ISSN 2408-2384 (ONLINE)

Environment and Natural Resources Journal

Volume 22 Number 4 July - August 2024

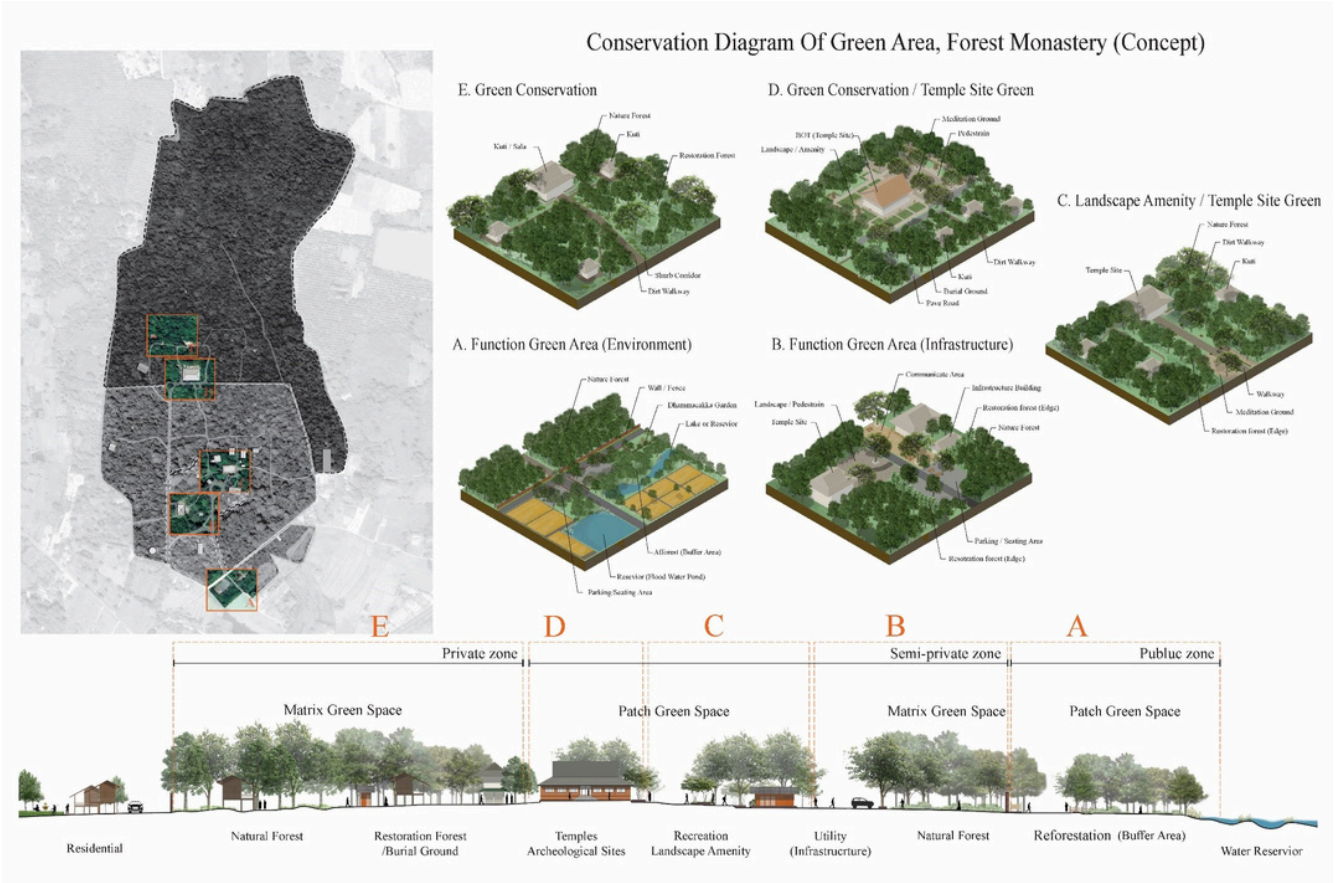

Area planning for ecological landscape conservation management of the Wat Pah

Source: Kongsombut P, Pattanakiat S, Rawang W, Srijuntrapun P, Phewphan U, Phutthai T, Vongvassana S, Jumpasingha J. Landscape ecological structures and patterns for green space conservation in forest monasteries in Northeast Thailand. Page 366-377.

Environment and Natural Resources Journal (EnNRJ)
Volume 22, Number 4, July - August 2024 ISSN: 2408-2384 (Online)

AIMS AND SCOPE

The Environment and Natural Resources Journal is a peer-reviewed journal, which provides insight scientific knowledge into the diverse dimensions of integrated environmental and natural resource management. The journal aims to provide a platform for exchange and distribution of the knowledge and cutting-edge research in the fields of environmental science and natural resource management to academicians, scientists and researchers. The journal accepts a varied array of manuscripts on all aspects of environmental science and natural resource management. The journal scope covers the integration of multidisciplinary sciences for prevention, control, treatment, environmental clean-up and restoration. The study of the existing or emerging problems of environment and natural resources in the region of Southeast Asia and the creation of novel knowledge and/or recommendations of mitigation measures for sustainable development policies are emphasized.

The subject areas are diverse, but specific topics of interest include:

- Biodiversity
- Climate change
- Detection and monitoring of polluted sources e.g., industry, mining
- Disaster e.g., forest fire, flooding, earthquake, tsunami, or tidal wave
- Ecological/Environmental modelling
- Emerging contaminants/hazardous wastes investigation and remediation
- Environmental dynamics e.g., coastal erosion, sea level rise
- Environmental assessment tools, policy and management e.g., GIS, remote sensing, Environmental Management System (EMS)
- Environmental pollution and other novel solutions to pollution
- Remediation technology of contaminated environments
- Transboundary pollution
- Waste and wastewater treatments and disposal technology

Schedule
Environment and Natural Resources Journal (EnNRJ) is published 6 issues per year in January-February, March-April, May-June, July-August, September-October, and November-December.

Publication Fees
There is no cost of the article-processing and publication.

Ethics in publishing
EnNRJ follows closely a set of guidelines and recommendations published by Committee on Publication Ethics (COPE).

Environment and Natural Resources Journal (EnNRJ)

Volume 22, Number 4, July - August 2024 ISSN: 2408-2384 (Online)

Editorial Office Address
Research Management and Administration Section,
Faculty of Environment and Resource Studies, Mahidol University
999, Phutthamonthon Sai 4 Road, Salaya, Phutthamonthon, Nakhon Pathom, Thailand, 73170
Phone +662 441 5000 ext. 2108 Fax. +662 441 9509-10
Website: https://ph02.tci-thaijo.org/index.php/ennrj/index
E-mail: ennrjournal@gmail.com

Environment and Natural Resources Journal (EnNRJ)

Volume 22, Number 4, July - August 2024 ISSN: 2408-2384 (Online)

CONTENT

Environment and Natural Resources Journal

Volume 22
Issue 4
2024

Burrow Morphological Characteristics of Soldier Crab (*Dotilla myctiroides*) on the Libong Island, Koh Libong Subdistrict, Kantang District, Trang Province, Thailand

Pimonrat Thongroy, Supaporn Saengkeaw, Panjan Sujjaritthurakarn, Waewruedee Waewthongrak, Sukallaya Hemmanee, and Somsak Buatip*

Department of Science, Faculty of Science and Technology, Prince of Songkla University, Pattani Campus, Pattani, Thailand

ARTICLE INFO

Received: 10 Nov 2023
Received in revised: 27 Apr 2024
Accepted: 8 May 2024
Published online: 10 Jun 2024
DOI: 10.32526/ennrj/22/20230316

Keywords:
Burrow/ Sandy beach/ Libong/ *Dotilla myctiroides*

*** Corresponding author:**
E-mail: somsak.bu@psu.ac.th

ABSTRACT

Dotilla myctiroides, the soldier crab, digs burrows in sand flats and extracts nutrients from sediment. The present study investigated the burrow morphology of this soldier crab, at Laem Juhoi Beach, Libong Island, Koh Libong Subdistrict, Kantang District, Trang Province, Thailand. Randomly selected burrows were examined by injecting molten paraffin into them. The crab found inside a burrow was collected and measured for its carapace length. The shapes of the complete burrow casts were identified, and various morphological characteristics of the burrow casts were recorded. A total of 84 burrows were identified, all of them were the I-shaped or single-tube burrows. The burrows were categorized into two groups based on the burrow opening diameter: the <12 mm group and the ≥12 mm group. The burrow opening diameter ranged from 7.50 to 20.10 mm while the end diameter at the burrow bottom ranged from 8.40 to 21.00 mm, and the total length of the burrows ranged from 27 to 206 mm. The carapace length showed a significant correlation ($p<0.05$) with the burrow opening diameter in both groups. Additionally, the burrow opening with a diameter <12 mm group had significantly greater hole distances than the burrow opening with a diameter ≥12 mm group ($p<0.05$). The observed variations in hole distances suggest potential differences in ecological and behavioral factors that influence the burrow morphology of *D. myctiroides* in distinct size categories.

1. INTRODUCTION

The burrow morphological characteristics of organisms are highly specific to their species, but their forms can change based on the physical and chemical characteristics of their habitats (Reise, 2002; Kristensen, 2008; Katrak et al., 2008). Some species may create or modify their burrow structures to adapt to the changing environmental conditions in their area (Griffis and Chavez, 1988; Griffis and Suchanek, 1991; Wolfrath, 1992). There have been several studies on the burrow structures of various crab species in different countries. For instance, a study was conducted in 2016, 2022, and 2023 on the burrow structure of *Ocypode ceratophthalmus* (Trivedi and Vachhrajani, 2016), *Dotilla blanfordi* (Upadhyay et al., 2022), *Austraca cryptica* (Min et al., 2023), and *A. sindensis* (Maheta and Vachhrajani, 2023) in India. Wang et al. (2015) also investigated the burrow structure of the *Macrophthalmus japonicas* and *Uca arcuate* in China. Additionally, Qureshi and Saher (2012) examined the burrow structures of several fiddler crab species, including *Uca* (*Paraleptuca*) *sindensis*, *U.* (*Paraleptuca*) *chlorophthalmus*, and *U. annulipes* in Pakistan.

Burrowing crabs are of great ecological importance. Soldier crabs belonging to the genus *Dotilla*, which are commonly found in the Indo-Pacific region, typically exhibit a preference for sandy substrates over muddy shores. They are generally observed inhabiting the lower regions of sandy shores

Citation: Thongroy P, Saengkeaw S, Sujjaritthurakarn P, Waewthongrak W, Hemmanee S, Buatip S. Burrow morphological characteristics of soldier crab (*Dotilla myctiroides*) on the Libong Island, Koh Libong Subdistrict, Kantang District, Trang Province, Thailand. Environ. Nat. Resour. J. 2024;22(4):301-309. (https://doi.org/10.32526/ennrj/22/20230316)

(MacNae and Kalk, 1962; McIntyre, 1968; Hartnoll, 1973; Hails and Yaziz, 1982; Matsumasa et al., 1992; Darmarini et al., 2019). The soldier crab plays a crucial role in the sandy beach ecosystem, as they are commonly found in large numbers and have adapted to thrive on the sandy shore. They are characterized by having a streamlined body shape, long legs, and elongated eyestalks, allowing them to move quickly and efficiently. *Dotilla myctiroides* showcases a rounded or oval body shape with nearly equal length and width, small size, and a round body form. Dorsal part lacks sculpturing. Fresh specimen is grayish-brown coloration. It possesses four pairs of robust legs. This species features short antennae ranging from orange to brown, accompanied by elongated brownish-black eyes. (Darmarini et al., 2019). Soldier crabs can dig burrows and have curved, shovel-like appendages for scooping up food. They also have bristle-like structures in their mouthparts that help filter organic matter from sand grains (Warner, 1977; Ansell, 1988). The process of burrowing and feeding by the soldier crab group results in the decomposition of organic matter on the sand surface, leading to the cycling of nutrients and the flow of energy within the sandy beach ecosystem. This contributes to an increase in oxygen levels in the sand, creating a nutrient-rich sandy substrate suitable for small-sized animals as habitat. Additionally, it enhances the rate of decomposition within the sandy soil (Warner, 1977). *D. myctiroides* has been the subject of a study regarding burrow structures in Thailand, specifically found in the Phuket Province. The study examined the diameters of burrows and food pellets at Ao Tung Khen (Lee and Lim, 2004). Additionally, there has been research on the distribution and shape of burrows in the seagrass *Enhalus acoroides* area (Matsumasa et al., 1992). In summary, further studies on burrow morphology in this crab species are essential to enhance the researchers understanding while gathering more comprehensive data. The main objective of the study was to investigate how burrow morphological characteristics relate to crab size and determine their link with hole density and distances between burrows.

Libong Island is covering area as 34 km^2 island located on 3.5 km off the west coast of peninsular Thailand. Its landscape features a forested western area rising to 344 m, while the central part is populated by humans which is now dominated by rubber plantations. The eastern side is characterized by tidal mangroves forest and grassy clearings on raised sandy patches. Open coastal habitats include sandy beaches, rocky outcrops, and extensive mudflats. Declared as a non-hunting area by the Royal Forest Department in 1979, Libong Island is part of the restricted wildlife hunting zone in the Libong Island group. Home to diverse reserved wildlife, including critically endangered and endangered species, the existence of the island is crucial for migratory shorebirds and threatened birds that is at the verge of extinction such as Great Knot, Great Hornbill, Black-capped Kingfisher, Grey-headed Fishing Eagle, Eurasian Curlew, Black-tailed Godwit, Bar-tailed Godwit, Red-necked Stint, and Curlew Sandpiper. Recognized as an important habitat for avian species facing challenges, Libong Island plays a vital role in supporting wildlife conservation efforts and contributing significantly to the region's overall biodiversity (Eve and Ann-Marie Guigue, 1982; Swennen et al., 1987; BirdLife International, 2001).

2. METHODOLOGY

2.1 Study area

In this study (7 º25'62" N, 99º44'86" E), the selected intertidal area for investigation is the sandy beach at Laem Juhoi Beach, situated at the eastern part of the island. During low tide, there is a large population of soldier crabs covering the area extensively (Figure 1).

2.2 Research methodology

The present study was carried out in March and October 2018. The burrows were selected randomly from lower to upper intertidal zone of the sandy shore. The study involved examining the burrow morphological characteristics by injecting molten paraffin into the crab burrows and allowing it to solidify. Once the paraffin had dried, the burrows were excavated and cleaned. If a crab was discovered inside a burrow, it was collected, and its carapace length (CL) was measured using digital vernier calipers (±0.01 mm; Pumpkin Model No. PTT-150VC01D). Subsequently, various measurements were taken, including the burrow opening diameter (B.O.D), end diameter at the burrow bottom (E.D), and the total length (T.L) using digital vernier calipers (±0.01 mm; Pumpkin Model No. PTT-150VC01D). The burrow shapes were also identified according to the modified method derived from Trivedi and Vachhrajani (2016) (Figure 2). These measurements and observations were conducted in a laboratory. In addition, random measurements of hole density (1×1 m^2) and the distance between holes.

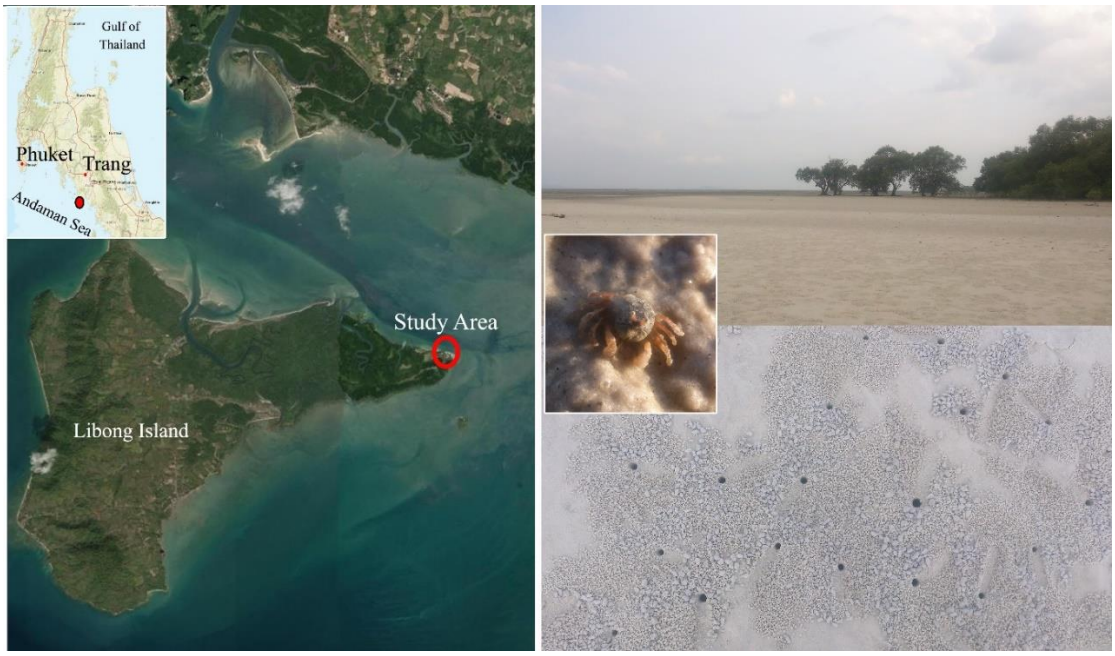

Figure 1. A map displaying the study area of Laem Juhoi Beach, Libong Island, Koh Libong Subdistrict, Kantang District, Trang Province

Figure 2. The method for measurements of the burrow morphological of soldier crab (*Dotilla myctiroides*)

2.3 Statistical analysis

The Pearson correlation coefficient was calculated to establish the relationship between morphological parameters of the burrow cast. While the crab size (carapace lengths) relationship between (1) burrow opening diameter (B.O.D), (2) end diameter at the burrow bottom (E.D), and (3) total length (T.L) were also analyzed. The hole distance was also compared using paired t-test. All of the statistical analysis was carried out using StatPlus in Windows 11.

3. RESULTS AND DISCUSSION

From the survey, it was found that soldier crabs are distributed across all of the sandy beach areas during the lowest tide periods. They share the area with fiddler crabs, ghost crabs, and sand bubbler crabs. Soldier crabs are predominantly found near the low tide zone. The soldier crabs are distributed approximately 6 m away from the shore to the low tide zone. Upon observation, two sizes of soldier crabs were identified. The distribution range of medium-sized soldier crabs start from approximately 6 m, while the larger soldier crabs start from approximately 16 m (Figure 3).

3.1 Burrow morphological characteristics

From a total of 84 burrow samples, it was found that all burrows exhibited an “I shape or single tube burrow”. These burrows could be categorized into two groups based on the burrow opening diameter (B.O.D) namely: B.O.D<12 mm group (n=41) (Figure 4(a)) and B.O.D≥12 mm group (n=43) (Figure 4(b)).

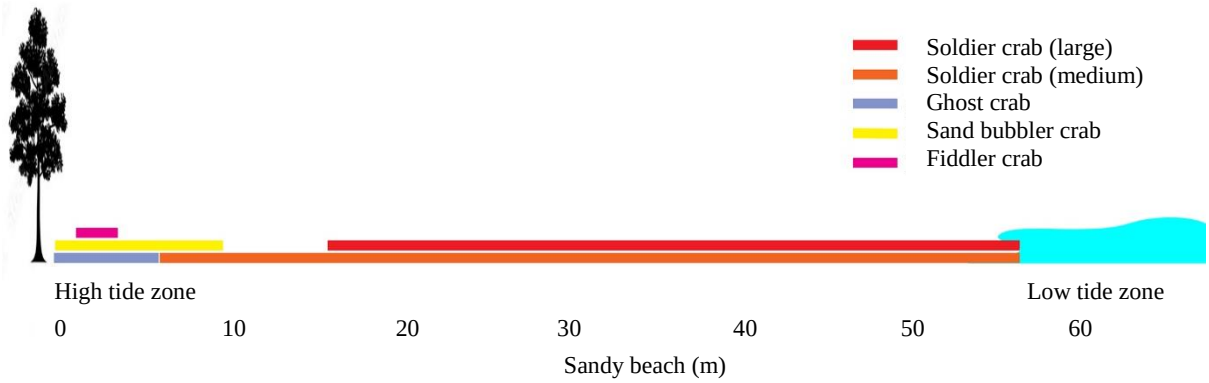

Figure 3. Distribution of soldier crab (*Dotilla myctiroides*) and other crabs on the sandy beach**,** Laem Juhoi Beach, Libong Island, Koh Libong Subdistrict, Kantang District, Trang Province

Figure 4. Burrow morphological of *Dotilla myctiroides*: (a) B.O.D<12 mm (medium) group, (b) B.O.D≥12 mm (large) group

In the B.O.D<12 mm group, the average burrow opening diameter is 10.08±1.17 mm while the average end diameter at the burrow bottom is 11.41±2.07 mm, and the average total length is 140.98±36.44 mm (Table 1, Figure 5(a)). In the B.O.D≥12 mm group, the average hole depth is less than B.O.D<12 mm group while the average burrow opening diameter is 13.74±1.74 mm with the average end diameter at the burrow bottom of 16.27±2.48 mm, and the average total length of 99.30±37.80 mm (Table 1, Figure 5(b)).

Table 1. Burrow morphological characteristics data of *Dotilla myctiroides*. (B.O.D: burrow opening diameter; E.D: end diameter at the burrow bottom; T.L: total length)

Parameters	B.O.D<12 mm group (n=41)			B.O.D ≥12 mm group (n=43)		
	B.O.D (mm)	E.D (mm)	T.L (mm)	B.O.D (mm)	E.D (mm)	T.L (mm)
Max	11.90	17.00	206.00	20.10	21.00	190.00
Min	7.50	8.40	58.00	12.00	12.00	27.00
Mean±SD	10.08±1.17	11.41±2.07	140.98±36.44	13.74±1.74	16.27±2.48	99.30±37.80

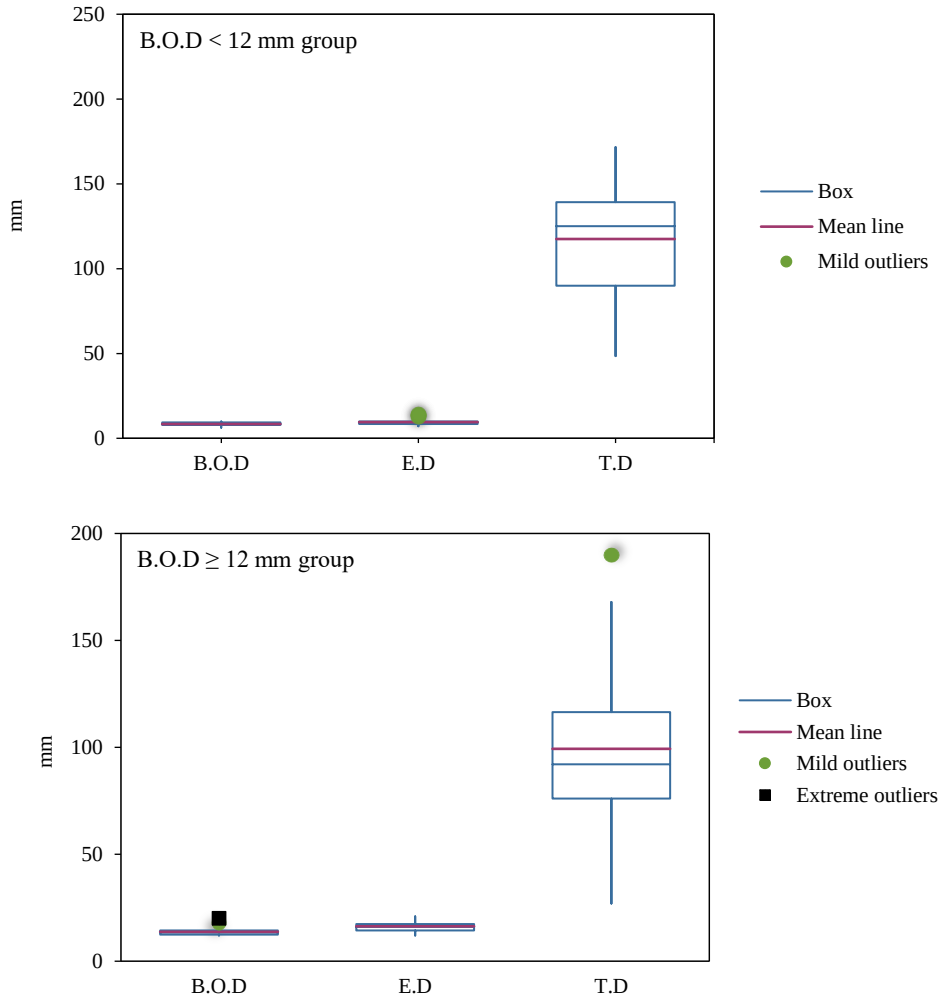

Figure 5. Boxplot: Burrow morphological characteristics of *Dotilla myctiroides*: (a) B.O.D<12 mm group, (b) B.O.D≥12 mm group

The analyzed data on the relationship between the morphological characteristics of the burrow using the Pearson Correlation Coefficient (r), found that only the T.L vs. E.D. within the B.O.D<12 mm group exhibited a non-significant correlation ($p>0.05$). In the B.O.D≥12 mm group, the sizes of B.O.D, E.D, and T.L showed a significantly correlated ($p<0.05$) situation. Specifically, B.O.D vs. E.D showed a positive correlation, while the B.O.D vs. T.L and T.L vs. E.D exhibited negative correlations (Table 2).

Table 2. Relationship between the morphological characteristics of the burrow (B.O.D: burrow opening diameter; E.D: end diameter at the burrow bottom; T.L: total length)

Burrow group	VAR vs. VAR	R	N	p-value
B.O.D<12 mm group	B.O.D vs. E.D	0.7910	51	4.9670E-12*
	B.O.D vs. T.L	0.4487	51	0.0010*
	T.L vs. E.D	0.2670	51	0.0582
B.O.D≥12 mm group	B.O.D vs. E.D	0.7384	84	0.0000*
	B.O.D vs. T.L	-0.3933	84	0.0002*
	T.L vs. E.D	-0.4713	84	6.0504E-6*

Asterisks indicate significant differences (*=p<0.05)

A total of 41 burrow samples in the B.O.D<12 mm group, 9 crabs were found to have attached individuals burrow, carapace width average of 5.55±0.50 mm (5.00-6.30 mm), and carapace length average of 5.68±0.59 mm (5.00-6.70 mm). And 43 burrow samples of B.O.D≥12 mm group, 11 crabs were found, carapace width an average 7.73±0.80 mm (6.90-9.00 mm), and carapace length an average 8.10±1.00 mm (6.90-9.80 mm). The analyzed data on the relationship between the morphology characteristics of the burrow and crab size using the Pearson Correlation Coefficient (r), found that only the carapace length (CL) vs. burrow opening diameter (B.O.D) within both groups are significantly correlated (p<0.05) (Table 3).

Table 3. Relationship between the morphological characteristics of the burrow and crab size (CL: carapace length; CW: carapace width; B.O.D: burrow opening diameter; E.D: end diameter at the burrow bottom; T.L: total length)

VAR vs. VAR	B.O.D<12 mm group			B.O.D≥12 mm group		
	R	N	p-value	R	N	p-value
CL vs. B.O.D	0.8386	9	0.0047*	0.6721	11	0.0235*
CL vs. E.D	0.2692	9	0.4836	0.5991	11	0.0515
CL vs. T.D	0.0144	9	0.9706	-0.4661	11	0.1485
CW vs. B.O.D	0.6386	9	0.0641	0.4882	11	0.1276
CW vs. E.D	0.2157	9	0.5773	0.4303	11	0.1865
CW vs. T.D	0.1217	9	0.7550	-0.5397	11	0.0866

Asterisks indicate significant differences (*=p<0.05)

The burrow morphological observed in this study are predominantly of the I-shape or single-tube burrow type. This basic burrow shape is commonly found among various crab species, including sand bubbler crabs, fiddler crabs, and ghost crabs. Subsequently, several crab species were found to modify their burrows into J, L, and other shapes according to their functional needs. Current research has revealed that I, J, and L shapes are prominent among burrow structures. The branching of burrows is most likely a strategy to evade pressure from predators and to accommodate both juveniles and adults together. Furthermore, an increased number of openings in some crab species' burrows may enhance their ability to escape from predators more easily (Gillikin and Kamanu, 2005; Min et al., 2023). This finding is consistent with the study conducted on the south-eastern shore of Phuket Island, Thailand, within the seagrass *Enhalus acoroides* zone (Matsumasa et al., 1992) whereby it was observed that this crab species exhibited two types of burrows, namely: tube-type and "igloo"-type burrows. However, the igloo-type burrows were not observed in this current study. Therefore, the data of environmental factors, such as slope, grain size, vegetation type, might need to be considered to explain the issue. This difference could be due to the fact that this study was conducted in sandy habitats, mainly with sandy sediment types, while the study by Matsumasa et al. (1992) was conducted in a seagrass zone with muddy sand sediment. The type of sediment may have affected the burrow structure.

Several studies in various areas in India had found that the I shape or single tube burrows morphological were very prominent, such as *Dotilla blanfordi* with 7 burrow shapes. These include single

tube burrows (predominant), single tube with branches, J, J shape with branches, U shaped with double openings, U shaped with a single opening, and bulb-shaped burrow (Upadhyay et al., 2022). Fiddler crab, *Austraca cryptica* exhibits only I shaped burrow, while *A. variegate* have J and I shaped burrow, *A. annulipes* have LL, Y, J, and I shaped burrow, and *A. occidentalis* exhibits JU, L, Y, and X shaped burrow (Min et al., 2023). In the case of *A. sindensis*, it exhibits 7 burrow shapes, including J shaped and single tube burrows predominantly, S, spiral, J-shaped with branches, U-shaped with single openings, and multi-branched burrow (Maheta and Vachhrajani, 2023). And ghost crab, *Ocypode ceratophthalmus* have 8 burrow shapes, including single tube burrow (predominant), J, Y, U, J-shaped with a branch at the base, bulb, multi-branched, and Y-shaped with double openings (Trivedi and Vachhrajani, 2016). In the case of *O. rotundata*, which was found on the Pakistan coastal belt, it exhibited 6 types of burrow shapes including single tube burrows (predominant), Y, C, L, J, and M shaped burrow (Odhano et al., 2022). The burrow shapes are typically specific to the species (Griffis and Suchanek, 1991; Wolfrath, 1992). However, modifications in burrow architecture may occur in response to variations in sediment type, grain size, average slope, average wave height, and vegetation, allowing the crabs to adapt to changing environmental conditions (Griffis and Chavez, 1988; Schlender et al., 2023).

In this study, it was found that carapace length (CL) showed a significant correlation with burrow opening diameter (B.O.D) in both groups, which is consistent with the findings of Lee and Lim (2004). In the case of other crab species, similar findings were found to be in line with the study on *Austruca sindensis.* However, in *A. sindensis*, crab carapace length demonstrated a significant positive correlation with total length, total burrow depth, and burrow volume (Maheta and Vachhrajani, 2023). In the case of *Ocypode ceratophthalmus*, crab carapace width showed a significant correlation with burrow opening diameter, total length, and burrow volume (Trivedi and Vachhrajani, 2016). And in the case of *Dotilla blanfordi*, these results emphasize the significant impact of crab body size on burrow morphology, a relationship that also varies across different life stages of the crab (Upadhyay et al., 2022).

3.2 Density and distance of the hole crab

Hole density was found to be between 50-85 holes/m^2 in the B.O.D<12 mm group, while the B.O.D≥12 mm group exhibited a hole density of between 53-119 holes/m^2

Hole distance was found to be between 3-18 cm with an average of 8.61±3.59 cm in the B.O.D<12 mm group (n=90), while the B.O.D≥12 mm group (n=60) had hole distances ranging from 2-12 cm with an average of 4.92±2.40 cm (Figure 6). Statistical analysis using t-test revealed that the hole distance in the B.O.D<12 mm group was significantly farther than the B.O.D≥12 mm group (t-statistic=7.5746, df=148, $p<0.05$).

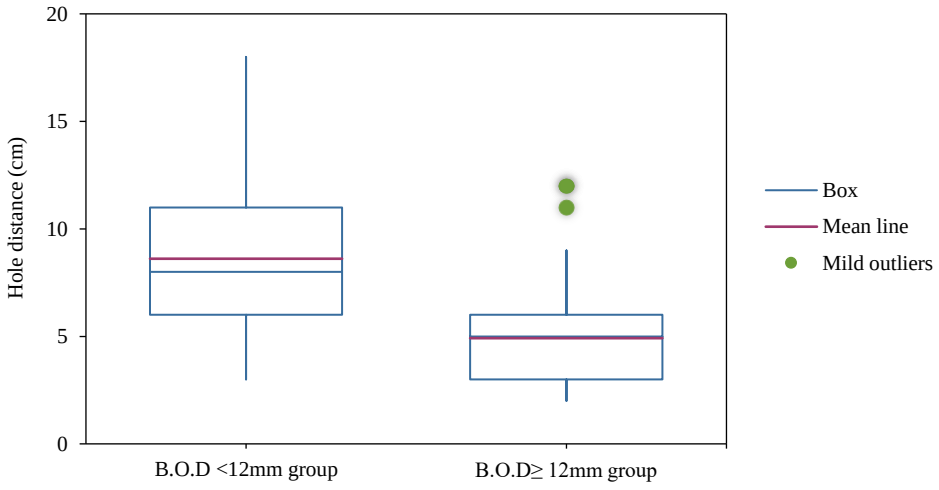

Figure 6. Boxplot: Hole distance of *Dotilla myctiroides* on Laem Juhoi Beach, Libong Island, Koh Libong Subdistrict, Kantang District, Trang Province

The density of burrows and the distances between them, as observed in the study, revealed that larger soldier crabs tend to create burrows in a denser arrangement compared to smaller soldier crabs. This also results in shorter distances between burrows, which could be attributed to variations in population size and the size of crabs in different age groups. Based on the study results, larger soldier crabs tend to have a narrower distribution range near the lowest water level, whereas smaller soldier crabs can spread out over a wider area (Figure 3). In contrast, it has been observed that the fiddler crab (*Uca bengali*) exhibited differences in behavior. Specifically, there is a dense distribution of larger-sized crabs in areas away from the water level, exhibiting a distinct pattern of dispersion (Tina et al., 2015). Larger soldier crab populations are generally more numerous than smaller ones. Furthermore, the distribution patterns differ among different-sized soldier crabs, with medium-sized soldier crabs establishing their burrows at approximately 6 meters apart, whereas larger soldier crabs start their burrows at around 16 meters apart. This leads to the larger soldier crabs being clustered closer together than the smaller ones. Hence, there would be a possibility that these differences might have been influenced by various factors, such as feeding behavior and food preferences, which are typically not explainable by a single mechanism. In addition, the profiles and natural characteristics of the beach environment may also play a role in shaping these patterns (Fisher and Tevesz, 1979; Milne and Milne, 1946; Turra et al., 2005; Branco et al., 2010; Gül and Griffen, 2018). Therefore, further research is needed to gain a deeper understanding on all factors related to these crab species.

4. CONCLUSION

The burrows of soldier crabs (*Dotilla myctiroides*) exhibited only an I-shaped (or single-tube structure). Based on the burrow opening diameter, the burrows were of two types namely, B.O.D<12 mm group and B.O.D≥12 mm group. There was a non-significant correlation between total length and end diameter within the group of burrow opening diameter was less than 12 mm. However, a significant correlation was found between carapace length and burrow opening diameter in both groups. Hole density was found to be between 50-119 holes/m^2 while the hole distance was between 2-18 cm. Future studies need additional factors, such as feeding behavior, food preferences, slope, as well as the physical and chemical characteristics of the beach environment. For the protection and management of the area, the responsible authorities should track and monitor those areas accessed by tourists and local fishermen so as to ensure that they benefit responsibly. This study suggested that there should be continuous monitoring to observe changes in the population or burrow structure of these crabs on the beach, which can easily assess environmental changes.

REFERENCES

Ansell AD. Migration or shelter? Behavioral options for deposit feeding crabs on tropical sandy shores. In: Chelazzi G, Vannini M. editors. Behavioral Adaptation to Intertidal Life. New York: Plenum Press; 1988. p. 15-6.

BirdLife International. Threatened Birds of Asia: the BirdLife International Red Data Book. Cambridge, UK: BirdLife International; 2001.

Branco JO, Hillesheim JC, Fracasso HAA, Christoffersen ML, Evangelista CL. Bioecology of the ghost crab *Ocypode quadrata* (Fabricius, 1787) (Crustacea: Brachyura) compared with other intertidal crabs in the Southwestern Atlantic. Journal of Shellfish Research 2010;29:503-12.

Darmarini AS, Soewardi K, Prartono T, Hakim AA, Nursiyamah S, Wardiatno Y. New distribution record of the soldier crab, *Dotilla myctiroides* (Milne-Edwards) from Lubuk Damar Coast, Aceh Province, Indonesia. AACL Bioflux 2019; 12(1):289-97.

Eve R, Ann-Marie Guigue AM. Birds on Ko Libong, Southern Thailand. Natural History Bulletin of the Siam Society 1982;30(2):91-104.

Fisher JB, Tevesz MJS. Within-habitat spatial patterns of *Ocypode quadrata* (Fabricius) (Decapoda Brachyura). Crustaceana Supplement 1979;5:31-6.

Gillikin DP, Kamanu CP. Burrowing in the East African mangrove crab, *Chiromantes ortmanni* (Crosnier, 1965) (Decapoda, Brachyura, Sesarmidae). Crustaceana 2005;78(10):1273-5.

Griffis RB, Chavez FL. Effects of sediment type on burrows of *Callianassa californiensis* Dana and *C. gigas* Dana. Journal of Experimental Marine Biology Ecology 1988;117(3):239-53.

Griffis RB, Suchanek TH. A model of burrow architecture and trophic modes in thalassinidean shrimp (Decapoda: Thalassinidea). Marine Ecology Progress Series 1991; 79:171-83.

Gül MR, Griffen BD. Impacts of human disturbance on ghost crab burrow morphology and distribution on sandy shores. PLoS ONE 2018;13(12):e0209977.

Hails AJ, Yaziz S. Abundance, breeding and growth of the ocypodid crab *Dotilla myctiroides* (Milne-Edwards) on a West Malaysian Beach. Estuarine and Coastal Marine Science 1982;15(2):229-39.

Hartnoll RG. Factors affecting the distribution and behaviour of the crab *Dotilla fenestrata* on East African shores. Estuarine Coastal and Marine Science 1973;1(2):137-43.

Katrak G, Dittmann S, Seuront L. Spatial variation in burrow morphology of the mud shore crab *Helograpsus haswellianus* (Brachyura, Grapsidae) in South Australian saltmarshes. Marine and Freshwater Research 2008;59(10):902-11.

Kristensen E. Mangrove crabs as ecosystem engineers; with emphasis on sediment processes. Journal of Sea Research 2008;59:30-43.

Lee S, Lim SS. Do diameters of burrows and food pellets provide estimates of the size structure of a population of *Dotilla myctiroides* at the sand-flats of Ao Tung Khen. Phuket Marine Biological Center Research Bulletin 2004;65:55-60.

MacNae W, Kalk M. The fauna and flora of sand flats of Inhaca Island, Mocambique. Journal of Animal Ecology 1962; 31(1):93-128.

Maheta NP, Vachhrajani KD. Burrow characteristics of the fiddler crab - *Austruca sindensis* (Alcock, 1900) from mudflats of Gulf of Khambhat, Gujarat, India. Arthropods 2023;12(1): 37-56.

Matsumasa M, Takeda S, Poovachiranon S, Murai M. Distribution and shape of *Dotilla myctiroides* (Brachyura: Ocypodidae) burrow in the seagrass *Enhalus acoroides* zone. Benthos Research 1992;43:1-9.

McIntyre AD. The meiofauna and macrofauna of some tropical beaches. Journal of Zoology 1968;156:377-92.

Milne LJ, Milne MJ. Notes on the behavior of the ghost crab. American Naturalist 1946;80(792):362-80.

Min WW, Kandasamy K, Balakrishnan B. Crab species-specific excavation and architecture of burrows in restored mangrove habitat. Journal of Marine Science and Engineering 2023;11:Article No. 310.

Odhano S, Saher NU, Rosenberg MS, Hassan MF, Soomro H. Burrow construction morphology of *Ocypode Rotundata* Miers 1882 (Ocypodidae: Brachyura) from the Sandy Coastal Areas of Karachi, Pakistan. Oceanography and Fisheries Open Access Journal 2022;15(4):Article No. 555917.

Qureshi NA, Saher NU. Burrow morphology of three species of fiddler crab (Uca) along the coast of Pakistan. Belgian Journal of Zoology 2012;142(2):114-26.

Reise K. Sediment mediated species interaction in coastal waters. Journal of Sea Research 2002;48(2):127-41.

Schlender K, Corte G, Durdall A, Habtes S, Grimes KW. Urbanization driving *Ocypode quadrata* burrow density, depth, and width across Caribbean beaches. Ecological Indicators 2023;153:Article No. 110396.

Swennen C, Ruttanadakul N, Ardseungnurn S, Howes JR. Foraging behaviour of the Crab Plover *Dromas ardeola* at Ko Libong, Southern Thailand. Natural History Bulletin of the Siam Society 1987;35:27-33.

Tina FW, Jaroensutasinee M, Sutthakiet O, Jaroensutasinee K. The fiddler crab, *Uca bengali* Crane, 1975: Population biology and burrow characteristics on a riverbank in southern Thailand. Crustaceana 2015;88:791-807.

Trivedi JN, Vachhrajani KD. On burrow morphology of the ghost crab, *Ocypode ceratophthalmus* (Decapoda: Brachyura: Ocypodidae) from sandy shore of Gujarat, India. International Journal of Marine Science 2016;6(15):1-10.

Turra A, Gonçalves MAO, Denadai MR. Spatial distribution of the ghost crab *Ocypode quadrata* in low-energy tide-dominated sandy beaches. Journal of Natural History 2005;39(23):2163-77.

Upadhyay KS, Patel KJ, Prajapati JM, Rabari VM, Thacker DR, Patel HV, et al. Burrow morphology of Brachyuran Crab *Dotilla blanfordi* Alcock, 1900 from Gulf of Khambhat, Gujarat, India. International Journal of Zoological Investigations 2022;8(2):251-61.

Wang J, Bertness MD, Li B, Chen J. Plant effects on burrowing crab morphology in a Chinese salt marsh: Native vs. exotic plants. Ecological Engineering 2015;74:376-84.

Warner GF. The Biology of Crabs. Great Britain: Paul Elek (Scientific Books) Ltd.; 1977.

Wolfrath B. Burrowing of the fiddler crab *Uca tangeri* in the Ria Formosa in Portugal and its influence on sediment structure. Marine Ecology Progress Series 1992;85:237-43.

Environment and Natural Resources Journal

Volume 22
Issue 4
2024

Life Cycle Assessment of Slaughtered Pork Production: A Case Study in Thailand

Monthita Joyroy[1], Patikorn Sriphirom[1], Direkrit Buawech[1], and Bhanupong Phrommarat[2*]

[1]Department of Environmental Science, Faculty of Science, Silpakorn University, Sanamchandra Campus, Nakhon Pathom 73000, Thailand
[2]Program of Biology, Faculty of Education, Chiang Rai Rajabhat University, Chiang Rai 57100, Thailand

ARTICLE INFO

Received: 22 Mar 2024
Received in revised: 29 Apr 2024
Accepted: 17 May 2024
Published online: 26 Jun 2024
DOI:10.32526/ennrj/22/20240074

Keywords:
Life cycle assessment/ Slaughtered pork/ Environmental impact/ Sustainable pork production/ Pig feed

*** Corresponding author:**
E-mail:
bhanupong.phr@crru.ac.th

ABSTRACT

Pork is a staple food in many cultures worldwide and plays a significant role in global food systems. However, the production of pork is associated with various environmental issues throughout its life cycle. This study employed a life cycle assessment (LCA) to evaluate the environmental impact of slaughtered pork production in Thailand. The system boundaries encompassed pig breeding, pig farming, and slaughtering. The primary focus was on identifying significant contributors to environmental burdens throughout the pork production chain. Three scenarios for pig feed compositions were assessed. The results indicated that pork production generated a total impact of 5.07 $kgCO_2$-eq on global warming, 1.16E-03 kgP-eq on freshwater eutrophication, 4.69 m^2a-eq on land use, and 4.97 m^3 on water consumption. Pig feed production, particularly maize cultivation, emerged as a hotspot within the life cycle, contributing the highest impact across all categories. According to scenario analysis, the substitution of rice by-products and sorghum in pig feed tended to reduce the magnitude of the impact. Opportunities were suggested to improve the environmental performance of pork production, especially through feed strategies such as substituting high-impact ingredients with more sustainable alternatives and utilizing waste from pig farming and slaughtering.

1. INTRODUCTION

Pork is recognized as one of the important protein sources contributing to global food security. It plays a significant role in various cuisines worldwide, with approximately 116 million tons of pork (11.3 kg per capita) consumed in 2023 (OECD, 2024). In Thailand, consumer demand for pork rose to 1.317 million tons in 2023, a 16.76 percent increase from 1.128 million tons in 2022. It is also exported to neighboring countries such as Hong Kong, Myanmar, and Laos, with an export volume of 1.771 tons in 2023 (Office of Agricultural Economics, 2023). Nonetheless, there has been increasing interest in recent years concerning sustainable food production due to depleting natural resources and environmental effects. Sustainable pork production is a promising practice that can enhance environmental quality, economic benefits, and social responsibility (Öhlund et al., 2017). There are various production factors as well as environmental emissions associated with pork production, such as pig feed, water, fossil fuels, electricity, wastewater, bio-waste, and transportation (Nguyen et al., 2011; McAuliffe et al., 2016; Winkler et al., 2016). These factors may contribute, directly or indirectly, to environmental impacts.

Increased pork demand has driven the expansion of intensive pig farming, causing a wide range of environmental impacts. This includes deforestation for pig pens, feed crops, and infrastructure, leading to habitat loss and biodiversity decline (Long et al., 2021). Various studies suggested that pork production contributes to greenhouse gas emissions occurring at different stages of the product life cycle, such as feed production, manure management, and fuel combustion (Dai et al., 2021; Pazmiño and Ramirez, 2021). In addition, pigs excrete large amounts of manure

Citation: Joyroy M, Sriphirom P, Buawech D, Phrommarat B. Life cycle assessment of slaughtered pork production: A case study in Thailand. Environ. Nat. Resour. J. 2024;22(4):310-320. (https://doi.org/10.32526/ennrj/22/20240074)

containing organic substances, i.e., nitrogen and phosphorus, which can cause eutrophication as well as pollution in surface water and groundwater (De La Mora-Orozco et al., 2018). The production of pig feed, often based on crops such as soy and corn, requires significant energy inputs for cultivation, processing, and transportation (De Quelen et al., 2021). Pig farming in South America contributes to deforestation due to its heavy reliance on soybean feed (Rajão et al., 2020).

Life Cycle Assessment (LCA), a standardized environmental assessment tool for a product or service based on a life cycle perspective, has been used to holistically assess the environmental impacts of pig farming and pork production. LCA is used extensively to quantify and highlight the significant environmental impacts (or hotspots) of a concerned product at every stage, ranging from raw material acquisition, manufacturing process, use, transportation, and waste management. LCA can be a valuable tool to inform decision-makers toward more sustainable pork production by identifying environmental hotspots, comparing different production systems, and evaluating the potential of new technologies (McAuliffe et al., 2016). In LCA studies concerning pork supply chains, system boundaries are often defined up to either the farm gate or slaughter gate. Among life cycle stages, the cultivation of feed used in pig farming is often identified as a primary contributor to environmental impacts. This is primarily due to its direct association with land use change as well as the intensive use of agrochemicals and fossil fuels (Bava et al., 2017; Dorca-Preda et al., 2021; Zira et al., 2021). Also, manure management can potentially contribute to greenhouse gas emissions and acidification, as suggested by Djekic et al. (2015). Changing feed composition, particularly a decrease in high-impact ingredients such as soybean meal and maize, can mitigate the overall influences of pig feed (Ottosen et al., 2021). Tailoring the nutrient content of the feed to the exact needs of the pig at each stage of growth, or precision feeding, can boost farm profitability and efficiency, and improve the environmental performance of pig feed (Pomar and Remus, 2019). Organic pig farming could be more environmentally beneficial than conventional farming as the environmental effects of organic pork were shown to be 38-80% lower than conventional pork in all impact categories (Zira et al., 2021).

While numerous LCA studies have been conducted on pork production in various regions globally, there remains an existing gap in research concerning the context of Thailand. Moreover, Thailand's reliance on rice by-products such as broken rice and bran for pig feed (Bureau of Animal Nutrition Development, 2017) might lead to different results compared to studies in other regions. This study aimed to investigate the life cycle environmental impacts of slaughtered pork in Thailand through a cradle-to-slaughterhouse gate case study, considering relevant stages of pig farming and slaughtering. In addition, the effects of different pig feed formulas and allocation methods on the life cycle impacts were also compared.

2. METHODOLOGY

This study employed the Life Cycle Assessment (LCA) method following the standards outlined in ISO 14040 and 14044 by the International Organization for Standardization (ISO, 2006a; ISO, 2006b). These standards define the four main phases of an LCA, comprising goal and scope definition, life cycle inventory, life cycle impact assessment, and interpretation.

2.1 Goal and scope definitions

The objective of this study was to investigate the environmental impacts of slaughtered pork throughout its life cycle. The functional unit for the assessment was 1 kg of packaged average pork cuts obtained from a whole carcass. Inedible parts were considered bio-waste. The system boundary of this research was defined as a cradle-to-slaughterhouse gate (Figure 1). The system was divided into three main phases: pig breeding, pig farming, and slaughtering. Primary data on pig farming were derived from four pig farms in a central province of Thailand, while data on slaughtering were collected from a slaughterhouse located in an adjacent area. Secondary data on pig breeding and the background system were supplemented from existing literature as well as the LCI database, Ecoinvent 3.4, embedded in OpenLCA software. The database used was based on the allocation of the point of substitution (APOS) system model. The default allocation method in this study was based on an economic approach to avoid overestimation for lower-valued by-products (Williams and Eikenaar, 2022). The environmental impacts of the product system were assessed based on the ReCiPe 2016 midpoint (Hierarchist) method (Huijbregts et al., 2017). Four categories were selected to be highly relevant to the product system, including global warming, land use, water consumption, and freshwater eutrophication.

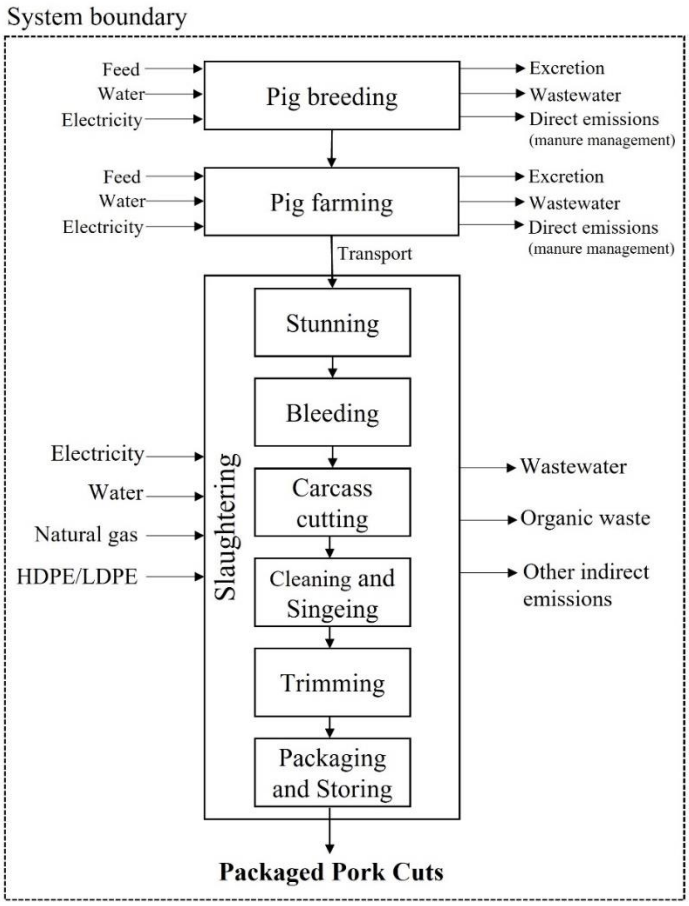

Figure 1. System boundary of slaughtered pork product system

2.2 Life cycle inventory

The product system comprised three main phases: pig breeding, pig farming, and slaughtering. Pig breeding focuses on managing boars and sows to produce healthy piglets. Pig farming is associated with the utilization of resources for raising pigs. The adult pigs are then transported to the slaughterhouse. There are six sub-processes at the slaughterhouse to produce the final product (packaged pork), including stunning, bleeding, carcass cutting, cleaning and singeing (hair removing), trimming, and packaging. The acquisition of data and assumptions used in the analysis for each life cycle stage are described as follows:

2.2.1 Pig breeding

During the breeding stage, sows are bred to produce piglets. Data on pig breeding, boar and sow handling, feed, water, and medication requirements were obtained from the Department of Livestock Development (DLD, 2005). This study assumed a sow could deliver 30 piglets annually (10 piglets/litter, 3 litters/year). Wastewater generation and direct emissions from manure, including methane (CH_4), nitrous oxide (N_2O), and ammonia (NH_3), were considered. Pig excretions were washed with water and discharged into a lagoon. The characteristics of wastewater were calculated based on data from the Pollution Control Department (2017). Direct greenhouse gas emissions from enteric fermentation and pig manure were calculated using the IPCC (2006) method, while ammonia emission was calculated based on IAEA (2008). Table 1 shows the data inventory associated with the pig breeding process to produce one weaning piglet.

2.2.2 Pig farming

Primary environmental data for pig farming were collected from four pig farms, focusing on raising weaning piglets (over 10 weeks old) with an average weight of 15 kg. The raising process primarily relied on pig feed and water. Pig feed was transported from the feed supplier to the pig farm over an average distance of 36.25 km by a 10-wheel truck. Additional inputs during this stage included disinfectants for cleaning pig houses, food supplements, and vaccines and medicines. Similar to the breeding stage, wastewater and direct air emissions were considered. A summarized inventory analysis of the farm process

per pig is presented in Table 2, providing an overview of the resources and emissions associated with this stage of pig farming.

Table 1. Inventory analysis of farm production per one weaning piglet

	Quantity	Unit
Input		
Water	1.12	m^3
Transport (feed to farm)	36.25	km
Disinfectants	0.20	g
Pig feed (mixed)	36.5	kg
Output		
Piglet	15	kg
BOD (to water)	623	g
COD (to water)	1,324	g
Suspended solids (to water)	701	g
TNK (to water)	273	g
CH_4 (to air)	267	g
N_2O (to air)	11.5	g
NH_3 (to air)	98	g
Organic waste	225.34	g

Table 2. Inventory analysis of farm production per one adult pig

	Quantity	Unit
Input		
Piglet	15	kg
Electricity	17.6	kWh
Water	7.65	m^3
Transport (feed to farm)	36.25	km
Disinfectants	0.2	g
Pig feed (mixed)	375	kg
Output		
Pig (live weight)	122	kg
BOD (to water)	9.0	kg
COD (to water)	19.4	kg
Suspended solids (to water)	10.8	kg
TNK (to water)	1.3	kg
CH_4 (to air)	3.29	kg
N_2O (to air)	0.14	kg
NH_3 (to air)	1.31	kg
Organic waste	375	kg

2.2.3 Feed

To understand how variations in feed formulas can have environmental effects, this study analyzed life cycle scenarios for pork production using different feed formulations. The three main feed formulas in this study, based on Wanasitthachaiwat and Rojanasathit (1999), are summarized in Table 3. Each formula met the key requirement of pig feed recommended by DLD (2005): a crude protein content of at least 18%. The nutritional content of each feed formula, calculated based on the INRAE-CIRAD-AFZ feed tables (INRAE-CIRAD-AFZ, 2021), is specified in Table 3. Maize and rice bran are generally used as the key ingredients supplemented by sorghum and soybean meal. In scenario 1 (the baseline scenario), pig feed was produced from a mixture of maize as the main raw material, followed by soybean meal, rice bran, and other minor ingredients. In scenario 2, rice bran and maize were the main raw materials, along with a mixture of sorghum, soybean meal, and other ingredients. In scenario 3, a large proportion of rice bran was applied, followed by sorghum and soybean meal without maize.

2.2.4 Slaughtering

Adult pigs with an average live weight of 122 kg were transported to the slaughterhouse by a 10-wheel truck over an average distance of 148.61 km. There were six sub-processes in the slaughterhouse, as depicted in Figure 1. The pigs were cleaned before being passed to the stunning and bleeding units. The pig carcasses were then cut and separated into various parts. All parts were cleaned with water. Parts with skin were singed to remove hair. Finally, the pork cuts were trimmed and packed in plastic packages. After processing, the weight of the pork cuts from the whole carcass was reduced to 96.26 kg. This process generated wastewater and organic wastes (approximately 20% of live weight), including bones, bristles, and fat. A summarized inventory of the data for the slaughter process per whole carcass is presented in Table 4.

Table 3. The environmental inventory for three pig feed scenarios (per 100 kg of feed)

	Scenario 1	Scenario 2	Scenario 3
Maize (kg)	61.3	25.2	-
Rice bran and broken rice (kg)	13.3	25.2	28.8
Soybean meal (kg)	17.8	17.9	12.2
Sorghum (kg)	-	23.9	51.3
Fish meal (kg)	5.95	5.95	5.95
Dicalcium phosphate (kg)	1.30	1.30	1.30

Table 3. The environmental inventory for three pig feed scenarios (per 100 kg of feed) (cont.)

	Scenario 1	Scenario 2	Scenario 3
Sodium chloride (kg)	0.25	0.25	0.25
Multivitamin (kg)	0.18	0.18	0.18
Crude protein (%)	18.0	19.3	18.0
Crude fat (%)	4.3	5.7	5.9
Crude fiber (%)	3.2	2.8	2.6
Net energy (kcal)	229448	216216	216216

Table 4. Inventory analysis of the slaughterhouse production of pork cuts per whole carcass

	Value	Unit
Input		
Pig (live weight)	122	kg
Water	0.49	m^3
Electricity	17.1	kWh
Natural gas	0.96	kg
Transportation from farm to slaughterhouse	148.61	km
HDPE	306.0	g
LDPE	14.3	g
Output		
Pork	96.26	kg
Organic waste (bone, bristles, etc.)	25.74	kg
Wastewater	0.35	m^3
BOD	8.66	kg
COD	11.55	kg
Organic nitrogen	1.64	kg
Ammonia nitrogen	0.08	kg

3. RESULTS AND DISCUSSION

3.1 Life cycle impact assessment

Life cycle environmental impacts (LCIA) were assessed by the ReCiPe 2016 midpoint (H) approach considering four impact categories, comprising global warming (GW), freshwater eutrophication (FE), land use (LU), and water consumption (WC). The LCIA results can be described as follows:

3.1.1 Baseline scenario

The characterization results of midpoint impact categories are summarized in Table 5. Figure 2 shows the comparison of results across three scenarios displayed on a percentage share by setting the greatest result to 100%. The impact assessment results for 1 kg of packaged pork cut demonstrated the pig farming stage made the greatest contribution, exceeding 85% across all impact categories. The total carbon footprint was 5.07 $kgCO_2$-eq. The key contributor to this footprint arose from the production of maize used in pig feed, as well as direct emissions (CH_4 and N_2O) from pig slurry. Considering activities and inputs specifically in the pig farming process (Figure 3), maize was the main raw material in pig feed. The cultivation of maize also significantly impacted FE, LU, and WC.

Maize cultivation, especially with fertilizer use, contributes to eutrophication by causing an imbalance in soil and water nutrient levels (N and P) (Powers, 2005). In terms of the impact on LU, maize and soybean meal contributed equally. Large-scale maize farming often involves monoculture practices, dedicating extensive areas solely to maize. This practice reduces biodiversity and disrupts natural ecosystems (Fuchs et al., 2021). In addition, soybean feed production has been linked to land use change and deforestation, especially in South America (Rajão et al., 2020). While the amount of rice bran in the pig feed was relatively low, its impact was almost as significant as maize. The results suggested that rice cultivation requires significantly more water than maize. Studies revealed that rice cultivation in tropical regions may necessitate nearly double the water usage compared to maize (2,497 L/kg versus 1,222 L/kg) (Rahaman and Shehab, 2018).

Table 5. Comparison of impacts in different feed scenarios (per functional unit)

		GW ($kgCO_2$-eq)	FE (kgP-eq)	LU (m^2a-eq)	WC (m^3)
Scenario 1	Breeding	3.96E-01	8.88E-05	4.16E-01	4.02E-01
	Farming	4.50E+00	9.92E-04	4.28E+00	4.35E+00
	Slaughtering	1.77E-01	8.22E-05	2.66E-03	2.10E-01
	Total	5.07E+00	1.16E-03	4.69E+00	4.97E+00
Scenario 2	Breeding	3.73E-01	6.67E-05	2.83E-01	4.06E-01
	Farming	4.27E+00	7.65E-04	2.92E+00	4.40E+00
	Slaughtering	1.77E-01	8.22E-05	2.66E-03	2.10E-01
	Total	4.82E+00	9.14E-04	3.20E+00	5.02E+00
Scenario 3	Breeding	3.24E-01	4.35E-05	1.31E-01	3.60E-01
	Farming	3.77E+00	5.26E-04	1.35E+00	3.93E+00
	Slaughtering	1.77E-01	8.22E-05	2.66E-03	2.10E-01
	Total	4.27E+00	6.52E-04	1.49E+00	4.50E+00

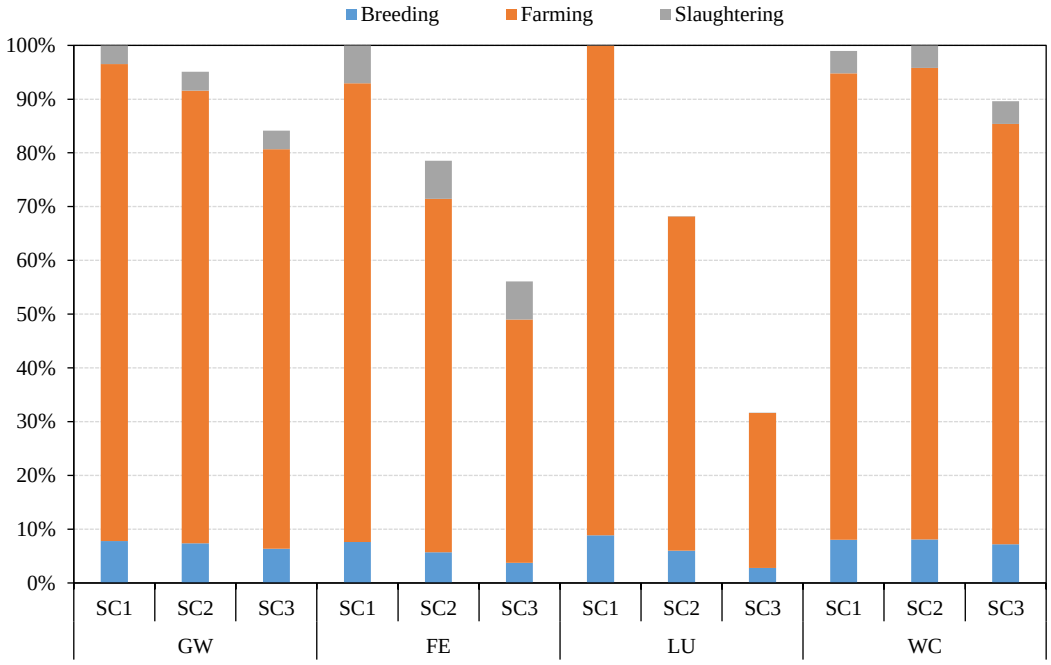

Figure 2. Impact assessment results of different feed scenarios

3.1.2 Alternative feed scenarios

In comparing the feed scenarios (Figures 2 and 3), the baseline scenario emerged as the one with the most significant impact on GW, FE, and LU, primarily due to its heavy reliance on maize, as discussed earlier. Scenario 3, on the other hand, had the lowest environmental impact across all categories. Scenarios 2 and 3 aimed to reduce the environmental impact of maize production on GW, FE, and WC by substituting raw materials. However, this substitution resulted in a proportional increase in the impact of rice. Since rice is a water-intensive crop, the higher proportion of rice bran for pig feed in Scenario 2 led to a greater impact on WC compared to the baseline scenario. Similar to the baseline scenario, maize and soybean remained the primary contributors to LU in Scenarios 2 and 3. Substituting maize with sorghum, particularly in Scenario 3, significantly reduced the impacts on FE and LU. Sorghum's high nitrogen usage efficiency and lower water requirement (one-third less than maize) make it a low-impact crop (Duff et al., 2019).

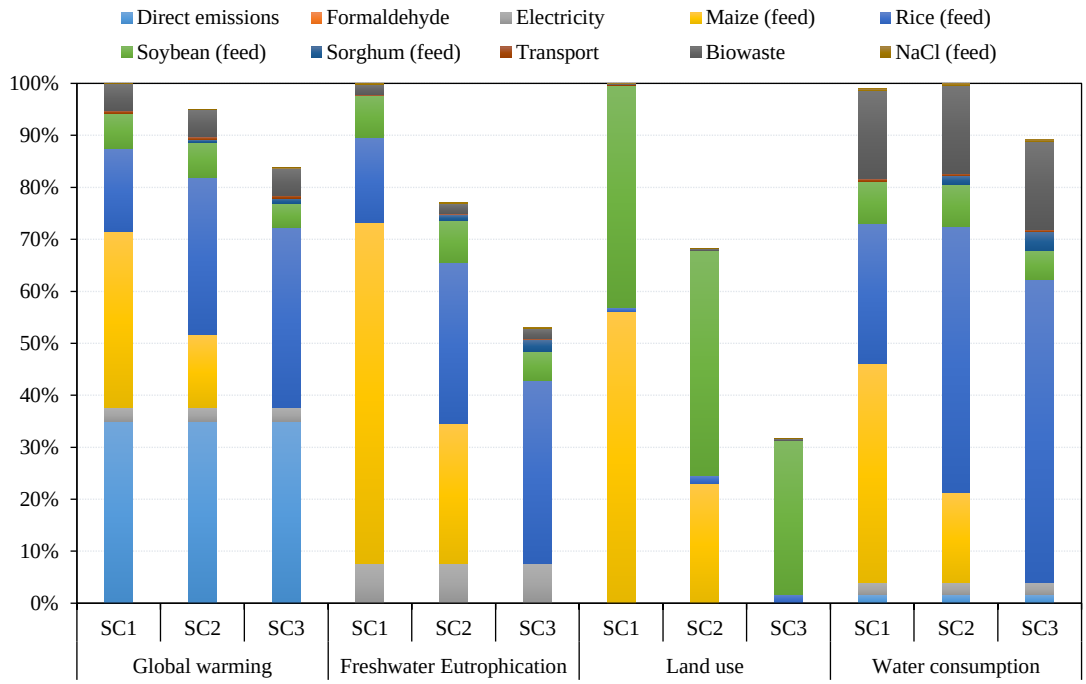

Figure 3. Comparison of impact contribution from pig farming in different scenarios

3.2 Sensitivity analysis

3.2.1 Variability of parameters

This study analyzed the impact of uncertain data in pork production through sensitivity analysis to identify the parameters that significantly influence the final results. This information can then be used to improve the reliability of the LCA and identify areas where further data collection is needed. Parameters with a percentage coefficient of variation (%CV) of at least 10% were selected and varied by ±10%. The impact on the product life cycle assessment (LCA) results was then assessed to identify the level of influence.

Six parameters were identified as having significant variability, including transport feed, HDPE, LDPE, water, organic waste, and slaughterhouse wastewater. Table 6 shows the changes in the three impacts resulting from the variation of these parameters. However, these changes had a minimal effect on the results of the overall sensitivity analysis (less than 1% impact). This suggested that, while some individual parameters might influence specific impact categories, the overall data used in the test was relatively robust to these variations.

3.2.2 Allocation method

The default allocation method in this study was based on economic value because the mass-based approach can lead to overestimation for lower-valued by-products (i.e., rice bran and broken rice) (Williams and Eikenaar, 2022). The average selling prices for rice (THB 20.40 per kg of rice) and its by-product (THB 11.47 per kg of rice bran) in 2023 (Ministry of Commerce, 2024) were used to calculate the default allocation factor. In this section, physical allocation was performed to investigate the effect of the allocation method on the LCA result. For every 1 kg of paddy rice processed in a mill, 0.1 kg of rice bran and broken rice are generated. Therefore, approximately 10% of the environmental burden from rice production was assigned to by-products.

Table 6. Sensitivity of impact results responding to parameter variations (±10%)

Parameter	%CV	%Sensitivity			
		GW	FE	LU	WC
Transport (feed to farm)	13.95	0.047	0.016	0.002	0.041
Organic waste (slaughterhouse)	23.83	0.032	0.012	0.002	0.103
HDPE (slaughterhouse)	29.43	0.004	0.012	0.000	0.011
LDPE (slaughterhouse)	29.43	0.001	0.000	0.000	0.000
Water (slaughterhouse)	17.05	0.000	0.000	0.000	0.010
Wastewater (slaughterhouse)	23.59	0.003	0.033	0.000	0.032

Table 7. Comparison of LCA results using physical and economic allocation methods

	Allocation method	GW ($kgCO_2$-eq)	FE (kgP-eq)	LU (m^2a-eq)	WC (m^3)
Scenario 1	Economic	5.07E+00	1.16E-03	4.69E+00	4.97E+00
	Physical	5.63E+00	1.29E-03	4.72E+00	5.88E+00
	%change	10.92%	10.70%	0.57%	18.36%
Scenario 2	Economic	4.82E+00	9.14E-04	3.20E+00	5.02E+00
	Physical	5.87E+00	1.15E-03	3.25E+00	6.75E+00
	%change	21.79%	25.83%	1.58%	34.47%
Scenario 3	Economic	4.27E+00	6.52E-04	1.49E+00	4.50E+00
	Physical	5.47E+00	9.22E-04	1.54E+00	6.47E+00
	%change	28.13%	41.37%	3.88%	43.97%

Utilizing the physical allocation method (as shown in Table 7) significantly increased the overall environmental impact compared to the economic allocation method, particularly in Scenario 3 with its heavy reliance on rice bran and broken rice in the feed formulation. This effect was most noticeable in FE and WC, where rice production is the key contributor. These results highlight the significant impact that the method selected for allocating environmental burdens from agricultural by-products in pig feed can have on the overall LCA findings.

3.3 Discussion

This study reaffirmed that an environmental hotspot of pork production was pig feed, consistent with previous studies (e.g., Pazmiño and Ramirez, 2021; Liu et al., 2021; Zira et al., 2021). The main ingredients of pig feed, particularly maize and rice by-products, played an important role in contributing to environmental impacts. Although the results of LCA are unable to be compared directly due to variations in methodology and system boundaries, a comparison of global warming or carbon footprint results, a key environmental concern, was conducted. As shown in Table 8, the life cycle GWP of pork can vary significantly, ranging from 2.46 to 9.04 $kgCO_{2\text{-eq}}$ per kg of pork at the slaughterhouse gate. Such variations likely stem from different data limitations, production practices, feed composition, and waste management scenarios. In the present study, Scenarios 1-3 yielded GW values of 5.07, 4.82, and 4.27 $kgCO_2$-eq/kg of pork cut, respectively, which fall within the range identified in the literature review with an average value of 4.63 $kgCO_2$-eq.

Table 8. Comparison of global warming potential impact results with other studies

Reference	Scenario/Country	GWP ($kgCO_2$-eq/FU[1])
Ndue and Pál (2022)	Conventional, EU	2.46
	Organic, EU	4.27
Pazmiño and Ramirez (2021)	Economic allocation, Ecuador	4.57
Liu et al. (2021)	Small-scale production, China	5.96
Reckmann et al. (2016)	Standard diets, Germany	3.01
Winkler et al. (2016)	Australia	4.75
Djekic et al. (2015)	Serbia	9.04
Nguyen et al. (2011)	Denmark	2.95

[1]Functional Unit: 1 kg of pig carcass or pork at the slaughterhouse gate

Pig feed composition significantly influences the life cycle impacts of pork products. In Europe, wheat, barley, and maize are commonly used feed ingredients supplemented with soybean meal (Djekic et al., 2015; Reckmann et al., 2016). However, this reliance on soybean meal creates an environmental concern, as it is often imported from South American countries where deforestation for soy cultivation is a significant issue (Rajão et al., 2020). Conversely, Asian pig feed relies primarily on maize and soybean meal (Liu et al., 2021; Ogino et al., 2013). Burning agricultural residues, such as maize stalks and rice straw, is currently a major environmental concern in Asia. This practice discharges large quantities of fine

particulate matter (PM2.5) directly into the atmosphere and leads to serious health problems in Southeast Asia (Oanh et al., 2018).

The scenario analysis in this study, investigating different feed options in Thailand, indicated that combining rice by-products (rice bran and broken rice) with sorghum had the potential to mitigate environmental impacts. However, rice use necessitates optimization as its cultivation requires a significant quantity of water. Although Thailand is located in a tropical, humid area, the country faces various challenges related to water availability, quality, and management. The increase in water demand due to population growth, the rapid growth of spatial development and economy, etc. causes water shortages (Wijitkosum and Sriburi, 2008). In addition to water consumption, rice cultivation requires fertilizers and contributes directly to greenhouse gas emissions. Apart from rice by-products, sorghum boasts a lower environmental footprint compared to maize and rice (Duff et al., 2019). Nonetheless, domestic production in Thailand is currently low, necessitating heavy reliance on imports (DOAE, 2019).

Several management strategies have been recommended to improve the environmental performance of pig feed. The substitution of crude protein content from soybean meal with, for example, synthetic amino acids can potentially reduce the overall environmental impact of pig feed and consequently lower N and CH_4 excretion of pigs (Ogino et al., 2013; Reckmann et al., 2016). The utilization of precision feeding techniques, which involves providing the right amount of feed with the perfect mix of nutrients at the right time, can reduce production costs and greenhouse gas emissions (6% lower) (Pomar and Remus, 2019). Dry legume seeds, particularly when combined from different species, offer the most accessible protein alternative to soybean; they can be effectively incorporated into pig diets without compromising meat quality (Parrini et al., 2023). Some countries incorporate recycled food waste into pig feed, which can be a sustainable practice if managed hygienically. Heller et al. (2018) highlighted feeding pigs with recycled food waste as a management strategy that can mitigate the associated greenhouse gas emissions by 24%. However, controversy about animal welfare and environmental sustainability emerges (Ndue and Pál, 2022).

Apart from feed management to improve the system, adequate management of farm waste is still required, even though manure and wastewater from pig production have a relatively low environmental impact. These residues can be utilized for generating biogas, fertilizers, and compost that can be used in feed production practices, subsequently reducing the life cycle impact of pork production. During the slaughtering process, all by-products should be prioritized for use as food or animal feed. For any inedible by-products, rendering or converting them into usable products should be strongly encouraged. This approach reduces reliance on virgin resources and promotes a more sustainable life cycle for pork production. Future research should prioritize the environmental impact of feed production, as it appears to have been the most significant contributor in this study. Due to data limitations, only three feed formulas were analyzed. However, investigating alternative feed ingredients, specifically from local crops or agricultural by-products, is crucial. Furthermore, the impact of these alternative feed nutrients on pig growth and biomass production should be explored.

4. CONCLUSION

A life cycle assessment was conducted to evaluate the environmental effects of 1 kg of average packaged pork cut from a whole carcass. This study identified the environmental impact of each stage of the pork life cycle and pinpointed hotspots for improvement. Three scenarios for feed composition were also assessed. The baseline scenario results showed that maize production in pig feed was the key contributor to all three key environmental damage categories, followed closely by rice production. The substitution of rice by-products and sorghum in Scenarios 2 and 3 tended to reduce the magnitude of any impact. On the other hand, rice cultivation requires a significant amount of water as well as fertilizers and is directly related to greenhouse gas emissions. Moreover, the method chosen for allocating environmental impacts from agricultural by-products in pig feed can significantly affect the overall results. The reason is that the mass of the by-products is typically much greater than their economic value compared to the main product. Significant opportunities exist to improve the environmental impact of pork production, with a focus on feed production strategies. This can be achieved by substituting ingredients with high environmental footprints for more sustainable alternatives. Additionally, utilizing the waste from pig farming and slaughtering can further reduce the environmental

impact. This information can be used by pig farmers, slaughterhouse owners, suppliers, and other stakeholders to enhance their environmental performance.

ACKNOWLEDGEMENTS

This study is kindly supported by Silpakorn University and Chiang Rai Rajabhat University. The authors would like to express gratitude to anonymous reviewers and editors for their useful comments and suggestions.

REFERENCES

Bava L, Zucali M, Sandrucci A, Tamburini A. Environmental impact of the typical heavy pig production in Italy. Journal of Cleaner Production 2017;140:685-91.

Bureau of Animal Nutrition Development. Pig feed ingredient [Internet]. 2017 [cited 2023 Dec 25]. Available from: https://nutrition.dld.go.th/nutrition/index.php/the-joomla-project/953-2017-09-01-05-06-54 (in Thai).

Dai XW, Zhanli SUN, Müller D. Driving factors of direct greenhouse gas emissions from China's pig industry from 1976 to 2016. Journal of Integrative Agriculture 2021; 20(1):319-29.

De La Mora-Orozco C, González-Acuña IJ, Saucedo-Terán RA, Flores-López HE, Rubio-Arias HO, Ochoa-Rivero JM. Removing organic matter and nutrients from pig farm wastewater with a constructed wetland system. International Journal of Environmental Research and Public Health 2018;15(5):Article No. 1031.

De Quelen F, Brossard L, Wilfart A, Dourmad JY, Garcia-Launay F. Eco-friendly feed formulation and on-farm feed production as ways to reduce the environmental impacts of pig production without consequences on animal performance. Frontiers in Veterinary Science 2021;8:Article No. 689012.

Department of Agricultural Extension (DOAE). Production of sorghum as feed cultivation year 2018/19 [Internet]. 2019 [cited 2024 Apr 24]. Available from: http://www.agriinfo.doae.go.th/year62/plant/rortor/agronomy/7.pdf (in Thai).

Department of Livestock Development (DLD). Pig Farming Manual. Bangkok: Department of Livestock Development; 2005 (in Thai).

Djekic I, Radović Č, Lukić M, Stanišić N, Lilić S. Environmental life cycle assessment in production of pork products. Scientific and Professional Section 2015;17;469-76.

Dorca-Preda T, Mogensen L, Kristensen T, Knudsen MT. Environmental impact of Danish pork at slaughterhouse gate a life cycle assessment following biological and technological changes over a 10-year period. Livestock Science 2021; 251:Article No. 104622.

Duff J, Vincent A, Bice D, Hoeffner I. Background on grain Sorghum Usage. In: Zhao ZY, Dahlberg J, editors. Sorghum: Methods in Molecular Biology, Volume 1931. New York: Humana Press; 2019. p. 245-56.

Fuchs A, Berger V, Steinbauer K, Köstl T. The long-term effects of monoculture maize cultivation on plant diversity. Phytocoenologia 2021;50(4):397-408.

Heller MC, Willits-Smith A, Meyer R, Keoleian GA, Rose D. Greenhouse gas emissions and energy use associated with production of individual self-selected US diets. Environmental Research Letters 2018;13:Article No. 044004.

Huijbregts MAJ, Steinmann ZJN, Elshout PMF, Stam G, Verones F, Viera M, et al. ReCiPe2016: A harmonised life cycle impact assessment method at midpoint and endpoint level. International Journal of Life Cycle Assessment 2017;22:138-47.

INRAE-CIRAD-AFZ. INRAE-CIRAD-AFZ feed tables: Table data (as fed) [Internet]. 2021 [cited 2024 Apr 20]. Available from: https://www.feedtables.com/content/table-as-fed.

International Atomic Energy Agency (IAEA). Guidelines for Sustainable Manure Management in Asian Livestock Production Systems. Vienna: IAEA; 2008.

Intergovernmental Panel on Climate Change (IPCC). 2006 IPCC Guidelines for National Greenhouse Gas Inventories. Kanagawa: IGES; 2006.

International Organization for Standardization (ISO). ISO 14040: Environmental Management-Life Cycle Assessment-Principles and Framework. Geneva: ISO; 2006a.

International Organization for Standardization (ISO). ISO 14044: Environmental Management-Life Cycle Assessment-Requirements and Guidelines. Geneva: ISO; 2006b.

Liu X, Cai Z, Yuan Z. Environmental burdens of small-scale intensive pig production in China. Science of the Total Environment 2021;770:Article No. 144720.

Long WT, Wang HL, Hou Y, Chadwick D, Ma YF, Cui ZL, et al. Mitigation of multiple environmental footprints for China's pig production using different land use strategies. Environmental Science and Technology 2021;55(8):4440-51.

McAuliffe GA, Chapman DV, Sage CL. A thematic review of life cycle assessment (LCA) applied to pig production. Environmental Impact Assessment Review 2016;56:12-22.

Ministry of Commerce (of Thailand). Prices of agricultural products [Internet]. 2024 [cited 2024 Feb 2]. Available from: https://data.moc.go.th/OpenData/GISProductPrice (in Thai).

Ndue K, Pál G. Life cycle assessment perspective for sectoral adaptation to climate change: Environmental impact assessment of pig production. Land 2022;11(6):Article No. 827.

Nguyen TL, Hermansen JE, Mogensen LI. Environmental Assessment of Danish Pork [dissertation]. Aarhus, Aarhus University; 2011.

Office of Agricultural Economics. Situation of important agricultural products and trends in 2024 [Internet]. 2023 [cited 2024 Jan 5]. Available from: https://www.oae.go.th/assets/portals/1/files/jounal/2566/trend2567.pdf (in Thai).

Öhlund E, Hammer M, Björklund J. Managing conflicting goals in pig farming: Farmers' strategies and perspectives on sustainable pig farming in Sweden. International Journal of Agricultural Sustainability 2017;15(6):693-707.

Ogino A, Osada T, Takada R, Takagi T, Tsujimoto S, Tonoue T, et al. Life cycle assessment of Japanese pig farming using low-protein diet supplemented with amino acids. Soil Science and Plant Nutrition 2013;59:107-18.

Organisation for Economic Co-operation and Development (OECD). Meat consumption (indicator) [Internet]. 2024 [cited 2024 Feb 10]. Available from: https://data.oecd.org/agroutput/meat-consumption.htm.

Ottosen M, Mackenzie SG, Filipe JA, Misiura MM, Kyriazakis I. Changes in the environmental impacts of pig production systems in Great Britain over the last 18 years. Agricultural Systems 2021;189:Article No. 103063.

Oanh NTK, Permadi DA, Hopke PK, Smith KR, Dong NP, Dang AN. Annual emissions of air toxics emitted from crop residue open burning in Southeast Asia over the period of 2010-2015. Atmospheric Environment 2018;187:163-73.

Parrini S, Aquilani C, Pugliese C, Bozzi R, Sirtori F. Soybean replacement by alternative protein sources in pig nutrition and its effect on meat quality. Animals 2023;13(3):Article No. 494.

Pazmiño ML, Ramirez AD. Life cycle assessment as a methodological framework for the evaluation of the environmental sustainability of pig and pork production in Ecuador. Sustainability 2021;13(21):Article No. 11693.

Pollution Control Department. Handbook for Using Waste Treatment Technology and Wastewater from Pig Farms, Focusing on Biogas in the Form of a Combined System. Bangkok: Pollution Control Department (of Thailand); 2017 (in Thai).

Pomar C, Remus A. Precision pig feeding: A breakthrough toward sustainability. Animal Frontiers 2019;9(2):52-9.

Powers SE. Quantifying Cradle-to-Farm Gate Life-Cycle Impacts Associated with Fertilizer used for Corn, Soybean, and Stover Production. United States: US Department of Energy; 2005.

Rahaman MM, Shehab MK. Is the propensity of increasing the rice production a sustainable approach? Experiences from India, Pakistan, and Bangladesh. Journal of Water Resource Engineering and Management 2018;5(2):2-18.

Rajão R, Soares-Filho B, Nunes F, Börner J, Machado L, Assis D, et al. The rotten apples of Brazil. Science 2020;369:246-8.

Reckmann K, Blank R, Traulsen I, Krieter J. Comparative life cycle assessment (LCA) of pork using different protein sources in pig feed. Archives Animal Breeding 2016;59(1):27-36.

Wanasitthachaiwat W, Rojanasathit S. Pig Food Recipes. Volume 16. Bangkok: Department of Livestock Development; 1999 (in Thai).

Wijitkosum S, Sriburi T. Impact of urban expansion on water demand: The case study of Nakhonrachasima City, Lam Ta Kong Watershed. Nakhara: Journal of Environmental Design and Planning 2008;4:69-88.

Williams E, Eikenaar S. Finding your way in multifunctional processes and recycling [Internet]. 2022 [cited 2024 Jan 24]. Available from: https://pre-sustainability.com/articles/finding-your-way-in-allocation-methods-multifunctional-processes-recycling/.

Winkler T, Schopf K, Aschemann R, Winiwarter W. From farm to fork: A life cycle assessment of fresh Austrian pork. Cleaner Production 2016;116:80-9.

Zira S, Rydhmer L, Ivarsson E, Hoffmann R, Röös E. A life cycle sustainability assessment of organic and conventional pork supply chains in Sweden. Sustainable Production and Consumption 2021;28:21-38.

Environment and Natural Resources Journal

Volume 22
Issue 4
2024

Oil and Grease Pollution in the West Coast of Sabah and Water Quality Index for the Conservation of Marine Biota

Phemela Koh Francis[1], Abentin Estim[2*], and Madihah Jafar Sidik[2]

[1]Sabah Marine Department, Kota Kinabalu, Sabah, Malaysia
[2]Borneo Marine Research Institute, Universiti Malaysia Sabah, Malaysia

ARTICLE INFO

Received: 9 Nov 2023
Received in revised: 1 May 2024
Accepted: 20 May 2024
Published online: 24 Jun 2024
DOI: 10.32526/ennrj/22/20230314

Keywords:
Oil and grease/ Marine pollution/ Water quality index/ West Coast Sabah

*** Corresponding author:**
E-mail: bentin@ums.edu.my

ABSTRACT

Oil and grease (O&G) concentrations were determined on the West Coast of Sabah to identify pollution hotspots and to understand the extent of the issue. Triplicate seawater samples were collected at twenty-five stations during the northeast (November 2020 to February 2021) and southwest (July 2021 to September 2021) monsoons. QGIS software was used to create a map model, and water quality indexes were used to provide information on the status of the marine ecosystem and marine biota preservation. O&G concentrations were significantly higher ($p<0.05$) in certain areas of the West Coast of Sabah, ranging from 0.05±0.03 mg/L to 39.34±1.01 mg/L. According to the Malaysian Marine Water Quality Standards, O&G concentrations in the study area were categorized into Class 3, which is directly exposed to the discharge of effluent from anthropogenic activities. Hence, ecosystems in these areas were susceptible to some degree of deterioration. This suggests a potential source of pollution that requires further investigation and remediation efforts. However, the Water Quality Index revealed that the study areas were classified into moderate, acceptable, and medium status, which were still within the acceptable limit for the conservation of marine biota. The findings underscore the need for continued research and proactive measures to minimize O&G pollution and protect ecosystems in the study area. With increased awareness of oil spills, this favorable trend is projected to endure through effective management methods and effective actions to prevent O&G pollution along the West Coast of Sabah. Oil and grease pollution have the potential to endure in the environment for extended periods, ranging from years to even decades, resulting in enduring ecological harm, and hindering the restoration of ecological systems.

1. INTRODUCTION

The West Coast of Sabah is renowned for its abundant biodiversity, encompassing coral reefs, and mangrove forests. These areas serve as crucial reproductive sites, nurseries, and feeding grounds for a wide range of marine animals. However, the region is subject to various environmental impacts that have been documented by various studies and reports (Sabah Parks, 2023; SFD, 2023; BMRI, 2022; SEPD, 2021; SEDIA, 2020; MOAFIS, 2015). These impacts include pollution from industrial activities, such as oil spills and chemical discharges, which can harm marine ecosystems and biodiversity. Overfishing and destructive fishing can reduce fish stocks and harm coral reefs. Furthermore, overfishing is a significant concern in the region, leading to the depletion of fish stocks and disrupting the delicate balance of the marine ecosystem (SFD, 2023). This threatens the livelihoods of local fishing communities and undermines the sustainability of the fisheries sector (SEDIA, 2020). The construction of resorts, ports, and other infrastructure has encroached upon sensitive marine ecosystems, such as coral reefs and mangroves, leading to their degradation and

Citation: Francis PK, Estim A, Sidik MJ. Oil and grease pollution in the West Coast of Sabah and water quality index for the conservation of Marine Biota. Environ. Nat. Resour. J. 2024;22(4):321-334. (https://doi.org/10.32526/ennrj/22/20230314)

destruction (SEPD, 2021). Coastal development and deforestation also contribute to sedimentation and runoff, leading to water pollution and habitat degradation. The discharge of untreated wastewater from coastal communities and industries has contributed to water pollution in the West Coast of Sabah waters (MOAFIS, 2015). This pollution, combined with oil spills from shipping and offshore activities, has had severe impacts on water quality, marine life, and the overall health of the ecosystem (Sabah Parks, 2023). Fossil fuel combustion is a significant contributor to CO_2 emissions, which in turn exacerbate global warming and its consequences, including rising sea levels, extreme weather occurrences, and ocean acidification (Perera, 2017).

O&G pollution can cause severe damage to these sensitive ecosystems, leading to the loss of biodiversity, degradation of habitats, and disruption of ecological balance. O&G is a significant marine pollutant that can potentially harm marine ecosystems due to its poor solubility and slow microbial breakdown (Bao et al., 2013). Oil spills from ships, illegal waste oil disposal, leaks from offshore oil and gas installations, and other factors can all contribute to this kind of pollution. The presence of O&G in the marine environment can have detrimental effects on the ecosystem, including the destruction of habitats, harm to marine life, and negative impacts on local communities that rely on coastal resources for their livelihoods. When it comes to marine biota, O&G pollution can have detrimental effects. These substances can coat the surfaces of marine organisms, impairing their ability to breathe, feed, and reproduce. When exposed to O&G, aquatic life suffers from decreased development, respiration rates, reproduction impairment, enlarged livers, detrimental effects on fish eggs, and larval survival (McNeill et al., 2012; Pilote et al., 2018). Moreover, O&G can contaminate the food chain, leading to the bioaccumulation and biomagnification of toxic substances in marine organisms. O&G pollution, which enters the food chain, may have a negative impact on human health and marine ecosystems, including mangroves and coastal wetland areas (Fahd et al., 2021). The primary source of contamination on beaches has been identified as sewage originating from the oil and gas industry (Schulz et al., 1994).

There are oil spillage cases reported around the West Coast of Sabah, especially offshore activity spillage (SECD, 2000). Oil discharges resulting from land-based activities have a negative impact on marine ecology, including coastal wetlands and mangroves. Additionally, the entry of these pollutants into the food chain poses a significant risk to human health (Fadzil et al., 2017). The researchers have documented the existence of aliphatic and polycyclic aromatic hydrocarbons in the sediment samples and have linked the occurrence of these substances to many sources, including port operations, shipping activities, accidental spills, and automobile emissions (Abdullah, 1995; Ching, 1996; Waheed et al., 2007; Annammala et al., 2013; Fadzil et al., 2017; Urzola et al., 2019).

Since 1976, the Department of Environment of Malaysia has conducted a monitoring program on marine water quality status (DOE, 2013; DOE, 2021). The Malaysian Marine Water Quality Criteria and Standard (MMWQS) is a tool used as a benchmark for water quality status in Malaysian marine waters. The Malaysian Department of Environment has been keeping an eye on O&G since 1976, one of the parameters in the MMWQS. MMWQS is divided into four classifications (Table 1). Besides, the Malaysian Marine Water Quality Index (MMWQI) is a quantitative and evaluative instrument used to determine the overall condition of water by considering a range of parameters, including physical, chemical, and biological attributes (DOE, 2013), and the O&G parameter is one of the seven total parameters included in the index. It produces a numerical value that measures the overall health of the water body and its appropriateness for supporting marine life (Table 2).

Table 1. Malaysia Marine Water Quality Standards (MMWQS) for the O&G concentration

Parameter (2012)	Class 1	Class 2	Class 3	Class E
O&G (mg/L)	0.01	0.14	5.00	0.14
Parameter (2019)	Class 1	Class 2	Class 3	Class E
O&G (mg/L)	0.01	0.14	5.00	1.00

Source: DOE (2021)

Table 2. Water Quality Indexes

Index	Acronym	Developed by	Equation	Classification	
Malaysian Water Quality Index proposed by DOE to reflect the marine water quality status and its category.	MWQI	Department of Environment (DOE), Malaysia	Equation 1	Excellent Good Moderate Poor	90-100 80-<90 50-<80 0-<50
Water Quality Index of Marine and Coastal Waters for the preservation of Marine biota	$ICAM_{PFF}$	The Marine and Coastal Research Institute José Benito Vives de Andréis (INVEMAR)	Equation 2	Optimum Adequate Acceptable Inadequate Poor	97-100 92-96 70-91 35-69 1-34
Water Quality Index developed in coastal area of Ha-Long Bay, Vietnam	WQI_{HL}	Loan, Nguyên, N.T., Hçi, N.	Equation 3	Excellent Good Medium Bad Very bad	97-100 92-96 70-91 35-69 1-34
Water Quality Index proposed by the Canadian Council of Ministers of the Environment	WQI CCME	Canadian Council of Ministers of the Environment	Equation 4	Excellent Good Acceptable Marginal Poor	95-100 80-94 65-79 45-64 0-44

The Water Quality Index (WQI) for marine biota considers specific parameters that are relevant to the health and well-being of marine life. These parameters may include dissolved oxygen levels, pH, temperature, turbidity, nutrient levels, and the presence of pollutants such as O&G. The WQI has been used for decades to simplify surface water physical, chemical, and microbiological properties into a single numerical number. This helps policymakers, scientists, engineers, non-scientists, and the public develop effective aquatic ecosystem and human well-being protection strategies. This article employs a water quality index to detect O&G pollution hotspots and causes in West Coast Sabah marine waters to conserve marine biota. This paper provides information about O&G concentration along the West Coast of Sabah and can be a guideline for local governments to manage marine ecosystems' sustainability by incorporating marine oil pollution concerns into policies related to the livelihoods of indigenous coastal fisheries and aquaculture communities, especially in combating oil spill pollution in the Sabah context.

By monitoring and assessing the WQI for marine biota, scientists and environmental agencies can identify areas of concern, implement appropriate measures to mitigate pollution, and protect the health and biodiversity of marine ecosystems. This helps to ensure the sustainable use of marine resources, the preservation of marine habitats for future generations, and their suitability for supporting marine life. Efforts are made to prevent and mitigate O&G pollution through strict regulations, monitoring, and response mechanisms to minimize the environmental and socio-economic impacts. O&G pollution on the West Coast of Sabah is a significant environmental concern that poses risks to the marine ecosystem and local communities. This region is home to diverse marine life and supports various economic activities such as fishing, tourism, and aquaculture. Efforts are being made to address these issues through conservation initiatives, stricter regulations, and community engagement to promote sustainable practices and protect the marine environment in the West Coast of Sabah waters. These environmental impacts highlight the urgent need for effective management strategies and sustainable practices in the West Coast of Sabah waters to mitigate further damage and ensure the long-term health and resilience of the marine environment (SBC, 2021).

2. METHODOLOGY

2.1 Sampling sites and water analysis

Sampling was taken along the coastal and river mouths of the West Coast of Sabah, Malaysia, which consists of 25 stations as shown in Table 3. Five significant locations were selected in consideration of the activities occurring on land, shore, and offshore (Figure 1). Sampling was conducted during the northeast (November 2020 to February 2021) and southwest (July 2021 to September 2021) monsoons, and triplicate seawater samples were collected using water sampler and kept in a 500 mL polyethylene bottle with caps. The concentration of O&G was

measured following the standard partition gravimetric method (5520B). All samples were preserved by refrigerating at 4°C, extracted within seven days, and analysed as soon as possible. The Partition-Gravimetric method involves the extraction of dissolved or emulsified O&G from water through close contact with a mixture of trichloro-trifluoroethane and petroleum ether in a ratio of 40/60. Take approximately 500 mL of sample and mark the level in the bottle for later determination of sample volume. Acidity to pH2 or lower; often, 5 mL of HCl is sufficient. Transfer to a separate funnel. Carefully rinse the sample container with 30 mL of trichlorotrifluoroethane before solvent washing the separating funnel. Shake vigorously for two minutes. However, if stable emulsion is suspected, gently shake for 5-10 min. Allow the layer to separate, then drain it through a funnel containing solvent-moisturized filter paper into a clean, evacuated distillation flask. If a clear solvent layer cannot be formed, add 1 g Na_2SO_4, as needed. Extract twice more with 30 mL of solvent each time, but first rinse the sample container with solvent. Combine the extracts in an evacuated distilling flask and mash the filter paper with an additional 10 mL to 20 mL solvent. Use a water bath set to 70°C to distil the solvent from the distilling jar. As soon as the solvent has drained, put the flask on a water bath set to 70°C for 15 min and use a hoover to pull air through it for 1 min. It is possible to see water in the residue. To get rid of it, add 2 mL of acetone and let it evaporate on a water bath. Do this again and again until there is no more water visible. Let it cool for 30 min in a desiccator and then weigh it. The amount of O&G in the sample can be calculated as, O&G (mg/L) = (A-B) 1,000/volume of the sample, where A is the mass of the evacuated flask and residue (g), B is the mass of the evacuated flask (g), and the amount of O&G in the given water sample is in mg/L.

Table 3. Coordinate and selected area of the 25 sampling stations in the five chosen locations (A, B, C, D, and E) of the West Coast of Sabah

Location	Station	Area	Coordinate	
			Latitude	Longitude
A	S1	Pulau Tiga, Kuala Penyu	5°43’14.8”	115°39’00.6”
	S2	Menumbok Jetty	5°18’09.9”	115°22’28.2”
	S3	Sipitang (Tg Pagar Fisherman Jetty)	5°04’09.4”	115°32’38.7”
	S4	Sipitang (Merintaman Beach)	5°04’04.4”	115°31’59.3”
	S5	Sipitang (Mengalong River Mouth)	5°00’49.3”	115°28’00.3”
B	S6	Pimping Beach, Membakut	5°31’48.6”	115°41’22.9”
	S7	Kimanis River Mouth	5°37’08.3”	115°53’20.0”
	S8	Benoni River	5°38’56.2”	115°53’46.7”
	S9	Manis Beach, Papar	5°44’05.2”	115°53’46.4”
	S10	Diniwan Island	5°50’38.9”	115°59’30.9”
C	S11	Sepanggar Port	6°05’29.3”	116°07’37.8”
	S12	Putatan Shore	5°52’43.3”	116°02’60.0”
	S13	Gaya and Manukan Island (Coastal water)	5°59’32.5”	116°00’41.8”
	S14	Gaya and Sepanggar Island (Coastal water)	6°02’52.6”	116°03’39.0”
	S15	Likas Bay	6°00’28.8”	116°06’35.4”
D	S16	Dalit Beach (Mengkabong River Mouth)	6°08’34.2”	116°08’14.1”
	S17	Sabandar Beach, Tuaran	6°12’02.0”	116°10’34.4”
	S18	Tuaran River Mouth	6°14’09.6”	116°11’55.5”
	S19	Usukan Island	6°23’26.6”	116°20’03.6”
	S20	Manis Beach, Kg Sarang	6°35’03.2”	116°32’18.6”
E	S21	Teringai Beach, KM	6°43’16.1”	116°38’39.2”
	S22	Sikuati Beach (River Mouth)	6°53’17.0”	116°40’54.3”
	S23	Tip of Borneo	7°02’12.4”	116°44’27.9”
	S24	Bangi Island	7°06’31.7”	117°05’06.6”
	S25	Kudat Port	6°52’44.6”	116°50’44.3”

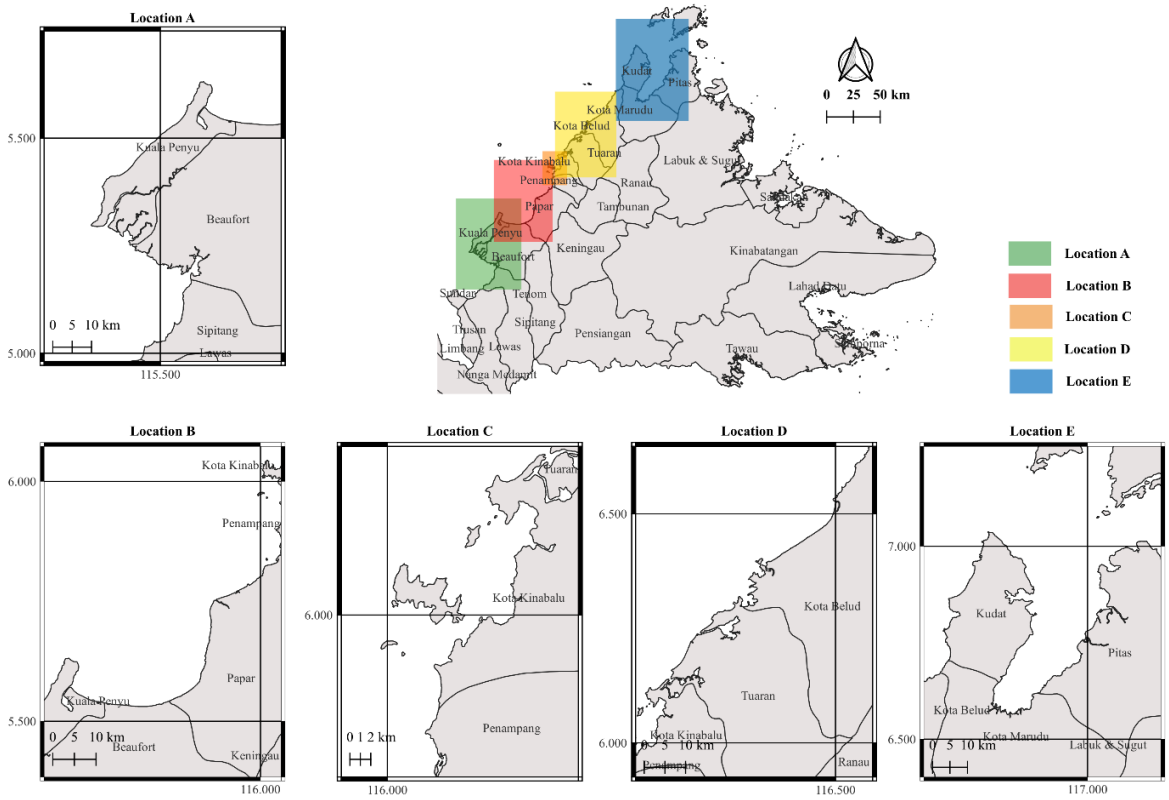

Figure 1. Five chosen locations (A, B, C, D, and E), at the West Coast of Sabah with each of the locations has five sampling stations

2.2 Marine Water Quality Standard and Water Quality Index

The Malaysian Marine Water Quality Standards (MMWQS) are environmental standards that focus on protecting and preserving the marine ecosystem, recognizing how important the ecosystem is to society, and doing so in a way that is cost-effective, useful, and socially appropriate. There are five classes classified in MMWQS (DOE, 2021). The use of the Marine Water Quality Standards (MMWQS) is predicated upon the established categorization of marine water based on its intended purpose within the ecosystem. Since 1985, the Department of Environment (DOE) has been engaged in the ongoing monitoring of marine water quality in Sabah. In addition, the Malaysian Marine Water Quality Index (MMWQI) serves as a comprehensive amalgamation of key marine water quality characteristics, with the objective of offering useful information on the status of marine water quality in a given water body. The index, denoted as Equation 1, is formulated by considering six distinct characteristics related to water quality (DOE, 2021). The MMWQI aggregate is measured on a scale ranging from 0 to 100, with a value of 0 representing low water quality and a value of 100 representing excellent water quality (Table 3).

$$\mathrm{MMWQI} = \mathrm{qiDO}^{0.18} \times \mathrm{qiFC}^{0.19} \times \mathrm{qiNH}^{0.15} \times \mathrm{qiNO}^{0.16} \times \mathrm{qiPO}^{0.17} \times \mathrm{qiTSS}^{0.15} \quad (1)$$

The water quality indices for O&G concentrations in marine waters were determined by utilizing the sub-index curves of $\mathrm{ICAM_{PFF}}$, as presented in Equation 2. These indexes were employed to assess the preservation of biota. The $\mathrm{ICAM_{PFF}}$ index has been recognized for its ability to determine fatal values and establish a normalized curve for O&G based on acute toxicity studies that have been previously documented in scientific literature. These studies exhibit a stronger correlation with the observed concentrations of O&G in marine environments and their associated toxicity (Urzola et al., 2019). Nguyên et al. (2013) also devised the water quality index ($\mathrm{WQI_{HL}}$) in line with the characteristics of the coastal zone. The authors proceeded to employ this index to evaluate the water quality in Ha Long Bay, Vietnam, as seen in Table 3. The estimation of the water quality index for the $\mathrm{WQI_{HL}}$ (Equation 3) utilizes a set of nine characteristics. These parameters are used to determine the water quality index, which is then classified into five categories ranging from 1 to 100. A value of 1 represents very poor water quality, while a value of 100 signifies exceptional water quality.

$$ICAM_{PFF} = \left[\prod_1^n X_i^{wi}\right]^{\frac{1}{\sum_1^n wi}} \quad (2)$$

$$WQI_{HL} = \left[\prod_1^n q_i^{wi}\right]^{\frac{1}{\sum_1^n wi}} \quad (3)$$

$$WQI\ CCME = 100 - \left(\frac{\sqrt{F_1^2 + F_2^2 + F_3^2}}{1.732}\right) \quad (4)$$

2.3 Modelling using QGIS and statistical analysis

QGIS software version 3.22 was used to create the map modeling for the area. The software functions such as shapefile and inverse distance weighting (IDW) interpolation were used to make the map layout and create the raster layer for concentration of O&G for specific areas based on the data. SPSS software 26.0 was used for the data and statistical analyses. The one-way analysis of variance (ANOVA) was employed to assess the statistical significance ($p<0.05$) of the differences in the O&G concentrations among the five locations of the 25 stations. A post-hoc analysis was performed to ascertain whether there was a statistically significant disparity among the various sites.

3. RESULTS AND DISCUSSION

3.1 O&G concentrations at the West Coast of Sabah

The range of O&G concentrations recorded at the West Coast of Sabah was 0.05±0.03 mg/L to 39.34±1.01 mg/L, respectively, at the S21 of location E and at the S9 of location B, as shown in Figure 2. The concentrations of O&G were significantly different ($p<0.05$) between the five locations, as shown by a one-way ANOVA (Figure 1). Figure 2 shows the highest O&G concentration was recorded at location B (Table 3), specifically at S9 (Manis Beach, Papar), followed by S8 (Sungai Benoni Station), and the lowest at S6 (Pimping Beach, Papar). Location C recorded the second highest O&G concentrations (mean±S.D.) with a range of 0.44±0.13 mg/L to 20.01±2.90 mg/L, followed by location D with a range of 0.38±0.02 mg/L to 17.86±5.97 mg/L, and the lowest was at location E with a range of 0.05±0.03 mg/L to 1.54±0.73 mg/L (Figure 2). Overall, Figure 3 shows interpolation O&G concentrations using QGIS at the coastal waters of the West Coast of Sabah.

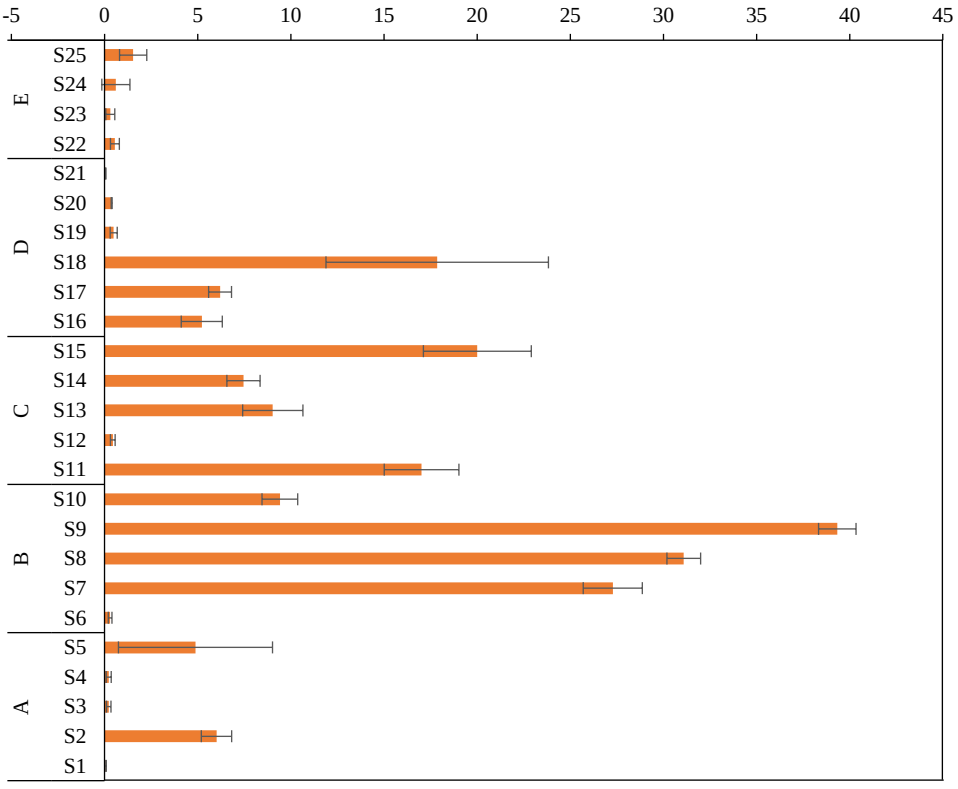

Figure 2. Means (±S.D.) concentrations of O&G at the 25 Stations of the West Coast of Sabah

Due to rapid activities and exploration from land, onshore, and offshore, there were high O&G concentrations at location B (Figure 1). The area of Manis Beach (S21) recorded 39.34±1.01 mg/L mean O&G concentration, which means it is critical erosion with immediate danger of damage or loss of values. The causes of the erosion are reclamation, dredging a navigational channel under construction, and a pipeline on the seabed that was observed at the location of Sabah Oil and Gas Terminal (SOGT) and

was the main activity of the operational underwater pipeline transferring crude oil and gas to SOGT from the offshore platform. The increased shipping activities along the coastal water might be one of the main factors leading to higher O&G concentrations in location B (Figure 4). The boom of industrial activities within Kimanis Bay, such as palm oil estates and factory fabrication yards, power plants, timber processing factories, concrete plants, and the Sabah Agro-Industrial Precinct (SAIP) located along the Benoni River, and runoff oil spillage, are visible along the Benoni River (Figure 4).

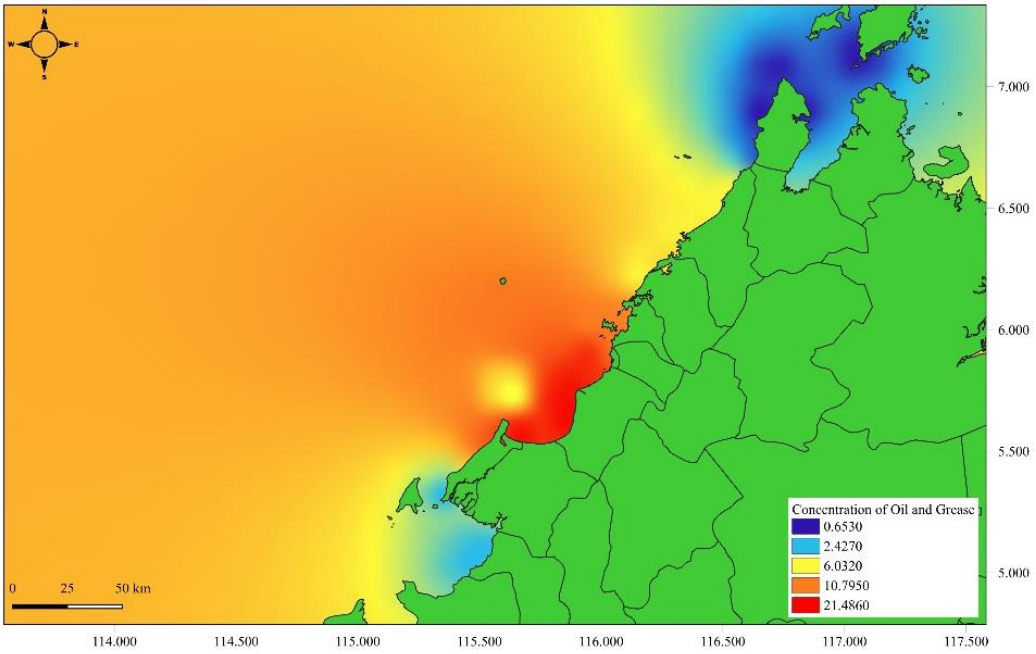

Figure 3. Distribution of O&G concentrations at the West Coast of Sabah

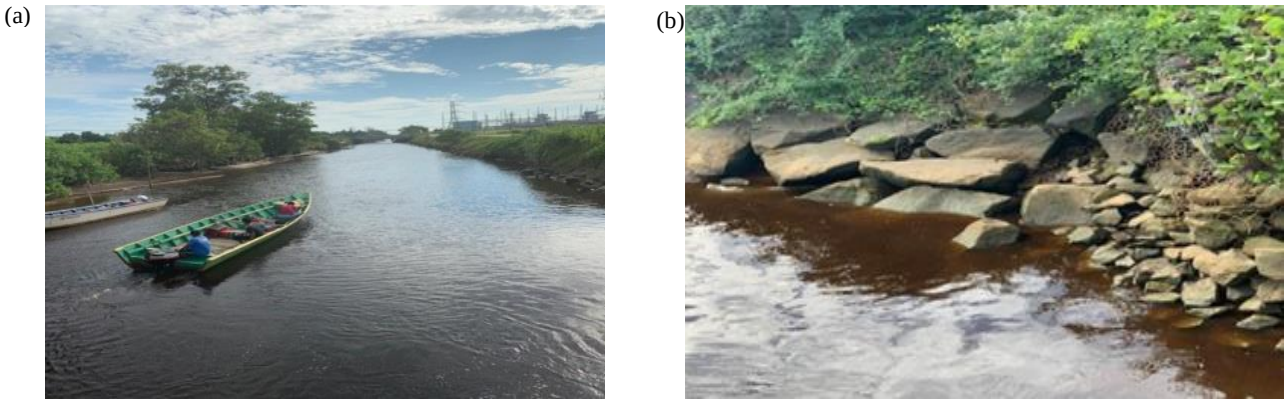

Figure 4. Trace of polluted water (a) and at the SOGT (b) of Sungai Benoni, Papar

3.2 Comparison of O&G concentrations with other studies

Table 4 shows the comparison of O&G concentrations between the present study and other research. It shows the O&G range concentrations were various. The O&G concentrations in the current study were marginally lower than those in the study by Annammala et al. (2013), which were 23.30 mg/L to 76.80 mg/L at the Manukan, Mamutik, and Sapi Islands of Sabah. They also reported that in the waters of Kota Kinabalu Port, the O&G concentration was 8.53 mg/L to 40.6 mg/L. However, the O&G concentrations in the present study were slightly higher compared to Fadzil et al. (2017) at the Kukup Island and Tanjung Piai coastal and estuary areas and Waheed et al. (2007) at the coastal and open sea of Brunei Bay (Table 4).

DOE (2013) reported that in the Malaysian waters of the Straits of Malacca coastal areas, the range of O&G concentrations was 1.45 mg/L (in Selangor waters) to 8.80 mg/L (in Penang waters), while Abdullah (1995) stated that the O&G concentrations in the Straits of Malacca coastal areas ranged from 0.40 mg/L (in Penang waters) to 3.50 mg/L (in Johor waters), as shown in Table 4. Abdullah (1995) also reported that in the South China Sea, the concentrations of O&G ranged from 0.30 mg/L to 2.40 mg/L. Those reported O&G concentrations were slightly lower compared to this study, which ranged from 0.05±0.03 mg/L (in location E) to 39.34±1.01 mg/L (in location B).

Table 4. Comparison of O&G concentrations in this study and other references

Location	Mean concentration (range) (mg/L)	References
Sipitang, Menumbok and Kuala Penyu (Location A)	Location A: 2.265 (0.055-6.011)	Present study
Membakut and Papar (Location B)	Location B: 21.486 (0.300-39.337)	
Kota Kinabalu (Location C)	Location C: 10.794 (0.443-20.014)	
Tuaran and Kota Belud (Location D)	Location D: 6.099 (0.383-17.860)	
Kota Marudu and Kudat (Location E)	Location E: 0.809 (0.330-2.537)	
Labuan (Manukan, Memutik and Sapi Islands)	43.3 (23.3-76.8)	Annammala et al. (2013)
Kota Kinabalu Port	24.6 (8.53-40.60)	Annammala et al. (2013)
Kukup Island	Kukup Island: 0.44 (0.09-1.50)	Fadzil et al. (2017)
Tg. Piai Coastal	Tg Piai: 0.28 (0.13-0.45)	
Sg Pulai Estuaries	Sg Pulai, Sg Pendas, and Sg Redan: 0.34 (0.06-0.90)	
Straits of Malacca Coastal Areas	Kedah: 2.79 (2.00-3.63)	DOE (2013)
	Melaka: 5.17 (5.00-7.00)	
	P.Pinang: 4.38 (2.40-8.80)	
	Selangor: 2.81 (1.45-5.60)	
Brunei Bay Costal and Open Aea	0.63 (0.20-1.00)	Waheed et al. (2007)
Straits of Malacca	Perak: 0.51 (0.10-0.90)	Abdullah (1995)
	Selangor: 0.53 (0.30-1.00)	
	N.Sembilan: 0.42 (0.10-0.60)	
	Johor: 1.07 (0.30-3.50)	
	Perlis: 0.75 (0.60-0.90)	
	Melaka: 0.58 (0.50-0.60)	
	P.Pinang: 0.86 (0.40-1.40)	
South China Sea	Sarawak: 0.68 (0.10-1.50)	Abdullah (1995)
	Pahang: 1.70 (0.80-2.40)	
	Terengganu: 0.97 (0.40-1.90)	
	Kelantan: 0.77 (0.30-1.30)	
	Sabah: 0.45 (0.40-0.60)	

3.3 Marine Water Quality Standards and Water Quality Index

Based on the classification by the MMWQS, the concentrations of O&G along the West Coast of Sabah were categorized into class 3 (Table 1). Class 3 is the established benchmark for marine water that is subject to direct effluent discharge resulting from human activities. Therefore, ecosystems in various regions are susceptible to varying degrees of deterioration. Thus, the equivalent degree of protection is intended to preserve the remaining ecosystem's health and enhance the quality of water in the impacted region.

Table 5 shows the marine water quality status for the West Coast of Sabah according to the four indexes. It shows that the five locations of the West Coast of Sabah in the present study were in moderate status according to the MWQI, except for one station, respectively at location C and location D, and two stations at location E, which were in good status (Table 5). Besides, other indexes also showed that the five locations were in the acceptable ($ICAM_{PFF}$ and WQI_{HL}) and Medium (WQI CCME) statuses. The results proved that, according to the indexes, the five locations on the West Coast of Sabah were still in acceptable concentrations for the preservation of marine biota, according to the $ICAM_{PFF}$ (Table 5). Acceptable status requires the study area to monitor, bioassay, control, and manage the water body, evaluate physicochemical and toxic parameters, and develop a quarterly contingency plan to improve water quality and ensure discharge prevention measures help the ecosystem studied.

Table 5. Marine Water Quality Status for the West Coast of Sabah, according to the indexes

Area	Station	MWQI			$ICAM_{PFF}$	WQI_{HL}	WQI CCME
		2020	2021	This study			
Location A	1	Moderate	Moderate	Moderate	Acceptable	Medium	Acceptable
	2	Moderate	Moderate	Moderate	Acceptable	Medium	Acceptable
	3	Moderate	Moderate	Moderate	Acceptable	Medium	Acceptable
Location B	1	Moderate	Moderate	Moderate	Acceptable	Medium	Acceptable
	2	Moderate	Moderate	Moderate	Acceptable	Medium	Acceptable
	3	Moderate	Moderate	Moderate	Acceptable	Medium	Acceptable
Location C	1	Moderate	Moderate	Moderate	Acceptable	Medium	Acceptable
	2	Moderate	Moderate	Good	Acceptable	Medium	Acceptable
	3	Moderate	Moderate	Moderate	Acceptable	Medium	Acceptable
Location D	1	Moderate	Moderate	Good	Acceptable	Medium	Good
	2	Moderate	Moderate	Moderate	Acceptable	Medium	Acceptable
	3	Moderate	Moderate	Good	Acceptable	Medium	Good
Location E	1	Moderate	Moderate	Good	Acceptable	Medium	Acceptable
	2	-	-	Good	Acceptable	Medium	Good

4. DISCUSSION

O&G pollution on the West Coast of Sabah is a significant environmental concern that poses risks to the marine ecosystem and local communities. This region is home to diverse marine life and supports various economic activities such as fishing, tourism, agriculture, and aquaculture (BMRI, 2022; SBC, 2021; SEDIA, 2020; SEPD, 2021; SFD, 2023). The primary sources of O&G pollution in this area include oil spills from shipping activities, illegal waste oil dumping, gas facilities, and leakage from offshore oil. These incidents can result in the release of large quantities of O&G into the marine environment, leading to immediate and long-term impacts. Based on the observations, all the activities from land, onshore, and offshore could contribute to the O&G pollution in the area and harm the marine environment, but if they were controlled and managed well, the marine pollution could be avoided and the impact would be minimized. The amount of O&G in water can have a substantial impact on water quality, and it can be a critical criterion in establishing a body of water's Water Quality Index (WQI). The link between O&G and WQI is mostly due to the environmental and health hazards connected with these pollutants. According to Samsudin and Azid (2018), the use of WQI is a straightforward procedure that offers an appropriate assessment of water quality.

The lowest O&G concentration was recorded in the coastal waters of location E, as shown in Figures 2 and 3, due to the nature of location E's shallow coastal water, which makes it difficult to operate shipping activities. O&G concentrations were still within the MWQS range, and the water quality was in a "good" MWQI status, which means that the water is safe to use and is just slightly degraded from its ideal state. The marine operations in the area are mostly based on passenger ships, fishing, and recreational activities. Similar to the Teringai Beach in Kota Marudu (Table 3), the O&G concentration was still in the range of MWQS because the station is in a remote area, the condition of the gravel road is poor, and the location is not strategic, being quite far from the main road compared to the beaches in the coastal waters of Kudat. However, in the Bangi Island waters (Table 3), the O&G concentration was slightly higher because of tourism activity involving passenger ships, fishing activities, exploration of O&G operations, and residential areas.

The highest concentration of O&G in location B is due to the rapid and active activities from land, onshore, and offshore within the coastal water. The higher and faster the activity, the greater the risk of pollution. The concentration of O&G at location B is classified as class 3 according to the MWQS. This classification indicates that the discharge of effluent from human activities has had a direct impact on the area. Therefore, the ecosystems in these regions are prone to varying degrees of deterioration (DOE, 2021). Location B is also known as an active offshore activity. The location of the platform is approximately 100 to 500 km in Sabah Economic Exclusive Zone (EEZ) water, and the risk of marine pollution in this location is higher compared to the other locations. The

highest cases of marine pollution from offshore, according to Department of Environment Sabah reports, demonstrate this. SOGT underwater pipelines connect to platforms from Sabah, Labuan, and Sarawak, which transport crude oil and gas. According to Schulz et al. (1994), offshore activities involving dredging, pipe-laying, and the establishment of support facilities result in the release of diverse contaminants into the maritime environment, therefore influencing its overall quality. According to DID (2012), the amount of oil and gas in location B is in category 1, which means that there is a high risk of damage or loss of value right away. This is because of the erosion and reclamation, construction of navigational channels, and pipelines on the seabed, especially close to the Sabah Oil and Gas Terminal (SOGT), Kimanis. Coastal erosion and siltation are two of the sources of marine pollution (Sarma, 2015). The exacerbation of siltation and coastal erosion has been attributed to the growth and modernization of ports, which involves the deepening of harbor channels (Sarma, 2015). Operative underwater pipelines transferring crude oil and gas to SOGT from the offshore platform made the shipping activities along Papar coastal water and might be one of the main factors that lead to marine pollution, as shown in the Nautical Chart of Malaysia version 2020. Underwater pipelines, which transport crude oil and natural gas, can have a variety of environmental implications both during construction and operation. The degree of these effects might vary based on factors such as the pipeline's location, the procedures used, and the efficiency of environmental control measures. Underwater pipelines, which transport crude oil and natural gas, can have a variety of environmental implications both during construction and operation.

There are a lot of industrial activities, including palm oil estates and factory fabrication yards, power plants, factories that process wood, concrete plants, and the Sabah Agro Industrial Precinct (SAIP) along the Benoni River. In 2015, there was a runoff oil spillage that caused a high reading of oil and gas and can still be seen in its tracks along the river (Figure 4).

The second highest concentration of O&G was recorded at location C (Figures 2 and 3). Land use activities are active in Kota Kinabalu (Table 3), especially coastal development, port activities, urbanization, tourism, and industrial activities. This can be seen along Likas Bay, which has the highest trace of O&G. Urbanization, commercial, tourism, residential, and industrial activities are leading to local development, which contributes to marine pollution in the environment (Vanderzwaag and Power, 2008). Sepangar Port became the hub for Sabah water, mostly container, oil tanker, chemical tanker, bulk container, and general cargo. Statistics are shown in Figure 5 from the Shipping Statistics and Notices from 2010-2019 of the Marine Department, Sabah. Kota Kinabalu coastal water is very active with the onshore activities from Kota Kinabalu Port, such as shipping operations involving de-ballasting, oil tank and cargo cleaning, fishing activities, and the maintenance of pipe lay barges on shore seabed water, which might cause a high density of traffic onshore. In the Straits of Malacca, one of Malaysia's busiest ports, industrial discharges are highlighted as the key contributions of O&G (Abdullah, 1995), and the situation is quite similar. Types of cargo and vessel operation are the main factors in identifying the potential for high risk in marine operations, and a high density of shipping traffic activities might cause marine pollution (Roy et al., 2006). Between 1990 and 2015, tanker cargo, oil tankers, and cargo vessels caused the greatest oil leak accidents, with crude oil, marine diesel, drilling fluids, and oily water accounting for over 80% (Maggi et al., 2014).

Tourism, fishing activities, and residence areas in Pulau Gaya, Pulau Manukan, and Pulau Sepanggar (Table 3) contribute to marine pollution from traffic from boats and ships. Illegal dumplings of oil were found at Pulau Sepanggar twice in 2017 and 2019, as stated in the DOE yearly reports, since the high traffic shipping onshore makes it difficult to trace who is accountable for the oil pollution. The high trace of O&G within coastal water between Pulau Gaya, Pulau Manukan, and Pulau Sepanggar proved that activities from land and onshore led to marine pollution (Annammala, 2013). Low concentration of O&G on the Putatan shore because of less activity onshore and offshore, based on the study observation.

The third highest O&G concentration was recorded at location D (Figures 2 and 3). From the observation, there are also many land use activities in the area, such as tourism, recreational, resorts, hotels, and jetties, which lead to marine pollution (Ching, 1996). Along the coastal water of Tuaran, there are resorts and hotels such as Karambunai hotel and villas, Rasa Ria Tuaran resort, and Mimpian Jadi resort. The area around the Mengkabong River Mouth, for example, is also a highly active area, with a few construction projects nearby and also villages (Figure 6), which may have impacted the coastal area and

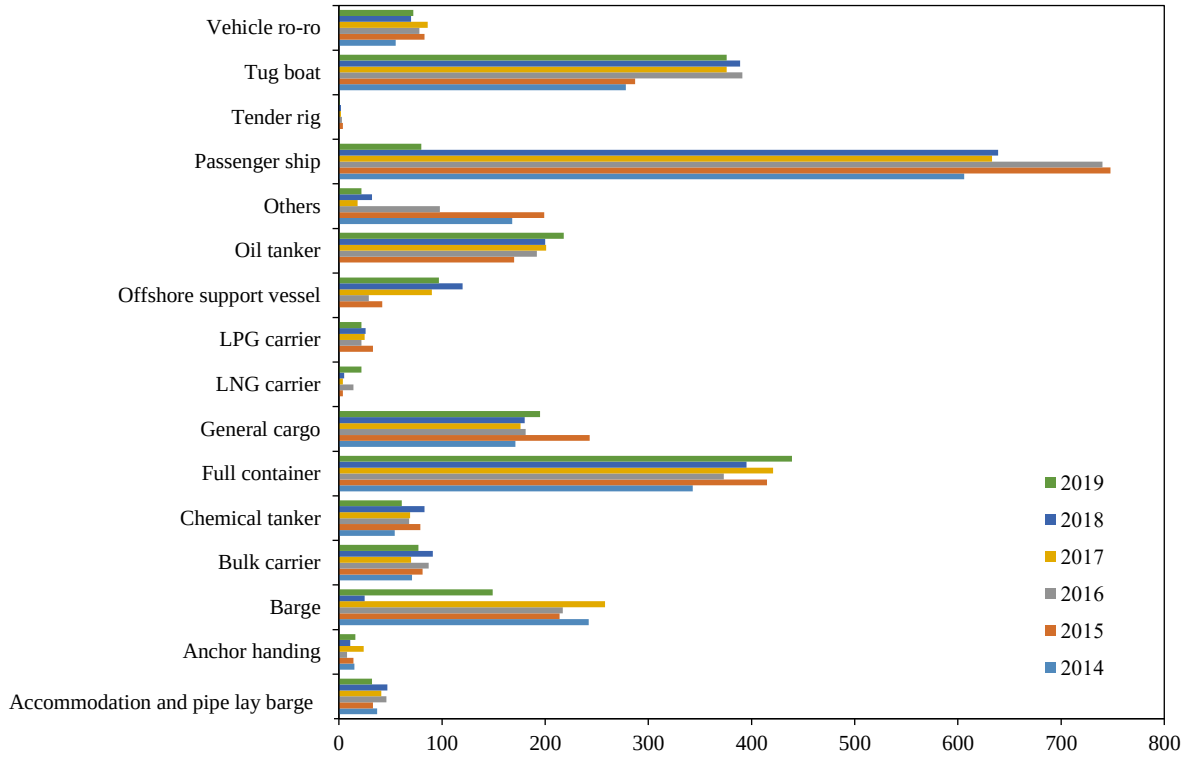

Figure 5. Data shown statistics of shipping activities in Kota Kinabalu, Sabah from year 2010-2019 (Source: Marine Department, Shipping statistics and notices, 2010-2019, Kota Kinabalu, Sabah)

(a)

(b)

(c)

Figure 6. Construction of Alia Hotel, nearby the Sungai Mengkabong River Mouth, Tuaran (a) and Manis Beach, Kampung Sarang, Kota Belud (b), Teringai Beach, Kota Marudu view from Teringai Hill halfway from the main road (c)

caused O&G pollution. The Tuaran River was detected to be polluted by O&G pollution, which may be due to the industrial and aquaculture activities nearby the area and also tourism operations, which may have contributed to the marine pollution in the area. Schulz et al. (1994), have identified sewage O&G as a significant constituent of substances contributing to beach contamination. Mengkabong River Mouth, Sabandar Beach, and Tuaran River fall under Category 2, which is significant erosion with loss of value over five to 10 years (DID, 2012). Low traffic density onshore in location D because only boats and fishing gear are currently active and because of the shallow water around Tuaran and Kota Belud. Offshore activities are not active on the St. Joseph Platform since most offshore activities are shifted to location B because of the new oil field.

The concentrations of O&G at location A exhibited a range of 0.06±0.04 mg/L to 6.01±0.81 mg/L, positioning it as the fourth highest among the locations (Figures 2 and 3). The highest O&G concentration at location A was recorded at Menumbok Terminal. This may be due to the traffic from passenger ships, roro, and boats from Labuan, Brunei, and Sipitang, as well as the increasing number of ship operators between Menumbok and Labuan. Mengalong River Mouth at Sipitang was traced to a high O&G because nearby the area was located with Sipitang Oil and Sabah Ammonia Urea Terminal (SAMUR) and Sabah Forest Industries (SFI). The Department of Environment Sabah reported a spill of marine fuel oil (MFO) in the SFI terminal in 2015, which may have resulted in a higher concentration of O&G in the Mengalong River Mouth. The location of Brunei Bay as an anchorage area nearby the Sipitang coastal water area may also cause a high concentration of O&G due to the shipping traffic onshore, which became an anchorage area and hub for vessel bunkering activities and ship-to-ship activities involving oil transfer (Bao et al., 2013). Due to the fact that Sabah Parks manages and maintains Pulau Tiga and has designated it as a protected marine park, there is a low concentration of O&G nearby (Sabah Parks, 2023).

One of the immediate consequences of O&G pollution is the coating of marine organisms' surfaces, such as fish, corals, and seabirds. This coating can disrupt their natural functions, including respiration, feeding, and reproduction. The toxic components present in O&G can also cause physiological and biochemical changes in marine organisms, leading to reduced growth rates, impaired immune systems, and increased mortality. Furthermore, O&G pollution can have cascading effects on the entire marine food chain. Plankton and other small organisms are capable of absorbing O&G particles, which larger organisms then consume. This process, known as bioaccumulation, can lead to the concentration of toxic substances at higher trophic levels, including commercially important fish species. Consuming contaminated seafood can pose risks to human health as well.

Numerous actions are now being taken along the West Coast of Sabah in order to reduce the amount of pollution caused by O&G. These include the construction of reaction procedures to deal with any accidents as quickly as possible, frequent monitoring of water quality, and stringent rules and enforcement to avoid unlawful dumping and oil spills. Additionally, public awareness campaigns and education programs are conducted to promote responsible environmental practices among industries, communities, and individuals. Efforts are also made to enhance emergency preparedness and response capabilities to minimize the impacts of O&G pollution. This involves training personnel, developing contingency plans, and deploying appropriate equipment and technologies for containment, recovery, and cleanup operations. Through the efficient management and mitigation of O&G pollution along the West Coast of Sabah, it is plausible to safeguard the marine ecosystem, conserve biodiversity, and promote the sustainable use of coastal resources to cater to the needs of both current and future generations.

Oil pollution can result in the deterioration of habitats, contamination of water sources, and damage to marine creatures due to ingestion or entanglement. Polluted waters can have adverse effects on fishing enterprises, tourism, and public health by contaminating seafood and making recreational water activities unsafe for humans. This phenomenon also leads to the degradation of marine habitats, including coral reefs, mangroves, and seagrass beds, resulting in a decline in biodiversity and a decrease in marine ecosystem resilience. These factors can have adverse effects on the reproductive, feeding, and sheltering processes of marine organisms. As a result of habitat degradation, humans can experience adverse effects on coastal protection, fisheries, and tourism businesses that rely on the well-being of ecological systems.

5. CONCLUSION

The study revealed that O&G concentrations were significantly higher in certain areas of the West Coast of Sabah. This suggests a potential source of pollution that requires further investigation and remediation efforts. A map model was created using the QGIS software to show the hotspot and the extent of O&G pollution in the region. According to the MWQS, the concentrations of O&G found along the West Coast of Sabah were categorized as class 3. This classification indicates that the area is subject to the direct discharge of effluent resulting from human activities. Therefore, the ecosystems in these regions are susceptible to varying degrees of deterioration. However, according to the water quality index, the West Coast of Sabah was in moderate status (MWQI) and still within the acceptable limit for the conservation of marine biota ($ICAM_{PFF}$). With the increasing awareness of oil spills, it is expected that this positive tendency will persist through the implementation of efficient management strategies and the use of effective measures to reduce O&G pollution along the West Coast of Sabah. It becomes feasible to safeguard the marine ecology, conserve biodiversity, and promote the sustainable utilization of coastal resources, therefore benefiting both current and future generations.

Undertaking studies regarding O&G pollution is crucial for environmental conservation, human health protection, economic support, and the advancement of sustainable development. Collaborative efforts among researchers, policymakers, and stakeholders can effectively tackle the significant environmental issue of O&G contamination by comprehending its origins, consequences, and approaches to mitigation. Discover cutting-edge remediation technology to tackle O&G contamination in aquatic environments. The process involves examining the origins and routes of O&G pollution in aquatic settings. This process may require locating both point and non-point sources, such as urban runoff or natural seepage. Understanding the processes that control the movement and destiny of O&G in aquatic environments can aid targeted management initiatives. The study's scope and accuracy may be constrained by the limited availability or quality of data pertaining to maritime ecosystems and human activities. Subsequent investigations may prioritise the enhancement of data gathering methodologies, the augmentation of monitoring endeavours, and the facilitation of data sharing initiatives among academics and relevant stakeholders.

ACKNOWLEDGEMENTS

This study was supported by grants from Universiti Malaysia Sabah (GUG 0332) and the Ministry of Higher Education, Malaysia (FRGS/1/2019/STG03/UMS/02/2). The authors would also like to thank Ms. Michelin Collyen Jimmy, Mr. Ismail Tajul, Mr. Jeffry Molius, Ms. Nur Effah Arsin, and Ms. Mezzy Ronin for their technical assistance during O&G lab analysis.

REFERENCES

Abdullah AR. Oil and grease in coastal waters: Relative contribution from various sources and evaluation of discharge sites. In: Abdullah AR, Wang CW, editors. Oil and Grease Pollution in the Malaysia Marine Environment. Malaysia: Department of Environment; 1995. p. 31-83.

Annammala KV, Abdullah MH, Moktar M, Joseph CG, Sakari M. Characterization of aromatic hydrocarbons in tropical coastal water of Sabah, Borneo. Asian Journal Chemistry 2013;25(7): 3773-80.

Bao XG, Wang F, Zheng PJ. Research on intelligent regulation of ship-to-ship crude oil transfer at sea based on internet of things. Advanced Materials Research 2013;860-863:2954-7.

Borneo Marine Research Institute (BMRI). Marine biodiversity in Sabah [internet]. 2022 [cited 20 May 2022]. Available from: https://www.ums.edu.my/ipmbv2/en/.

Ching LL. Tourism, pollution and the marine environment in Malaysia. Proceedings of the 13th Annual Seminar of the Malaysian Society of Marine Sciences; 1996 Oct 26; Petaling Jaya: Malaysia; 1996.

Department of Irrigations and Drainage Sabah (DID). Integrated Shoreline Management Plan for Sabah Report. Malaysia: Department of Irrigations and Drainage of Sabah; 2012.

Department of Environment, Malaysia (DOE). Environmental Quality Report 2013; Year 2013. Selangor: Ministry of Environment and Water; 2013.

Department of Environment, Malaysia (DOE). Environmental Quality Report 2021; Year 2021. Selangor: Ministry of Environment and Water; 2021.

Fadzil MF, Pang SY, Razal AR, Poh SC, Suratman S, Dagang NS, et al. Oil and grease and total petroleum hydrocarbons in the waters of RAMSAR gazette mangrove area, Johor. Journal of Sustainability Science and Management 2017;12(1):30-9.

Fahd F, Yang M, Khan F, Veitch B. A food chain-based ecological risk assessment model for oil spills in the Arctic environment. Marine Pollution Bulletin 2021;166:Article No. 112164.

Maggi P, Morgado CDRV, de Almeida JCN. Offshore oil spill incidents: Creating a database in Brazil. Proceedings of the International Oil Spill Conference; 2014 May 5-8; Savannah International Trade and Convention Center, Georgia: USA; 2014.

McNeill SA, Arens CJ, Hogan NS, Köllner B, van den Heuvel MR. Immunological impacts of oil sands-affected waters on rainbow trout evaluated using an *in-situ* exposure. Ecotoxicology and Environmental Safety 2012;84:254-61.

Ministry of Agriculture and Food Industry of Sabah (MOAFIS). Third Sabah Agricultural Policy 2015-2024 (SAP3). Sabah, Malaysia: Ministry of Agriculture and Food Security; 2015.

Nguyên TTN, Loan DK, Hoi NC. Development of water quality index for coastal zone and application in the Ha Long Bay. VNU Journal of Earth and Environmental Sciences 2013;29(4):43-52.

Perera F. Pollution from fossil-fuel combustion is the leading environmental threat to global pediatric health and equity: Solutions exist. International Journal of Environmental Research and Public Health 2017;15(1):Article No. 16.

Pilote M, André C, Turcotte P, Gagné F, Gagnon C. Metal bioaccumulation and biomarkers of effects in caged mussels exposed in the Athabasca oil sands area. Science of the Total Environment 2018;610-611:377-90.

Roy DL, Volcaert A, Vermoote S, Wachter BD, Maes F, Coene J, et al. Risk Analysis of Marine Activities in the Belgian Part of the North Sea (RAMA) Final Report. Brussels, Belgium: Belgian Science Policy; 2006.

Sabah Biodiversity Centre (SBC). Sabah biodiversity strategy 2012-2022 [internet]. 2021 [cited 12 Oct 2021]. Available from: https://sabc.sabah.gov.my/content/sabah-biodiversity-strategy-2012-2022.

Sabah Economic Development and investment authority (SEDIA). SDC blueprint [internet]. 2020 [cited 15 Jan 2020]. Available from: https://sedia.com.my/news-resources/sdc-blueprint/.

State Environmental Conservation Department (SECD). Handbook for Environmental Impact Assessment (EIA) in Sabah. Sabah, Malaysia: The Environmental Conservation Department; 2000.

Sabah Environment Protection Department (SEPD). Action Plan for Beach Cleaning Due to Oil Spills in Sabah Edition 2021. Sabah, Malaysia: Environment Protection Department of Sabah and Department of Environment; 2021 (in Indonesian).

Sabah Fisheries Department (SFD). Fisheries Management [internet]. 2023 [cited 15 Nov 2023]. Available from: https://fishdept.sabah.gov.my/policies-guidelines/.

Sabah Parks. Marine Parks [internet]. 2023 [cited 20 May 2023]. Available from: https://www.sabahparks.org.my/ resource-centre/publication#.

Samsudin MS, Azid A. Assessment of marine water quality index in mangrove estuarine: Case study in Setiu river estuary. Journal Clean WAS 2018;2(2):16-8.

Sarma K. Siltation and coastal erosion at shoreline harbours. Procedia Engineering 2015;116:12-9.

Schulz TJ, Marczan PJ, Fane AG. Behavior of sewage effluent oil and grease in the ocean. Water Environment Research 1994; 66(6):800-4.

Urzola ME, Sierra NR, Cabarcas LS, Martínez DV, Bolaños ÉQ. Oil and grease as a water quality index parameter for the conservation of marine biota. Water 2019;11(4):Article No. 856

Vanderzwaag DL, Powers A. The protection of the marine environment from land-based pollution and activities: Gauging the tides of global and regional governance. International Journal of Marine and Coastal Law 2008;23:423-52.

Waheed Z, Al-Alzad S, Syed Hussein MA, Aguol KA, Saleh M, Vairappan CS. Biological resources. In: Mustafa S, Saleh E, editors. Coastal Environmental Profile of Brunei Bay Sabah. Sabah, Malaysia: Universiti Malaysia Sabah; 2007. p. 47-94.

Environment and Natural Resources Journal

Volume 22
Issue 4
2024

Role of Correlation among Physical Factors in Probabilistic Simulation of Emissions of Volatile Organic Compounds from Floating Storage and Offloading Vent Stack

Chalee Seekramon, Chalor Jarusutthirak, and Pawee Klongvessa*

Department of Environmental Technology and Management, Faculty of Environment, Kasetsart University, Bangkok 10900, Thailand

ARTICLE INFO

Received: 7 Dec 2023
Received in revised: 16 May 2024
Accepted: 21 May 2024
Published online: 8 Jul 2024
DOI: 10.32526/ennrj/22/20230339

Keywords:
Floating storage and offloading (FSO)/ Multiple linear regression (MLR)/ Probabilistic simulation/ Volatile organic compound (VOC) emission

*** Corresponding author:**
E-mail: ecpwk@ku.ac.th

ABSTRACT

This research investigated the roles of correlations among physical factors in the probabilistic simulation of volatile organic compounds (VOCs) emitted from a marine vessel (known as floating storage and offloading, FSO), located in the Gulf of Thailand. The physical factors in this study were wave height, ambient temperature, storage temperature, storage quantity, Reid vapor pressure, and the daily incoming rate. These physical factors were transformed into normally distributed data and a second-order multiple linear regression (MLR) with interaction effects, that were then used to determine the relationship between the transformed physical factors and the VOC venting volume from the FSO. The dataset of relevant predictors (transformed physical factors and interactions) that provided the maximum adjusted coefficient of determination was chosen for inclusion in the MLR. After that, two datasets of 1,000 venting volumes (one with and one without correlations among physical factors) were simulated. In the simulation, 1,000 datasets of six physical factors were generated according to observed averages and standard deviations. Cholesky randomization was used to generate the correlated physical factors for the simulation with correlation among physical factors. The averages of VOC venting volumes calculated from the generated physical factors when correlations among physical factors were and were not applied were 211,610 and 210,906 ft^3, respectively (observed average was 210,984 ft^3), with standard deviations of 38,828 and 40,787 ft^3, respectively (observed standard deviation was 67,961 ft^3), and skewness values of 0.74 and 0.51, respectively (observed skewness was 0.71). Therefore, correlation among the physical factors improved the skewness and provided better simulation results for VOC emission.

1. INTRODUCTION

Volatile organic compounds (VOCs) contribute to the formation of tropospheric ozone, which causes negative impacts on human health and the environment (Shao et al., 2020). Under normal atmospheric conditions, the VOCs emitted from natural gas liquids (NGLs) comprise 2.63% ethane, 14.60% propane, 14.87% butane, 1.96% pentane, 0.26% hexane, and 0.17% heptane (Seekramon, 2015; Drysdale, 2019). While operating a marine vessel, called floating storage and offloading (FSO), the increase in incoming NGLs into the storage tank raises the internal pressure, leading to VOC evaporation and accumulation in the tanks. The accumulated VOCs are eventually released to the atmosphere via the FSO vent stack to prevent an explosion and deformation of the FSO storage tanks (Seekramon, 2015; Vos et al., 2007). VOCs are key factors in forming ozone and fine particulates in the atmosphere. Human exposure to such pollutants at high concentrations over extended

Citation: Seekramon C, Jarusutthirak C, Klongvessa P. Role of correlation among physical factors in probabilistic simulation of emissions of volatile organic compounds from floating storage and offloading vent stack. Environ. Nat. Resour. J. 2024;22(4):335-345. (https://doi.org/10.32526/ennrj/22/20230339)

periods has long-term adverse health effects, such as prolonged eye, nose, and throat irritation among the exposed workforce (Mo et al., 2021).

It has been reported that VOC emissions from storage tanks were associated with several physical factors relating to the NGLs and/or oil products and operating conditions, including Reid vapor pressure (RVP), storage quantity, storage temperature, product incoming rate, and turbulence from NGLs or oil movement (Rudd and Hill, 2001). Additionally, the VOC emission from an FSO tank is affected by ambient conditions (Alam et al., 2019), including solar radiation, ambient temperature, and turbulence from wave height (Hu et al., 2020; Lin et al., 2009; Yang et al., 2017; Lang et al., 2017). However, there has been no integrated investigation of these physical factors and applied probabilistic simulation to predict the VOC emission.

Probabilistic simulation is a statistical technique for exploring the impact of uncertainty in data (Alshanbari et al., 2023). In a probabilistic simulation, various inputs are used to calculate the outputs under different probabilities. Lynd and O'brien (2004) used a second-order Monte Carlo simulation to estimate disease risks to produce a risk-benefit acceptability curve. Cao et al. (2013) used a probabilistic simulation to model oil spilled concentration based on time, magnitude, and location. The obtained simulation was used to quantify risk analysis and to support a comprehensive spill management framework. Lin et al. (2022) used probabilistic simulation to estimate the exposures and risks of indoor VOCs and formaldehyde based on their concentrations, inhalation rates, exposure frequencies, and the body weights of the receptors. The current study used probabilistic simulation to predict the VOC venting volume based on various physical factors during the FSO operation. Typically, the physical factors are correlated with each other. Therefore, the simulation result may be inaccurate if such correlations are ignored. Thus, simulation with correlation among physical factors can produce more accurate results.

In this study, six physical factors (wave height, ambient air temperature, storage temperature, storage quantity, RVP, and daily incoming rate of the NGLs) were used in the probabilistic simulation of the venting volume associated with VOC emission. In addition, the role was investigated of correlations among these physical factors in probabilistic simulation. The results from this study can be applied to simulate the venting volume of VOC-contained gas from the FSO stack under different probabilities, which, in turn, would be useful for many purposes, especially those involving risk assessment.

2. METHODOLOGY

2.1 Data gathering and screening

The data used in this study consisted of the VOC venting volume from the stack of an FSO in the Gulf of Thailand and six relevant physical factors influencing the venting volume (wave height, ambient temperature, storage temperature, storage quantity, RVP, and daily incoming rate of the NGLs). Wave heights were collected using a wave buoy (Fugro; Norway). Data were collated 100 times per day but only 33 middle-range data out of 100 daily wave height data were used to calculate the average and reported as daily wave height. Ambient temperatures were measured using temperature sensors (PT100; SMA Solar Technology; Germany). Storage temperature was measured using a temperature sensor and storage quantity was measured based on a radar beam method. These instruments were included in the tank monitoring system (Kongsberg GL-300; Norway). The daily incoming NGL rate was calculated as the difference between the storage quantities on 2 consecutive days. RVP was defined as the absolute vapor pressure of the liquid at 37.8 ºC (100 ºF). Its value was obtained based on the ASTM-D323 test method, using the Holler Bomb Test (Koehler Instrument Co. Ltd.; USA). The VOC venting volume from the stack of the FSO was measured daily using an ultrasonic flare gas flow meter (GF868; GE; USA). This instrument was installed on the vent stack of the FSO. These data were collected throughout 2020. However, the data on the VOC venting volume on some days might be discontinuous due to closure of the vent stack during bad weather or stack maintenance, resulting in less venting volume than usual. For this reason, venting volume data of less than 90,000 ft^3 were excluded from this study.

2.2 Determination of relationship between physical factors and venting volume

Multiple linear regression (MLR) is a statistical technique that can be used to analyze the relationship between the physical factors and venting volume. However, since this research conducted probabilistic simulation and Cholesky randomization, one of the steps of probabilistic simulation requires the inputs to be normally distributed. Therefore, the data on

physical factors were transformed for normality before determining the relationship.

2.2.1 Two-step normality transformation

Two-step normality transformation was applied to transform each physical factor for normality (Templeton and Burney, 2017). First, the data were transformed for uniformity. In this step, the data of each physical factor were converted to a percentile rank (Equation 1) and uniformly distributed:

$$\text{Percentile Rank}\,(X_i) = \frac{\text{Rank}(X_i)}{100(n+1)} \quad (1)$$

Where; X_i is the i^{th} smallest data, Percentile Rank (X_i) is the percentile rank of X_i, $\text{Rank}(X_i)$ is an ascending rank of X_i, and n is the count of data.

The second step was a transformation of data from uniformity to normality. In this step, the inverse normal distribution was used to convert the percentile ranks (resulting from the first step) to provide normally distributed z-scores (Equation 2):

$$p = \mu + \sqrt{2}\ \sigma\, \text{erf}^{-1}(-1 + 2P_r) \quad (2)$$

Where; p is the transformed data, μ is the mean of the data, σ is the standard deviation of the data, erf^{-1} is the inverse of the error function, and P_r is a probability calculated from the percentile rank.

2.2.2 Second-order multiple linear regression with interaction effects and selection term of terms and measurement of accuracy

MLR was used to predict the VOC venting volume from the six independent variables (transformed wave height, transformed ambient temperature, transformed storage temperature, transformed storage quantity, transformed RVP, and transformed daily incoming rate). Since the effect of each independent variable may vary, the relationships between the VOC venting volume and the independent variables were determined based on a second-order MLR with interaction effects, as shown in Equation 3 (Cho and Lee, 2018; Jia et al., 2020):

$$Y = a + \sum_{i=1}^{n} b_i x_i + \sum_{i=1}^{n}\sum_{j=i}^{n} c_{ij} x_i x_j \quad (3)$$

Where; Y is the VOC venting volume, a, b_i, and c_{ij} are constants, n is a number of factors, and x_i and x_j are the values of i^{th} and j^{th} independent variables, respectively.

Since not all interaction effects were necessary for the prediction of the VOC venting volume, the adjusted coefficient of determination (adjusted R^2) was calculated to determine the usefulness of each term in the MLR. The adjusted R^2 was calculated using Equation 4 (Alam et al., 2019; Pham, 2019):

$$R^2_{adj} = 1 - (1 - R^2)\left(\frac{n-1}{n-p-1}\right) \quad (4)$$

Where; R^2_{adj} is the adjusted coefficient of determination (adjusted R^2), R^2 is the coefficient of determination, n is the number of data, and p is the number of predictors.

The terms in the MLR were selected by maximizing the adjusted R^2. In other words, only the terms that improved the value of the adjusted R^2 were included in the MLR. After the selection of terms, the root mean squared error (RMSE) and coefficient of determination (R^2) were calculated to evaluate the accuracy of the MLR. Finally, the significance of each term in the MLR was appraised based on a t-test at a significance level of 0.05 (Cho and Lee, 2018).

2.3 Probabilistic simulation of venting volume

Probabilistic simulation was used to generate different values of the venting volume. First, the average and standard deviation of each physical factor were calculated, as well as the correlation coefficients among physical factors. Then, 1,000 datasets of relevant physical factors were generated according to the calculated averages, standard deviations, and correlations. After that, the 1,000 datasets were used to calculate 1,000 venting volumes. The distribution of these 1,000 venting volumes represented the venting volume at different probabilities. The diagram of probabilistic simulation is shown in Figure 1.

In generating the 1,000 datasets of physical factors, the Cholesky randomization method was used to create a dataset with specified correlation coefficients. First, the physical factors (wave height, ambient air temperature, storage temperature, storage quantity, daily incoming rate, RVP) were transformed to normally distributed data. After that, the correlation matrix was determined (the matrix containing the correlation coefficients among variables-transformed wave height, transformed ambient air temperature, transformed storage temperature, transformed storage quantity, transformed daily incoming rate, and transformed RVP-calculated from the MLR). Then, the Cholesky decomposition process was used to decompose the correlation matrix into a triangular matrix and its transpose, as shown in Equation 5 (Golub and Loan, 1983; Trefethen and Bau, 1997):

$$A = LL^T \quad (5)$$

Where; A is the correlation matrix, L is the lower triangular matrix with real and positive diagonal entries, and L^T is the transpose of L.

After that, a 6 × 1,000 matrix, containing random numbers between 0 and 1, was created (denoted as P). The six columns in matrix P represented the six variables (transformed wave height, transformed ambient air temperature, transformed storage temperature, transformed storage quantity, transformed daily incoming rate, and transformed RVP). Then, a matrix containing the inverse of the standard normal distribution of the elements of the matrix P was generated (denoted as X). After that, matrix X was multiplied by matrix L, as shown in Equation 6. The result was a matrix (denoted as X^*) containing random numbers, the correlation coefficients of which are matrix A:

$$X^* = XL \quad (6)$$

Finally, each column of matrix X^* was multiplied by the standard deviation of each variable (the variable each column represented) and the average of each variable was added to the product (the multiplication result). This process yielded 1,000 sets of random variables, the average, standard deviation, and correlation of which were according to those of the observed values. In the step of calculating venting volumes, 1,000 sets of random variables were used in the MLR to calculate the VOC venting volumes.

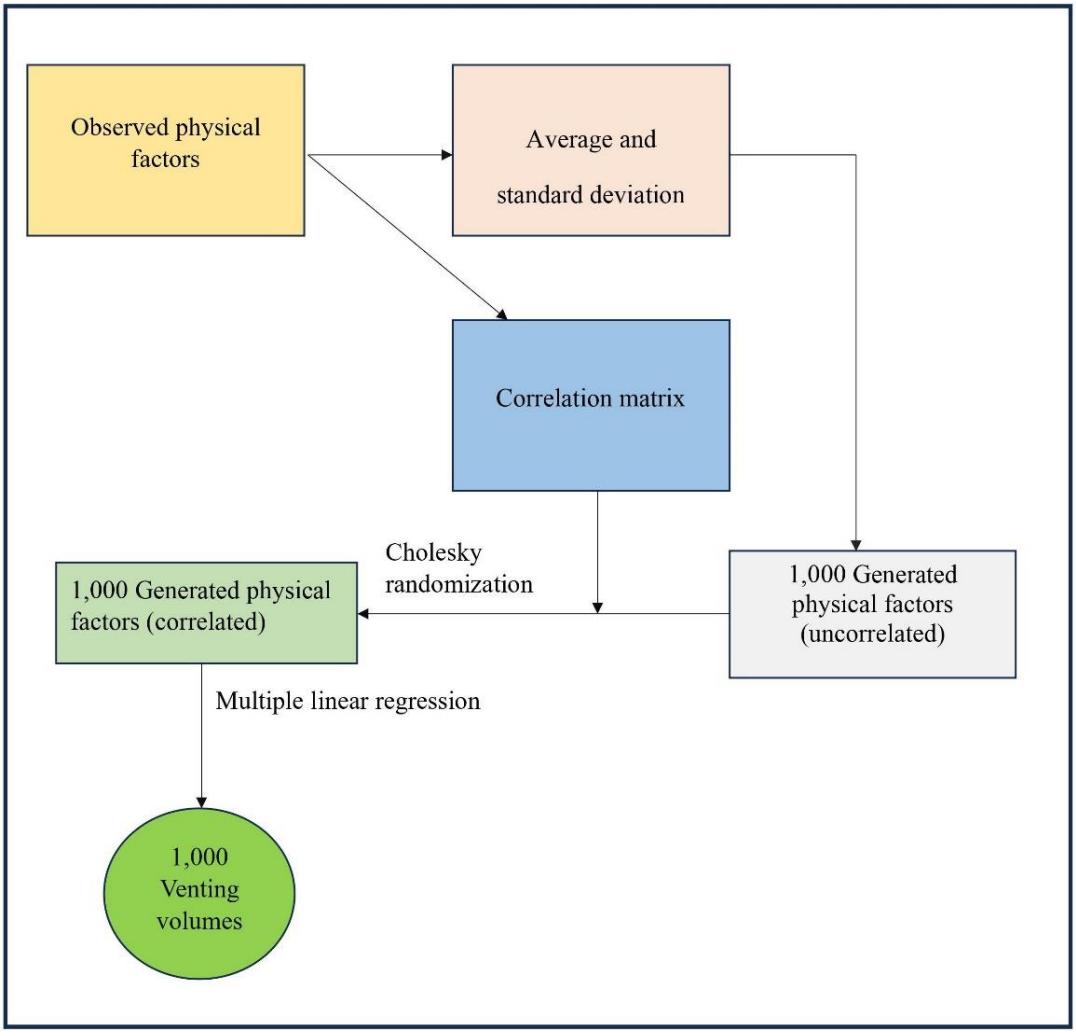

Figure 1. Flowchart of probabilistic simulation

2.4 Evaluation of role of correlation among physical factors

To evaluate the role of correlation among the physical factors, 2 probabilistic simulations were conducted. The first simulation was conducted without correlation among the physical factors. In that simulation, matrix X in section 2.3 was not multiplied by matrix L. The variables were generated by the multiplication of each column of matrix X using the standard deviation of each variable and the addition of the average of each variable to the multiplication result. The second simulation applied correlation among physical factors, which followed all the steps mentioned in section 2.3. The difference between moments (averages, standard deviations, and skewness) and percentiles of the VOC venting volumes from these 2 simulations were used to determine the role of correlation among physical factors.

3. RESULTS AND DISCUSSION

3.1 Data transformation

In the gathered data, there were 40 days for which the VOC venting volumes were less than 90,000 ft^3 due to closure of the vent stack, resulting from poor weather conditions or stack maintenance. Therefore, the data on these 40 days were excluded and only the data on the remaining 326 days were used. The summarized values of physical factors, both before and after the two-step normality transformation, during the study period are shown in Table 1. The ambient air temperature (average of 28.4°C and standard deviation of 0.9°C) was higher and had less variability than those from other studies because the study area was located in the tropical zone (Gjesteland et al., 2019; Hu et al., 2020; Stricklin, 2014). The RVP value had low variability because the NGLs of each batch had a consistent composition. Because of the application of the two-step normality transformation, the transformed data followed a normal distribution. The comparison between the non-transformed and transformed data revealed that the skewness of the transformed data was close to zero.

3.2 Relationship between VOC venting volume and physical factors

The set of terms producing the highest adjusted R^2 of the MLR and the coefficients of these terms, together with the results of the t-test, are shown in

Table 1. Summary of non-transformed and transformed physical factors

Statistic	Wave height		Ambient air temperature		Storage temperature		Storage quantity		RVP		Daily incoming rate	
	Non-transformed	Transformed	Non-transformed	Transformed	Non-transformed	Transformed	Non-transformed	Transformed	Non-transformed	Transformed	Non-transformed	Transformed
Average	1.1 m	1.1 m	28.5°C	28.5°C	29.4°C	29.4°C	492,012 bbls	493,508 bbls	12.1 psi	12.1 psi	43,163 bbls	43,181 bbls
Standard deviation	0.7 m	0.7 m	0.9°C	0.9°C	0.6°C	0.6°C	94,768 bbls	92,919 bbls	0.3 psi	0.3 psi	7,160 bbls	7,142 bbls
Skewness	1.30	-0.05	-0.54	0.10	0.57	0.01	0.33	0.17	0.75	0.33	-0.06	0.00

The abbreviation "bbls" stands for "barrels".

Table 2. The significant terms were: 1) transformed RVP; 2) transformed wave height; 3) transformed storage temperature; 4) transformed daily incoming rate; 5) transformed RVP × transformed daily incoming rate; 6) transformed RVP × transformed wave height; and 7) transformed RVP^2. Therefore, these sets of terms in the MLR were the best to estimate the VOC venting volume. The significant factors were consistent with those determined using the non-transformed data, as described by Seekramon (2023), except for the addition of the daily incoming rate, which was significant in the current study. The daily incoming rate related to the liquid velocity feeding into the tank. (A high daily incoming rate caused a high velocity and enhanced the turbulence of NGLs, leading to high VOCs venting volume). The other significant factors have been discussed in Seekramon (2023). The significance of the terms 5-7 above (transformed RVP × transformed daily incoming rate, transformed RVP × transformed wave height, and transformed RVP^2) suggested that the effects of RVP, wave height, and daily incoming rate were not constant. For example, a high RVP promoted NGL evaporation, corresponding to the VOC venting volume (Rudd and Hill, 2001; Stricklin, 2014), and at a high daily incoming rate and wave height promoted VOC venting volume (Deligiannis et al., 2016).

Table 2. Terms from MLR between transformed physical factors and VOC venting volume providing highest value of adjusted R^2

Term	Coefficient	Standard error	t- statistic	p-value
Intercept (ft^3)	24,539,128	8,158,959.184	-3.008	0.003
Transformed RVP (psi)	-1,570,508	765,865.167	-2.051	0.041*
Transformed wave height (m)	-681,298.9	328,061.780	-2.077	0.039*
Transformed storage temperature (ºC)	-1,017,555	506,203.820	-2.010	0.045*
Transformed daily incoming rate (bbl)	43.547	20.554	2.119	0.035*
Transformed RVP (psi) × transformed daily incoming rate (bbl)	-3.372	1.696	-1.989	0.048*
Transformed wave height (m) × transformed storage quantity (bbl)	0.064	0.046	1.391	0.165
Transformed storage temperature (ºC)^2	16,673.849	8,158.886	1.957	0.051
Transformed RVP (psi) × transformed wave height (m)	69,035.092	17,789.893	3.881	<0.001*
Transformed storage quantity (bbl)^2	-9.59×10^{-8}	6.13×10^{-8}	-1.565	0.119
Transformed wave height (m) × transformed ambient temperature (ºC)	5,453.376	3,288.785	-1.658	0.098
Transformed wave height (m) × transformed storage temperature (ºC)	-11,429.679	9,310.032	-1.228	0.221
Transformed RVP (psi)^2	68,773.81	31,713.808	2.169	0.031*

* p-value<0.05 (significant); The abbreviation "bbl" stands for "barrel".

The observed and modeled venting volumes are shown in Figure 2. The model produced increases and decreases in the venting volume consistent with the observed values. However, the standard deviation of the modeled data was less than that of the observed data. The MLR had values for R^2 of 0.370, adjusted R^2 of 0.345, and standard error of 54,863 ft^3. The venting volume was high during September-December (days 274-366) because of the influence of the northeast monsoon, which led to an increased wave height. This proved that wave height significantly increased the VOC venting volume.

3.3 Estimation of VOC venting volume based on probabilistic simulation

3.3.1 Cholesky decomposition of correlation matrix

Correlations among the transformed physical factors are shown in Table 3. There were positive correlations between transformed wave height and transformed storage quantity, between transformed wave height and transformed daily incoming rate, between transformed ambient air temperature and transformed storage temperature, between transformed temperature (both ambient and storage

temperatures) and transformed RVP, and between transformed storage quantity and transformed daily incoming rate. In addition, there were negative correlations between transformed wave height and transformed temperature (both ambient and storage temperatures), between transformed wave height and transformed RVP, between transformed temperature (both ambient and storage temperatures) and transformed storage quantity, between transformed temperature (both ambient and storage temperatures) and transformed daily incoming rate, between transformed storage quantity and transformed RVP, and between transformed RVP and transformed daily incoming rate.

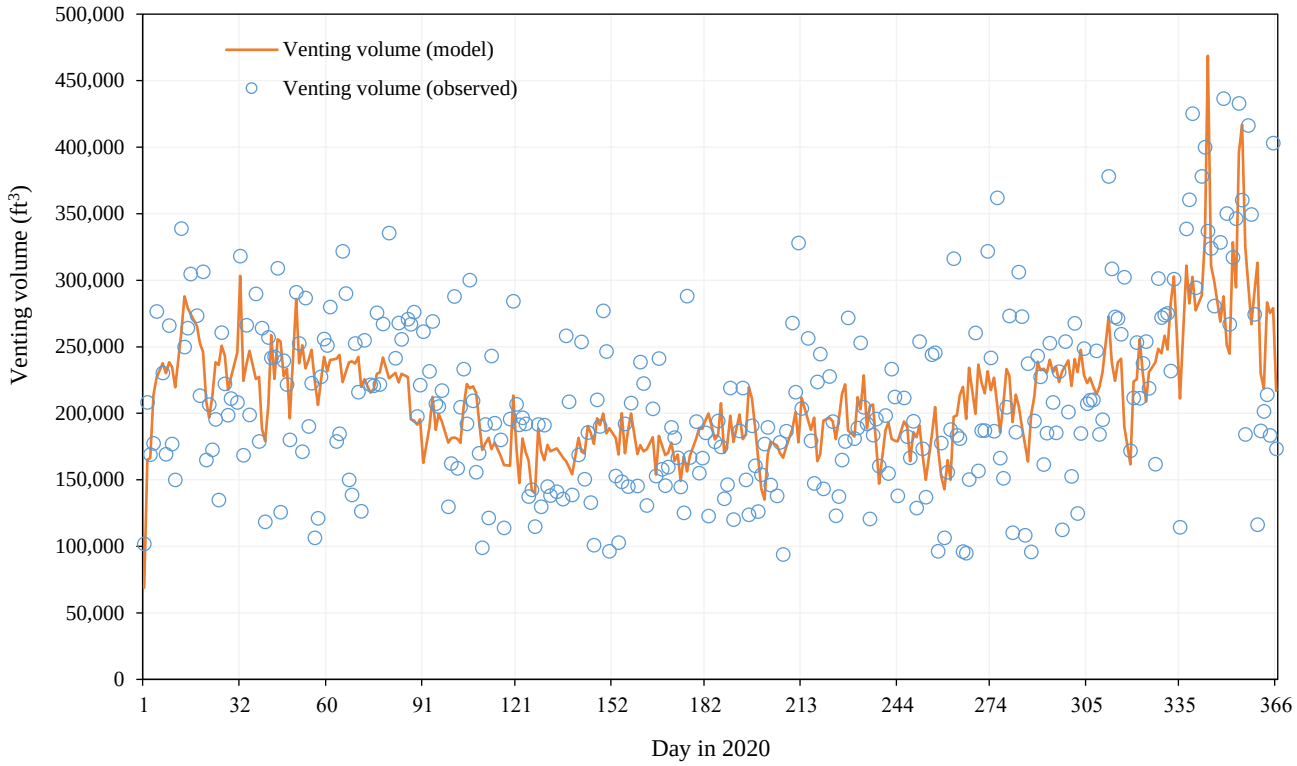

Figure 2. Observed and modeled VOC venting volume from FSO

Table 3. Correlations between each pair of observed transformed physical factors

Transformed wave height	1.000					
Transformed ambient air temperature	-0.326	1.000				
Transformed storage temperature	-0.403	0.592	1.000			
Transformed storage quantity	0.052	-0.116	-0.206	1.000		
Transformed daily incoming rate	0.188	-0.330	-0.194	0.240	1.000	
Transformed RVP	-0.046	0.144	0.189	-0.020	-0.070	1.000
	Transformed wave height	Transformed ambient air temperature	Transformed storage temperature	Transformed storage quantity	Transformed daily incoming rate	Transformed RVP

Based on Table 3, the correlation matrix (A) can be written as shown below:

$$A = \begin{matrix} 1.000 & -0.326 & -0.403 & 0.052 & 0.188 & -0.046 \\ -0.326 & 1.000 & 0.592 & -0.116 & -0.330 & 0.144 \\ -0.403 & 0.592 & 1.000 & -0.206 & -0.194 & 0.189 \\ 0.052 & -0.116 & -0.206 & 1.000 & 0.240 & -0.020 \\ 0.188 & -0.330 & -0.194 & 0.240 & 1.000 & -0.070 \\ -0.046 & 0.144 & 0.189 & -0.020 & -0.070 & 1.000 \end{matrix}$$

Which yields the result of Cholesky decomposition (L), as shown below:

$$L = \begin{matrix} 1.000 & 0.000 & 0.000 & 0.000 & 0.000 & 0.000 \\ -0.326 & 0.945 & 0.000 & 0.000 & 0.000 & 0.000 \\ -0.403 & 0.487 & 0.775 & 0.000 & 0.000 & 0.000 \\ 0.052 & -0.104 & -0.173 & 0.978 & 0.000 & 0.000 \\ 0.188 & -0.284 & 0.026 & 0.210 & 0.916 & 0.000 \\ -0.046 & 0.137 & 0.133 & 0.020 & -0.033 & 0.980 \end{matrix}$$

3.3.2 Randomized physical factors

The average, standard deviation, and skewness of the uncorrelated and correlated randomized variables are shown in Table 4. It can be seen that the averages, standard deviations, and skewness were close to those of the observed transformed variables (Table 1).

Tables 5 and 6 show the correlations among randomized variables when the actual correlations among physical factors were and were not applied in the randomization, respectively. When the actual correlations were applied, the correlations among randomized variables (Table 5) were close to those among the observed variables (Table 3). However, when the actual correlations were not applied, the correlations among randomized variables (Table 6) and those among the observed variables differed. Therefore, the Cholesky randomization successfully represented the correlations among physical factors.

3.4 Probabilistic simulation of VOC venting volume

Comparisons between the observed VOC venting volume and the probabilistic simulated VOC venting volumes with and without correlation among physical factors are shown in Table 7. It was found that regardless of whether or not correlations among physical factors were applied, the average simulated venting volumes were close to the observed venting volumes (approximately 210,000 ft^3), and the standard deviations of the simulated venting volumes (approximately 40,000 ft^3) were lower than those for the observed venting volumes (approximately 67,961 ft^3). However, when the correlations were applied, the skewness of the VOC venting volume was more accurate than when the correlations were not applied.

Table 4. Average, standard deviation, and skewness of the correlated and uncorrelated randomized variables

Randomized variable	Transformed wave height		Transformed ambient air temperature		Transformed storage temperature		Transformed storage quantity		Transformed daily incoming rate		Transformed RVP	
	Correlated	Uncorrelated	Correlated	Uncorrelated	Correlated	Uncorrelated	Correlated	Uncorrelated	Correlated	Uncorrelated	Correlated	Uncorrelated
Average	1.1 m	1.1 m	28.5°C	28.5°C	29.4°C	29.4°C	495,266.9 bbls	495,386.4 bbls	43,134.8 bbls	43,071.8 bbls	12.1 psi	12.1 psi
Standard deviation	0.7 m	0.7 m	0.9°C	0.9°C	0.6°C	0.6°C	94,650.3 bbls	94,920.4 bbls	7,041.7 bbls	7,154.8 bbls	0.3 psi	0.3 psi
Skewness	-0.017	-0.017	0.001	0.005	0.016	0.003	0.129	0.136	0.070	0.121	0.030	0.046

The abbreviation "bbls" stands for "barrels".

Table 5. Correlation between each pair of randomized variables with correlations among physical factors

Transformed wave height	1					
Transformed ambient air temperature	-0.343	1				
Transformed storage temperature	-0.405	0.557	1			
Transformed Storage quantity	0.067	-0.098	-0.196	1		
Transformed daily incoming rate	0.137	-0.309	-0.168	0.228	1	
Transformed RVP	-0.023	0.104	0.139	-0.015	-0.050	1
	Transformed wave height	Transformed Ambient air temperature	Transformed storage temperature	Transformed storage quantity	Transformed daily incoming rate	Transformed RVP

Table 6. Correlation between each pair of randomized variables without correlation among physical factors

Transformed wave height	1					
Transformed ambient air temperature	0.004	1				
Transformed storage temperature	0.013	-0.034	1			
Transformed storage quantity	0.018	0.011	0.004	1		
Transformed daily incoming rate	-0.064	-0.009	-0.014	-0.017	1	
Transformed RVP	0.020	-0.027	-0.032	-0.009	0.009	1
	Transformed wave height	Transformed ambient air temperature	Transformed storage temperature	Transformed storage quantity	Transformed daily incoming rate	Transformed RVP

Table 7. Comparison between observed and probabilistic simulated venting volumes

Statistic	Observed venting volume	Venting volume from probabilistic simulation (correlation applied)	Venting volume from probabilistic simulation (correlation not applied)
Mean (ft^3)	210,984	211,610	210,906
Maximum (ft^3)	436,548	369,461	372,812
Minimum (ft^3)	94,052	120,958	78,711
Standard deviation (ft^3)	67,961	38,828	40,787
Skewness	0.71	0.74	0.51

This finding coincided with other studies that used probabilistic simulation to generate non-normally distributed data (Cao et al., 2013; Headrick and Kowalchuk, 2007; Lin et al., 2022).

The standard deviations of the simulated venting volumes were low because the MLR accounted for only 37.0% of the variability of the venting volume (R^2=0.370). For this reason, the variability of the simulated value was less than that of

the observed value (Figure 2). It can be seen in Figure 3 that the simulated venting volumes were accurate at the 54th-63rd percentiles. At lower percentiles, the simulated venting volumes appeared to be higher than the observed venting volumes, while at higher percentiles, the simulated venting volumes appeared to be lower than the observed venting volumes.

The skewness of the simulated VOC venting volume was improved when the correlations among physical factors were applied, because of the natural characteristics of the physical factors that were correlated with each other. Ignoring the correlations among physical factors could result in unrealistic occurrence probability estimates for physical factors, leading to unrealistic skewness. When the correlations were not applied at low percentiles, the simulated venting volumes decreased with decreasing percentile at a higher rate than the observed data. However, when the correlations were applied, the rate of decrease was less, which was more accurate. Therefore, the results of the current study showed that applying correlations among physical factors in the probabilistic simulation of venting volume could improve simulation accuracy by improving the skewness of the simulated VOC venting volume, which was consistent with Batterman et al. (2014). Nevertheless, it should be noted that the observed and simulated venting volumes may not be close to each other when the venting volume is low because days with venting volumes of less than 90,000 ft^3 were excluded from the current study.

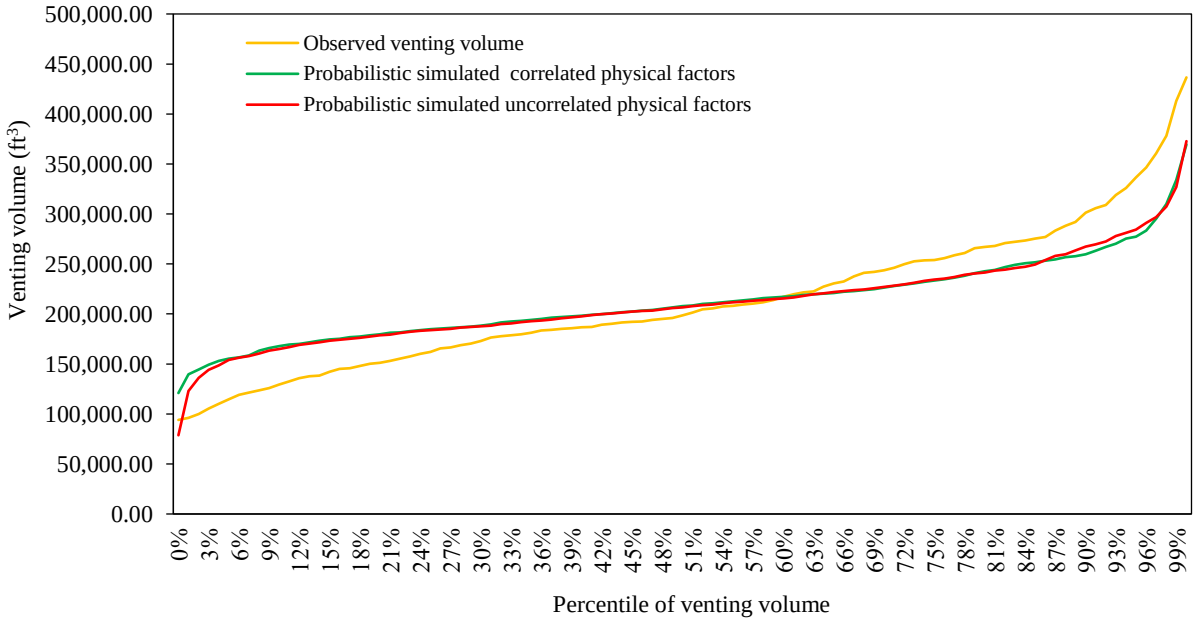

Figure 3. Percentiles of observed and probabilistic simulated venting volumes

4. CONCLUSION

This research highlighted the importance of implementing correlations among physical factors in predicting VOC venting volume emitted from the FSO. Physical factors affecting VOC venting volume, including wave height, ambient temperature, storage temperature, storage quantity, RVP, and daily incoming rate, were transformed to normally distributed data. Second-order MLR with interaction effects was used to determine the relationship between the transformed physical factors and the VOC venting volume. The selection of terms (transformed physical factors and interaction effects) in the MLR was based on maximizing the adjusted R^2, with the significance of each term being tested using a t-test. The significant terms for the prediction of VOC venting volume were: 1) transformed RVP; 2) transformed wave height; 3) transformed storage temperature; 4) transformed daily incoming rate; 5) transformed RVP × transformed daily incoming rate; 6) transformed RVP × transformed wave height; and 7) transformed RVP^2. The MLR had values for R^2 of 0.370, for adjusted R^2 of 0.345, and for standard error of 54,863 ft^3. Then, probabilistic simulation was applied to generate 1,000 sets of probable physical factors in 2 scenarios (implementing and not implementing the correlations among physical factors). The generated physical factors were used to estimate 1,000 VOC venting volumes. The averages of the estimated VOC venting volumes corresponded to the observed data for all scenarios. However, the standard deviations of the estimated VOC venting volumes were low because of

the low goodness of fit of the MLR. Nevertheless, the skewness of the simulated VOC venting volume was improved when the correlations among physical factors were applied. Therefore, the implementation of correlations among physical factors provided better simulation results. This improvement should benefit many works using probabilistic simulation, such as benefit-risk assessment.

ACKNOWLEDGEMENTS

The Department of Environmental Technology and Management, Faculty of Environment, Kasetsart University, Bangkok, Thailand provided support with resources and facilities that were essential in conducting the data analysis and staff who facilitated the smooth progress of this research.

REFERENCES

Alam MS, Nikolova I, Singh A, MacKenzie AR, Harrison RM. Experimental vapour pressures of eight n-alkanes (C17, C18, C20, C22, C24, C26, C28 and C31) measured at ambient temperatures. Atmospheric Environment 2019;213:739-45.

Alshanbari HM, Odhah OH, Ahmad Z, Khan F, El-Bagoury AA-AH. A new probability distribution: Model, theory and analyzing the recovery time data. Axioms 2023;12(5):477-94.

Batterman S, Su FC, Li S, Mukherjee B, Jia C. Personal exposure to mixtures of volatile organic compounds: Modeling and further analysis of the RIOPA data. Research Reports: Health Effects Institute 2014;181:3-63.

Cao W, Li J, Joksimovic D, Yuan A, Banting D. Probabilistic spill occurrence simulation for chemical spills management. Journal of Hazardous Materials 2013;256:517-26.

Cho JH, Lee JH. Multiple linear regression models for predicting non point-source pollutant discharge from a highland agricultural region. Water 2018;10(9):Article No. 1156.

Deligiannis P, Zouridis P, Galis A. VOC emissions assessment from the cargo area of tanker vessels. Proceedings of Smart and Green Technology for the Future of Marine Industries International Conference; 2016 Apr 25-26; Glasgow: UK; 2016.

Drysdale R. OCIMF annual report 2019 [Internet]. 2019 [cited 2023 Sep 20]. Available from: https://www.ocimf.org/document-libary/29-ocimf-annual-report-2019/file.

Gjesteland I, Hollund BE, Kirkeleit J, Daling PS, Sørheim KR, Bråtveit M. Determinants of airborne benzene evaporating from fresh crude oils released into seawater. Marine Pollution Bulletin 2019;140:395-402.

Golub GH, Loan CFV. Matrix Computations. Baltimore: The Johns Hopkins University; 1983.

Headrick TC, Kowalchuk RK. The power method transformation: Its probability density function, distribution function, and its further use for fitting data. Journal of Statistical Computation and Simulation 2007;77(3):229-49.

Hu G, Butler J, Littlejohns J, Wang Q, Guoneng L. Simulation of cargo VOC emissions from petroleum tankers in transit in Canadian waters. Engineering Applications of Computational Fluid Mechanics 2020;14(1):522-33.

Jia Z, Wang J, Zhou X, Zhou Y, Li Y, Li B, et al. Identification of the sources and influencing factors of potentially toxic elements accumulation in the soil from a typical karst region in Guangxi, Southwest China. Environmental Pollution 2020;256:Article No. 113505.

Lang J, Zhou Y, Chen D, Xing X, Wei L, Wang X, et al. Investigating the contribution of shipping emissions to atmospheric $PM_{2.5}$ using a combined source apportionment approach. Environmental Pollution 2017;229:557-66.

Lin C-C, Yu K-P, Zhao P, Lee GW-M. Evaluation of impact factors on VOC emissions and concentrations from wooden flooring based on chamber tests. Building and Environment 2009;44(3):525-33.

Lin W-T, Tsai R-Y, Chen H-L, Tsay Y-S, Lee C-C. Probabilistic prediction models and influence factors of indoor formaldehyde and VOC levels in newly renovated houses. Atmosphere 2022;13(5):Article No. 675.

Lynd LD, O'brien BJ. Advances in risk-benefit evaluation using probabilistic simulation methods: An application to the prophylaxis of deep vein thrombosis. Journal of Clinical Epidemiology 2004;57(8):795-803.

Mo Z, Lu S, Shao M. Volatile organic compound (VOC) emissions and health risk assessment in paint and coatings industry in the Yangtze River Delta, China. Environmental Pollution 2021;269:Article No. 115740.

Pham H. A new criterion for model selection. Mathematics 2019;7(12):Article No. 1215.

Rudd HJ, Hill NA. Measures to reduce emissions of VOCs during loading and unloading of ships in the EU [Internet]. 2001 [cited 2023 Sep 18]. Available from: http://ec.europa.eu/environment/archives/air/pdf/vocloading.pdf.

Seekramon C. Emission of Volatile Organic Compounds from Natural Gas Liquid Tank Vessel [dissertation]. Thailand, Mahidol University; 2015.

Seekramon C. Application of Simulation Models for Estimation of Benzene Emission on Floating Storage and Offloading (FSO) and Health Risk Assessment of Benzene Exposure [dissertation]. Thailand, Kasetsart University; 2023.

Shao P, Xu X, Zhang X, Xu J, Wang Y, Ma Z. Impact of volatile organic compounds and photochemical activities on particulate matters during a high ozone episode at urban, suburb and regional background stations in Beijing. Atmospheric Environment 2020;236:Article No. 117629.

Stricklin E. Evaporation loss measurement from storage tanks [Internet]. 2014 [cited 2023 Oct 10]. Available from: https://technokontrol.com/pdf/evaporation/evaporation-loss-measurement.pdf.

Templeton GF, Burney LL. Using a two-step transformation to address non-normality from a business value of information technology perspective. Journal of Information Systems 2017;31(2):149-64.

Trefethen LN, Bau D. Numerical Linear Algebra. Philadelphia, United States: Society for Industrial and Applied Mathematics; 1997.

Vos D, Duddy M, Bronneburg J. The evolution of inert-gas systems on SBM FPSOs: The problem of venting and a straightforward solution. SPE Projects Facilities and Construction 2007;2(2):1-11.

Yang T, Zhang P, Xu B, Xiong J. Predicting VOC emissions from materials in vehicle cabins: Determination of the key parameters and the influence of environmental factors. International Journal of Heat and Mass Transfer 2017;110: 671-9.

Environment and Natural Resources Journal

Volume 22
Issue 4
2024

Assessment of Health Risk from Exposure to Respirable Particulate Matter (RPM) among Motorcycle Taxi Drivers in Bangkok and Adjacent Provinces, Thailand

Kamonwan Samana[1], Kimihito Ito[2], Orasa Suthienkul[3], and Arroon Ketsakorn[1*]

[1]Faculty of Public Health, Thammasat University, Pathumthani, Thailand
[2]Division of Bioinformatics, International Institute for Zoonosis Control, Hokkaido University, Japan
[3]Faculty of Public Health, Mahidol University, Bangkok, Thailand

ARTICLE INFO

Received: 5 Dec 2023
Received in revised: 30 May 2024
Accepted: 22 May 2024
Published online: 8 Jul 2024
DOI: 10.32526/ennrj/22/20230335

Keywords:
Health risk assessment/ Respirable particulate matter/ Motorcycle taxi drivers/ Personal air sampling/ Bangkok/ Adjacent Provinces

*** Corresponding author:**
E-mail: arroon.k@fph.tu.ac.th

ABSTRACT

Exposure to outdoor air pollutants, particularly respirable particulate matter (RPM), can cause adverse health outcomes. The cross-sectional study aimed to assess motorcycle taxi driver's health risk from exposure to RPM. A total of 153 motorcycle taxi drivers were recruited in Bangkok and five adjacent provinces during May and June 2022. The standardized questionnaire for data collection contained exposure time (hour/day), frequency of exposure (days/years), duration of exposure (year), body weight (kg), and averaging time (days). The average RPM concentration from six provinces were assessed personal air sampling pumps and ranged from 0.006-0.031 mg/m^3. Bangkok showed the highest average RPM concentration (0.031 mg/m^3), followed by Pathumthani (0.028 mg/m^3), Samut Prakan (0.009 mg/m^3), Nakhon Pathom (0.008 mg/m^3), Nonthaburi (0.007 mg/m^3), and Samut Sakhon (0.006 mg/m^3), respectively. The Hazard Quotient (HQ) values for a non-carcinogenic risk to human health caused by RPM exposure in each province indicated a negligible risk (HQ=0.005-0.028). HQ averages (HQ=0.013) from all provinces were also at an acceptable level (≤1). Not all motorcycle taxi drivers are safe from RPM exposure, although their exposure is within acceptable limits depending on their individual susceptibility. Therefore, this is the first report on quantifying exposure to RPM from personal air sampling and health risk assessment among motorcycle taxi drivers. These findings would be useful information for further preventing and controlling ambient air pollution including policies and strategies to mitigate the risks for motorcycle-taxi drivers and the other exposed populations.

1. INTRODUCTION

Outdoor air pollution is the leading cause of more than 3 million deaths and premature deaths worldwide each year (Thurston et al., 2017). Respirable particulate matter (RPM) is defined by its diameter for air quality regulatory purposes. Those with a diameter of 10 microns or less (PM_{10}) are inhalable into the lungs and can induce adverse health effects. Fine particulate matter is defined as particles that are 2.5 microns or less in diameter ($PM_{2.5}$). Therefore, $PM_{2.5}$ comprises a portion of PM_{10}. The World Health Organization (WHO) estimates that more than 90% of the world's population lives in areas where air quality is below recommended values. From the literature review on air quality in Thailand during 2010-2020, it was found that the annual average concentration of PM_{10} and $PM_{2.5}$ mostly exceeded the Thailand and WHO standard especially in Bangkok and adjacent provinces (Pollution Control Department, 2022). Those areas are urban communities with dense populations and heavy traffic. The main source of PM_{10} and $PM_{2.5}$ in these areas is

Citation: Samana K, Ito K, Suthienkul O, Ketsakorn A. Assessment of health risk from exposure to respirable particulate matter (RPM) among motorcycle taxi drivers in Bangkok and Adjacent Provinces, Thailand. Environ. Nat. Resour. J. 2024;22(4):346-353. (https://doi.org/10.32526/ennrj/22/20230335)

traffic (Pollution Control Department, 2022). Motorcycle taxi drivers are at risk of exposure to PM_{10} and $PM_{2.5}$ because they are likely to be directly exposed to air pollution. In addition, their working posture requires sitting on an open motorcycle, and the environment where the motorcycle taxi terminals are located on the roadside, which may affect their respiratory problems. Around 76.0% of them work in the central region of Thailand (Bureau of Highway Safety, Department of Highways, 2021). They must drive to pick up or drop off passengers outside buildings throughout their working hours, on average 10 hours per day, and ranging from 4-19 hours per day (Suebsuk et al., 2014). Therefore, there is more chance of exposure to ambient air pollution than in other occupations. In addition, previous studies have focused on commuter's exposure to BTEX in public transportation modes in Bangkok (Ongwandee and Chavalparit, 2010), occupational exposure of gasoline station workers to BTEX compounds in Bangkok (Tunsaringkarn et al., 2012), health risk levels to benzene, toluene, ethylbenzene, and xylenes (BTEX) and carbonyl compounds (CCs) inhalation exposure of traffic policemen working in the inner city of Bangkok (Kanjanasiranont et al., 2017), and BTEX exposure including health risk assessment among car park workers (Loonsamrong et al., 2017). There have also been studies to determine the relationship between personal factors and pulmonary function abnormalities in Indonesia, Malaysia as well as in Tak, Chiang Mai, and Bangkok in Thailand (Suebsuk et al., 2014; Kheunpeck and Tantipanchaporn, 2016; Damayanti et al., 2019; Putri Anis Syahira et al., 2020). These studies were unable to demonstrate exposure to RPM and health effects, making health surveillance of such occupations ineffective.

Assessment of health risk from exposure to RPM consists of four steps according to the USEPA (USEPA, 2022).

1) Hazard identification

This process is to identify the RPM exposure to a stressor which can cause an increase in the incidence of specific adverse health effects (e.g., pneumonia, emphysema, tuberculosis, cerebrovascular disease, chronic obstructive pulmonary disease, ischemic heart disease, acute lower respiratory tract infection). When motorcycle taxi drivers are inhaled the RPM into their bodies, and a specific process of absorption, distribution, metabolism, and excretion takes place. This process is called toxicokinetics (Phanprasit, 2014).

2) Dose-response assessment

The term exposure-response relationship describes either a dose-response or a concentration-response, or other specific exposure conditions. Typically, as the dose increases, the measured response also increases. At low doses there may be no response. The scientific information is evaluated for adverse health effect or response; the understanding of the response is called the mode of action. Based on this mode of action, the agency determines the nature of the extrapolation, either through non-linear or linear dose-response assessment. A nonlinear assessment uses a dose-response relationship whose slope was zero (i.e., no response) at a dose of zero. No-Observed-Adverse-Effect Level (NOAEL) is used as a reference dose for nonlinear assessment. However, in cases where NOAEL has not been experimentally demonstrated, the term of Lowest-Observed-Adverse-Effect Level (LOAEL) is used as the lowest or reference dose instead of the NOAEL. The reference dose (RfD) is an oral or dermal dose derived from the NOAEL or LOAEL by application of generally order of magnitude uncertainty factors (UFs). These uncertainty factors take into account the variability and uncertainty that are reflected in possible differences between test animals and humans, and variability within the human population. On the part of assessing linear dose response, in this type of assessment, there is theoretically no level of exposure for such a chemical that does not pose a small, but finite, probability of generating a carcinogenic response. The extrapolation phase of assessment does not use UFs; rather, a straight line is drawn from the point of departure for the observed data to the origin (where there is zero dose and zero response). The slope of this straight line, called the slope factor or cancer slope factor, is used to estimate risk at exposure levels that fall along the line. When linear dose-response is used to assess cancer risk, the cancer risk is determined by considering the exposure and slope factor.

3) Exposure assessment

Average Daily Dose (ADD) is used to describe the exposure assessment. The potential dose of a RPM is the product of the RPM concentration, inhalation rate, exposure time, exposure frequency, and exposure duration divided by the product of averaging time and body weight.

4) Risk characterization

This step is to summarize and integrate information from the proceeding steps of the risk

assessment to synthesize an overall conclusion about risk.

Exposure to RPM affects health, thereby increasing the risk of acute and chronic respiratory disease and impaired lung function (Sonjai, 2001; Boonchu, 2005; Kheunpeck and Tantipanchaporn, 2016). At present, the number of registered motorcycles in Thailand has increased to approximately 21.7 million units (Statista, 2022). However, up to date, there is still a lack of studies assessing health risks from exposure to RPM of motorcycle taxi drivers. More evidence is still required to assess the health risk of RPM among motorcycle taxi drivers. Therefore, this study determined the assessment of health risk from exposure to RPM in the working environment among motorcycle taxi drivers in Bangkok and adjacent provinces in Thailand. The findings provided the crucial data based on health risk assessment to assist in proper prevention actions and controlling strategies.

2. METHODOLOGY

2.1 Study area

The motorcycle taxi drivers were selected from the central region of Thailand. Those areas included Bangkok, Pathum Thani, Samut Prakan, Samut Sakhon, Nonthaburi, and Nakhon Pathom. Bangkok and adjacent provinces occupy 7,762 km^2 with a population of 10,899,786 people and 5.6 million inhabitants respectively (National Statistical Office, 2021).

2.2 Study design and participants

This cross-sectional study was used in 153 motorcycle taxi drivers who worked to pick up or drop off passengers outside buildings. The study was conducted from May to June 2022. The participants were all over 20 years old motorcycle taxi drivers who were chosen through random sampling. The recruitment process was based on the inclusion and exclusion criteria. These criteria for the study are shown in Table 1.

Table 1. Inclusion and exclusion criteria for a cross-sectional study of motorcycle taxi drivers

Inclusion criteria	Exclusion criteria
Over 20 years of age	Diagnosis of chronic respiratory disease or any other chronic respiratory disease
Motorcycle taxi drivers who worked in ambient outdoor more than one year in Bangkok and adjacent provinces	Having an intermittent period working outdoor such as a stopping to work for other jobs outdoor and moving to indoor for doing work
Thai nationality and able to speak Thai language	Refusal to give informed consent

All participants must have a negative result for COVID-19 with a screening antigen test kit prior to interview and RPM measurement.

2.3 Data collection and instruments

The questionnaires were developed and adopted from previous studies by researchers which were approved by 3 experts before data collection with IOC; 0.70-1.00. Questionnaires were completed by face-to-face interviews with all participants. Exposure time (hour/day), frequency of exposure (days/years), duration of exposure (year), body weight (kg), and averaging time (days) were assessed via questionnaires.

The exposure to RPM of participants was measured using personal air sampling pumps with an aluminum cyclone and PVC membrane filter of 5.0 µm pore size (UNIVERSAL PCXR8, SKC, Inc., USA). Personal air sampling pumps were calibrated and set up at 2.5 L/min; NIOSH Method 0600 using the gravimetric (filter weight) technique for analyzing the mass of RPM in the air (National Institute for Occupational Safety and Health, 1998). After RPM samples were completed, questionnaires were collected and analyzed.

2.4 Data analysis

The data were analyzed with the statistical program Statistical Package for Social Sciences (SPSS version 23). Descriptive statistics were used for analyzing the data. Furthermore, health risk assessment was conducted by using data analysis from the questionnaires and RPM measurements. The RPM concentration limit of 3 mg/m^3 (inhalation slope factor) was used as a reference concentration for this study (USEPA, 2019). The equation parameter in Equation (1) was used to describe the potential dose of RPM among motorcycle taxi drivers.

$$\text{Average Daily Dose (ADD)} = \frac{\text{C}\times\text{IR}\times\text{ET}\times\text{EF}\times\text{ ED}}{\text{BW}\times\text{AT}} \quad (1)$$

Where; ADD=Average Daily Dose (mg/kg·day); C=RPM concentration (mg/m^3); IR= Intake rate (m^3/h);

ET=Exposure time (h/day); EF=Frequency of exposure (days/year); ED=Duration of exposure (year); BW=Body weight (kg); AT=Averaging time (days).

Hazard Quotient (HQ) was used to describe risk to human health caused by RPM exposure. HQ was the ratio of the potential exposure to RPM and the level at which no adverse effects are expected, as shown in Equation (2). HQ less than or equal to 1 indicates that adverse effects are not likely to occur, and thus can be considered to have negligible hazard. HQ greater than 1 are not statistical probabilities of harm occurring.

$$HQ = \frac{ADD}{RfC} \quad (2)$$

2.5 Ethical approval

Ethical approval to conduct this study was received from the Human Research Ethics Committee of Thammasat University, No.3. Ethical approval number 031/2565, and the approval date was April 29, 2022.

3. RESULTS AND DISCUSSION

3.1 Demographics information for health risk assessment

Table 2 shows the demographic information of the participants. Data collection was grouped by the six areas, consisting of Bangkok (BKK), Pathumthani (PTT), Samut Prakan (SPK), Samut Sakhon (SKN), Nonthaburi (NBI), and Nakhon Pathom (NPT). The distribution of the collected sample was determined by the density of motorcycle taxi drivers. BKK collected the most samples (37.3%), followed by SPK (22.2%), PTT (13.7%), NBI (9.8%), SKN (10.5%), and NPT (6.5%). There were 153 participants, including 7 females and 146 males. The results showed that 41.8% of the male participants were between 50-59 years old, 39.9% of the participants had never smoked before. Most of the participants (58.8%) had more than 10 years of experience in this occupation and took 11 hours a day to perform their work almost every day. Almost all of the participants used respiratory protection equipment while performing work. The types of respiratory protective equipment used by the participants were surgical masks (92.2%), hygienic masks made from cotton (7.8%), muslin masks (7.8 %), N95 masks (3.9%), and buff masks (2.6%), respectively.

3.2 Parameters of the ADD and HQ for RPM

HQ was used to describe the potential exposure to RPM in terms of average daily dose and level at which no adverse effects were expected, also known as the reference dose. Both ADD and HQ for RPM in each province are shown in Table 3.

Table 2. Demographics of the participants by six provinces (n=153).

Characteristics		No. (%) of participant						
		BKK	Adjacent provinces					Total
			NBI	PTT	SPK	SKN	NPT	
Gender	Male	55 (96.5)	14 (93.3)	20 (95.2)	33 (97.1)	15 (93.8)	9 (90.0)	146 (95.4)
	Female	2 (3.5)	1 (6.7)	1 (4.8)	1 (2.9)	1 (6.2)	1 (10.0)	7 (4.6)
Age (year)	20-29	4 (7.0)	0 (0.0)	1 (4.8)	1 (2.9)	1 (6.3)	0 (0.0)	7 (4.6)
x̄±SD (min.-max.) = 50.75±10.38 (20.0-79.0)	30-39	11 (19.3)	0 (0.0)	3 (14.3)	0 (0.0)	1 (6.3)	0 (0.0)	15 (9.8)
	40-49	16 (28.1)	2 (13.3)	3 (14.3)	12 (35.3)	5 (31.1)	4 (40.0)	42 (27.5)
	50-59	21 (36.8)	7 (46.7)	13 (61.8)	12 (35.3)	8 (50.0)	3 (30.0)	64 (41.8)
	≥60	5 (8.8)	6 (40.0)	1 (4.8)	9 (26.5)	1 (6.3)	3 (30.0)	25 (16.3)
Smoking history	Never-smoker	30 (52.6)	5 (33.3)	3 (14.3)	14 (41.2)	7 (43.8)	2 (20.0)	61 (39.9)
	Current smoker	24 (42.1)	6 (40.0)	10 (47.6)	8 (23.5)	2 (12.4)	8 (80.0)	58 (37.9)
	Former smoker	3 (5.3)	4 (26.7)	8 (38.1)	12 (35.3)	7 (43.8)	0 (0)	34 (22.2)

Table 2. Demographics of the participants by six provinces (n=153) (cont.)

Characteristics		No. (%) of participant						
		BKK	Adjacent provinces					Total
			NBI	PTT	SPK	SKN	NPT	
Work experience (year)	<5	19	3	8	6	4	1	41
x̄±SD (min.-max.) =		(33.3)	(20.0)	(38.1)	(17.6)	(25.0)	(10.0)	(26.8)
12.24±9.05 (1.0-40.0)	5-10	9	0	4	6	1	2	22
		(15.8)	(0)	(19.0)	(17.6)	(6.3)	(20.0)	(14.4)
	>10	29	12	9	22	11	7	90
		(50.9)	(80.0)	(42.9)	(64.8)	(68.7)	(70.0)	(58.8)
Work hour	<8	4	1	3	2	1	1	12
(hour per day)		(7.0)	(6.7)	(14.3)	(5.9)	(6.3)	(10.0)	(7.8)
x̄±SD (min.-max.) =	≥8	53	14	18	32	15	9	141
11.89±2.75 (3.0-18.0)		(93.0)	(93.3)	(85.7)	(94.1)	(93.7)	(90.0)	(92.2)
Working day per week	≤6	6	3	3	3	0	1	32
(days)		(10.5)	(20.0)	(14.3)	(8.8)	(0)	(10.0)	(20.9)
x̄±SD (min.-max.) =	7	51	12	18	31	16	9	121
6.61±0.92 (2.0-7.0)		(89.5)	(80.0)	(85.7)	(91.2)	(100.0)	(90.0)	(79.1)
Respiratory protection	Use	56	15	21	34	16	10	152
equipment while work		(98.2)	(100.0)	(100.0)	(100.0)	(100.0)	(100.0)	(99.3)
performing	Not use	1	0	0	0	0	0	1
		(1.8)	(0)	(0)	(0)	(0)	(0)	(0.7)
Types of respiratory protection equipment	Surgical masks							
	Yes	54	15	19	30	14	9	141
		(94.7)	(100.0)	(90.5)	(88.2)	(87.5)	(90.0)	(92.2)
	No	3	0	2	4	2	1	12
		(5.3)	(0)	(9.5)	(11.8)	(12.5)	(10.0)	(7.8)
	Hygienic masks made from cotton							
	Yes	1	0	2	4	5	0	12
		(1.8)	(0)	(9.5)	(11.8)	(31.3)	(0)	(7.8)
	No	56	15	19	30	11	10	141
		(98.2)	(100.0)	(90.5)	(88.2)	(68.7)	(100.0)	(92.2)
	Muslin masks							
	Yes	6	0	1	2	1	2	12
		(10.5)	(0)	(4.8)	(5.9)	(6.3)	(20.0)	(7.8)
	No	51	15	20	32	15	8	141
		(89.5)	(100.0)	(95.2)	(94.1)	(93.7)	(80.0)	(92.2)
	N95 masks							
	Yes	1	0	4	0	1	0	6
		(1.8)	(0)	(19.0)	(0)	(6.3)	(0)	(3.9)
	No	56	15	17	34	15	10	147
		(98.2)	(100.0)	(81.0)	(100.0)	(93.7)	(100.0)	(96.1)
	Buff masks							
	Yes	0	0	3	0	1	0	4
		(0)	(0)	(14.3)	(0)	(6.3)	(0)	(2.6)
	No	57	15	18	34	15	10	149
		(100.0)	(100.0)	(85.7)	(100.0)	(93.7)	(100.0)	(97.4)

The average RPM concentration from six provinces ranged from 0.007-0.031 mg/m^3. BKK showed the highest average RPM concentration (0.031 mg/m^3), followed by PTT (0.028 mg/m^3), SPK (0.009 mg/m^3), NPT (0.008 mg/m^3), NBI (0.007 mg/m^3), and SKN (0.006 mg/m^3), respectively. The RPM concentration of all areas did not exceed the OSHA (5 mg/m^3) and ACGIH (3 mg/m^3) standards. Additionally, the overall average RPM exposure concentration among motorcycle taxi drivers was 0.015 mg/m^3, and the maximum RPM exposure concentration was 0.365 mg/m^3. This is the first report on RPM exposure concentration among motorcycle taxi drivers by using air personal sampling. Most previous studies collected data on RPM concentration from ambient air (ChooChuay et al., 2020; Kirwa et

Table 3. Parameters of the ADD and HQ for RPM in each province

Parameter	Unit	BKK		Adjacent provinces								Total	
				PTT		SPK		SKN		NBI		NPT			
		Mean	Max	Mean	Max	Mean	Max	Mean	Max	Mean	Max	Mean	Max	Mean	Max
C	mg/m^3	0.031	0.365	0.028	0.099	0.009	0.025	0.006	0.024	0.028	0.099	0.008	0.018	0.015	0.365
IR	m^3/hr	15.2	15.2	15.2	15.2	15.2	15.2	15.2	15.2	15.2	15.2	15.2	15.2	15.2	15.2
ET	hr/day	12.4	18.0	11.1	15.0	12.1	16.0	11.4	16.0	11.1	15.0	10.7	13.0	11.6	18.0
EF	day/year	316.8	336.0	316.8	336.0	316.8	336.0	326.4	336.0	316.8	336.0	326.4	336.0	316.0	336.0
ED	year	29.00	30.00	34.00	35.00	29.00	30.00	28.00	30.00	34.00	35.00	38.00	40.00	31.17	40.00
BW	kg	69.90	120.00	67.10	100.00	74.00	100.00	72.50	105.00	67.10	100.00	59.00	71.00	69.17	120.00
AT	day	9,187	10,080	10,771	11,760	9,187	10,080	9,139	10,080	10,771	11,760	12,220	13,440	9,832	13,440
ADD	mg/kg-day	0.084	0.832	0.070	0.226	0.022	0.061	0.014	0.056	0.070	0.226	0.022	0.050	0.038	0.832
HQ	-	0.028	0.277	0.023	0.075	0.007	0.020	0.005	0.019	0.023	0.075	0.007	0.017	0.013	0.277

al., 2021; Ibrahim et al., 2021; Glenn et al., 2022; Wright et al., 2023; Dondi et al., 2023), which did not demonstrate their outdoor workers had been exposed to RPM. The advantage of personal air sampling showed the participants were actually exposed to respirable dust when compared to ambient air pollution sampling. Therefore, personal air sampling study has a clearer relationship to the health risk, especially in the respiratory system among outdoor workers than area sampling.

In Bangkok and adjacent provinces, the health risk assessment for RPM was concerned with the health impact of exposure to pollutants. HQ values were used to calculate the non-carcinogenic risk of RPM exposure. Non-carcinogenic risk refers to all adverse health effects in an organism caused by environmental factors other than cancer. This risk is calculated based on the ADD and took the reference values or RfC doses (3 mg/m^3; inhalation slope factor) into account. Table 3 indicates the ADD values for motorcycle taxi drivers in Bangkok and adjacent provinces.

The average ADD value (0.084 mg/kg-day) from RPM exposure in Bangkok was higher than each of the adjacent provinces (PTT, SPK, SKN, NBI, and NPT), and the overall average ADD value (0.038 mg/kg-day) from exposure to RPM in the adjacent provinces was lower than the Bangkok average. In addition, the maximum ADD value (0.832 mg/kg-day) from RPM exposure in Bangkok was higher than in any of the adjacent provinces and also it was observed that the average HQ values for motorcycle taxi drivers from inhalation RPM exposure ranged from 0.005-0.028, while the maximum HQ values ranged from 0.016-0.277. All areas for data collection showed average and maximum HQ values of between 0.013 and 0.277. The average and maximum HQ values from RPM exposure in Bangkok were higher than the adjacent provinces. However, the HQ values of all areas were less than 1.0 which indicated a low hazard risk. The low hazard risk results may be due to the sampling period overlapping with the rainy season in Thailand, which can affect RPM concentrations. This is an important parameter for HQ values. This result differed from the previous studies (Yunesian et al., 2019; Algarni et al., 2021; Neamhom et al., 2021; Gruszecka-Kosowska et al., 2021; Tian et al., 2022; Sah, 2023) which stated that particulate matter from resuspended dust (PM10 and PM2.5) caused a higher health risk. Those studies collected data during the winter and summer seasons.

For uncertainty of source-specific risks, HQ is sensitive for different variables, because they are dominated by components with different uncertainties. Moreover, these findings were consistent with previous studies (Thongthammachart, 2018; Mbazima, 2022; Zhou et al., 2023). These studies revealed that HQ values for $PM_{2.5}$-bound polycyclic aromatic hydrocarbons (PAHs) from the atmosphere were far lower than 1 for all populations, which was considered to have negligible hazard. In addition to $PM_{2.5}$-bound PAHs, it was also found that the ecological risk assessment of PM_{10} exposure was gradually acceptable risk in almost all data collection areas. A few data collection areas were found to be of high risk to human health. However, the human health risk for people in sensitive groups would be risk from exposure to RPM in Bangkok and adjacent provinces (Arphorn et al., 2018; Amnuaylojaroen et al., 2022).

4. CONCLUSIONS

Outdoor air pollution is a leading cause of death and premature death globally. Motorcycle taxi drivers are most at risk associated with occupational exposure to ambient air pollution in urban areas. They must drive to pick up or drop off passengers outside buildings throughout their working hours, on average 12 hours per day, ranging from 3-18 hours per day. Therefore, there is a greater chance of exposure to ambient air pollution than in other occupations. RPM was measured in Bangkok and adjacent provinces during the rainy season in Thailand. Bangkok indicated the highest average RPM concentration. The HQ values for Bangkok and adjacent provinces indicated a negligible risk ($HQ \leq 1$). Most of the motorcycle taxi drivers were without adverse health effects because these values are at acceptable levels. However, some of them may have adverse health effects due to individual sensitivities. Motorcycle taxi drivers might have a decreased lung function from direct exposure to RPM in their work environment. Even though exposure to RPM is minimal, it is continuous exposure that gradually causes long-term effects on lung function. Our research assists in conveying prevention measures to delay lung dysfunction in motorcycle taxi drivers.

ACKNOWLEDGEMENTS

This research project is supported by National Research Council of Thailand (NRCT): NRCT5-RGJ63008-103.

REFERENCES

Algarni S, Khan RA, Khan NA, Mubarak NM. Particulate matter concentration and health risk assessment for a residential building during COVID-19 pandemic in Abha, Saudi Arabia. Environmental Science and Pollution Research 2021;28 (46):65822-31.

Amnuaylojaroen T, Parasin N, Limsakul A. Health risk assessment of exposure near-future $PM_{2.5}$ in Northern Thailand. Air Quality, Atmosphere and Health 2022;15:1963-79.

Arphorn S, Ishimaru T, Hara K, Mahasandana S. Considering the effects of ambient particulate matter on the lung function of motorcycle taxi drivers in Bangkok, Thailand. Journal of the Air and Waste Management Association 2018;68(2):139-45.

ChooChuay C, Pongpiachan S, Tipmanee D, Suttinun O, Deelaman W, Wang Q, et al. Impacts of $PM_{2.5}$ sources on variations in particulate chemical compounds in ambient air of Bangkok, Thailand. Atmospheric Pollution Research 2020;11(9):1657-67.

Boonchu W. Comparative Study of Lung Function of Street Sweepers between the Inner and Outer Districts of Bangkok [dissertation]. Mahidol University; 2005.

Bureau of Highway Safety, Departmant of Highways. Traffic volume on highways in Bangkok Metropolitan Region [Internet]. 2021 [cited 2022 Oct 22]. Available from: http://bhs.doh.go.th/download/traffic.

Damayanti T, Pradipta J, Susanto A. Respiratory symptoms and lung function among online motorcycle taxi drivers. Proceedings of the Chest Annual Meeting; 2019 Oct 19-23; New Orleans; LA, USA; 2019.

Dondi A, Carbone C, Manieri E, Zama D, Del Bono C, Betti L, et al. Outdoor air pollution and childhood respiratory disease: The role of oxidative stress. International Journal of Molecular Sciences 2023;24(5):Article No. 4345.

Glenn BE, Espira LM, Larson MC, Larson PS. Ambient air pollution and non-communicable respiratory illness in sub-Saharan Africa: A systematic review of the literature. Environmental Health 2022;21(1):Article No. 40.

Gruszecka-Kosowska A, Dajda J, Adamiec E, Helios-Rybicka E, Kisiel-Dorohinicki M, Klimek R, et al. Human health risk assessment of air pollution in the regions of unsustainable heating sources. Case study-The tourist areas of southern poland. Atmosphere 2021;12(5):Article No. 615.

Ibrahim MF, Hod R, Nawi AM, Sahani M. Association between ambient air pollution and childhood respiratory diseases in low- and middle-income Asian countries: A systematic review. Atmospheric Environment 2021;256:Article No. 118422.

Kanjanasiranont N, Prueksasit T, Morknoy D. Inhalation exposure and health risk levels to BTEX and carbonyl compounds of traffic policeman working in the inner city of Bangkok, Thailand. Atmospheric Environment 2017;152:111-20.

Kheunpeck C, Tantipanchaporn T. Predicting factors of preventive behaviors from air pollution exposure among motorcycle taxi drivers in Mae Sot District, Tak Province. Journal of Safety and Health 2016;9(33):14-25 (in Thai).

Kirwa K, Eckert CM, Vedal S, Hajatet A, Kaufman JD. Ambient air pollution and risk of respiratory infection among adults: Evidence from the multiethnic study of atherosclerosis (MESA). BMJ Open Respiratory Research 2021; 8(1): e000866.

Loonsamrong W, Taneepanichskul N, Puangthongthub S, Tungsaringkarn T. Health risk assessment and BTEX exposure among car park workers at a parking structure in Bangkok, Thailand. Journal of Health Research 2017;29(4):285-92.

Mbazima SJ. Health risk assessment of particulate matter 2.5 in an academic metallurgy workshop. International Journal of Indoor Environmental and Health 2022;32(9):e13111.

National Institute for Occupational Safety and Health. NIOSH manual of analytical methods (NMAM), method 0600 particulates not otherwise regulated respirable [Internet]. 1998 [cited 2022 Dec 10]. Available from: https://www.cdc.gov/niosh/docs/2003-154/pdfs/0600.pdf.

National Statistical Office. Number of employed people in formal and informal workers Classified by age group, sex, region and province, 2011 - 2020 [Internet]. 2021 [cited 2021 Aug 16]. Available from: http://statbbi.nso.go.th/staticreport/page/sector/th/02.aspx.

Neamhom T, Patthanaissaranukool W, Pinatha Y, Chommueang B. Health risk and predictive equation for $PM_{2.5}$ using TSP and PM_{10} variables in office buildings. Songklanakarin Journal of Science and Technology 2021;43(3):834-9.

Ongwandee M, Chavalparit O. Commuter exposure to BTEX in public transportation modes in Bangkok, Thailand. Journal of Environmental Sciences 2010;22(3):397-404.

Phanprasit W. Industrial Hygiene: Strategy Assessment Control and Management. 1st ed. Bangkok: Mahidol University; 2014. (in Thai).

Pollution Control Department. Overall air quality reporting [Internet]. 2022 [cited 2022 Oct 22]. Available from: http://air4thai.pcd.go.th/webV3/#/Home.

Putri Anis Syahira MJ, Karmegam K, Nur Athirah Diyana MY, Irniza R, Shamsul Bahri MT, Vivien H, et al. Impacts of $PM_{2.5}$ on respiratory system among traffic policemen. Work 2020;66(1):25-9.

Sah D. Concentration, source apportionment and human health risk assessment of elements in $PM_{2.5}$ at Agra, India. Urban Climate 2023;49:Article No. 101477.

Sonjai P. Knowledge and Behavior of Self-Protection from Air Pollution and Noise of Motorcycle Taxi Drivers in Nakhon Pathom Municipality [dissertation]. Mahidol University; 2001.

Statista. Number of registered motorcycles in Thailand from 2012 to the first eight months of 2021 [Internet]. 2022 [cited 2022 Apr 22]. Available from: https://www.statista.com/statistics/1179962/thailand-number-of-registered-motorcycles/.

Suebsuk P, Pongnumkul A, Leartsudkanung D, Sareewiwatthana P. Predicting factors of lung function among motorcycle taxi drivers in the Bangkok metropolitan area. Journal of Public Health 2014;44(1):79-92 (in Thai).

Thongthammachart T. PM_{10} and $PM_{2.5}$ Concentrations in Bangkok over 10 Years and Implications for Air Quality [dissertation]. Chulalongkorn University; 2018.

Thurston GD, Kipen H, Annesi-Maesano I, Balme J, Brook RD, Cromar K, et al. A joint ERS/ATS policy statement: What constitutes an adverse health effect of air pollution? An analytical framework. European Respiratory Journal 2017;49(1):Article No. 1600419.

Tian Y, Jia B, Zhao P, Song D, Huang F, Feng Y. Size distribution, meteorological influence and uncertainty for source-specific risks: $PM_{2.5}$ and PM_{10}-bound PAHs and heavy metals in a Chinese megacity during 2011-2021. Environmental Pollution 2022;312:Article No. 120004.

Tunsaringkarn T, Siriwong W, Rungsiyothin A, Nopparatbundit S. Occupational exposure of gasoline station workers to BTEX compounds in Bangkok, Thailand. The International Journal of Occupational and Environmental Medicine 2012;3(3):117-25.

United States Environmental Protection Agency (USEPA). Human health risk assessment [Internet]. 2022 [cited 2022 Oct 24]. Available from: https://www.epa.gov/risk/human-health-risk-assessment#tab-1.

United States Environmental Protection Agency (USEPA). Regional screening level (RSL) summary table [Internet]. 2019 [cited 2022 Dec 10]. Available from: https://www.epa.gov/risk/regional-screening-levels-rsls-generic-tables.

Wright N, Newell K, Chan KH, Gilbert S, Hacker A, Lu Y, et al. Long-term ambient air pollution exposure and cardio-respiratory disease in China: Findings from a prospective cohort study. Environmental Health 2023;22(1):Article No. 30.

Yunesian M, Rostami R, Zarei A, Fazlzadeh M, Janjani H. Exposure to high levels of PM_{10} and $PM_{2.5}$ in the metropolis of Tehran and the associated health risks during 2016-2017. Microchemical Journal 2019;150:Article No. 104174.

Zhou J, Guo Z, Liu J, Gao M, Sun X, Sheng Y, et al. $PM_{2.5}$ -bound polycyclic aromatic hydrocarbons (PAHs) from the atmosphere of Xi'an, China: Seasonal variation, sources, and health risk assessments. Hygiene and Environmental Health Advances 2023;5:Article No. 100041.

Environment and Natural Resources Journal

Volume 22
Issue 4
2024

Optimization of Diclofenac Treatment in Synthetic Wastewater using Catalytic Ozonation with Calcium Peroxide as Catalyst

Papitchaya Chookaew[1], Apiradee Sukmilin[2], and Chalor Jarusutthirak[1*]

[1]Department of Environmental Technology and Management, Faculty of Environment, Kasetsart University, Bangkok, Thailand
[2]Environmental Science and Technology Program, Faculty of Science and Technology, Phranakhon Rajabhat University, Bangkok, Thailand

ARTICLE INFO

Received: 11 Apr 2024
Received in revised: 12 Jun 2024
Accepted: 19 Jun 2024
Published online: 18 Jul 2024
DOI: 10.32526/ennrj/22/20240102

Keywords:
Box-Behnken experimental design/ Calcium peroxide/ Catalytic ozonation/ Diclofenac/ Response surface methodology

*** Corresponding author:**
E-mail: ecclj@ku.ac.th

ABSTRACT

This research studied the performance of ozonation process combined with calcium peroxide (CaO_2) as a catalyst for the removal of diclofenac (DCF) from synthetic wastewater. The experiments were conducted using venturi-type ozonation with an ozone production rate of 96.30 mg/h. Response surface methodology (RSM) with a Box-Behnken experimental design (BBD) was used to investigate the DCF removal efficiency by optimizing the catalytic ozonation process and analyzing the influence of key parameters: solution pH (5.0-9.0), initial DCF concentration (10-25 mg/L), CaO_2 dosage (1-3 g/L), and reaction time (30-90 min), on the DCF removal efficiencies. Analysis of variance (ANOVA) indicated that the experimental model derived from the RSM-BBD was best suited to a quadratic regression model, with a coefficient of determination (R^2) of 0.84. The model demonstrated that the optimal conditions for achieving the highest DCF removal efficiency of up to 100% were an initial DCF concentration of 10 mg/L, solution pH of 7, CaO_2 dosage of 2 g/L, and reaction time of 90 min. Using these conditions, the actual DCF removal efficiency from a confirmation test was 97.6%. The accuracy of the model was verified; the root mean square error (RMSE) was 5.90 and the mean absolute percentage error (MAPE) was 6.10%, indicating that the regression model could be used to predict the DCF removal efficiency under various conditions. The results showed that catalytic ozonation using CaO_2 as a catalyst could effectively remove DCF in synthetic wastewater.

1. INTRODUCTION

Diclofenac (DCF) is a non-steroidal anti-inflammatory drug of the phenylacetic acid class that is widely used in analgesics for humans, livestock, and domestic animals, for the treatment of muscle, joint, and bone pain from both rheumatic and non-rheumatic origins (Tra et al., 2023). The annual worldwide usage of DCF was approximately 940 t, as indicated by trend analysis from 2020 to 2027 based on pharmaceutical consumption (Alessandretti et al., 2021). Generally, DCF is continuously introduced into the environment in waste by pharmaceutical industries, hospitals, and household drainage, raising major environmental concerns. This emerging contaminant can readily enter wastewater and surface water through various routes, including excretion by humans and animals, as well as in discharges from industrial and municipal wastewater treatment facilities (Davies and Anderson, 1997; Sathishkumar et al., 2020; Thalla and Vannarath, 2020). DCF has been detected in the environment in both its original form and as metabolites at concentrations ranging from nanograms per liter (ng/L) to milligrams per liter (mg/L), with the actual value dependent on its source and the effectiveness of wastewater treatment methods (Lonappan et al., 2016). Although the contamination of DCF in water sources has been detected only at relatively low amounts (micro or nano levels), DCF is toxic to various aquatic organisms in the ecosystem, including green algae, microcrustaceans, and

Citation: Chookaew P, Sukmilin A, Jarusutthirak C. Optimization of diclofenac treatment in synthetic wastewater using catalytic ozonation with calcium peroxide as catalyst. Environ. Nat. Resour. J. 2024;22(4):354-365. (https://doi.org/10.32526/ennrj/22/20240102)

invertebrates (Zind et al., 2021). DCF was reported to induce lethal effects by causing damage to renal and gastrointestinal tissues in various vertebrates such as fish (Lonappan et al., 2016). In addition, DCF may present an adverse ecological risk to non-target organisms due to biomagnification within the food chain (Sathishkumar et al., 2020). Therefore, appropriate treatment of wastewater containing DCF is necessary prior to releasing it into natural water sources, to minimize its environmental impact.

Conventional wastewater treatment, such as activated sludge, cannot effectively remove DCF due to the complicated structure of DCF that resists biological degradation (Jabbari et al., 2020). An adsorption process can remove DCF in rapidly, however, it causes adsorbent disposal problems (Beltran et al., 2009). Nanofiltration (NF) and reverse osmosis (RO) are very effective at removing DCF and other pharmaceutically active compounds (PhAcs), however, retentate streams with high concentrations of pollutants must be removed before discharge into water sources (Maryam et al., 2020; Alonso et al., 2024). Chemical oxidation using potassium permanganate ($KMnO_4$) and chlorine (Cl_2) are effective in DCF treatment as they have strong oxidizing properties (Wang et al., 2023). However, they have a limitation on toxic residuals in the environment (Gomes et al., 2019; M'Arimi et al., 2020). Ozone oxidation is effective in the removal of DCF because ozone is a powerful oxidant with a high oxidation potential of 2.07 V (Alharbi et al., 2022). It reacts with the organic compounds either directly as molecular ozone or indirectly through the hydroxyl radical (OH·). Nevertheless, direct ozonation has a main drawback due to the selective nature of ozone, its limited mass transfer, and slow rate of reaction (Malik et al., 2020). Catalytic ozonation, an effective method of advanced oxidation processes (AOPs), is a promising technology for the treatment of recalcitrant contaminants present in wastewater (Bilińska et al., 2022). It generates reactive free radicals (primarily the hydroxyl radical) with a higher oxidation potential than that of ozone (E°=2.80 V). It is capable of oxidizing and completely mineralizing refractory organic compounds to CO_2 and H_2O with increasing rates of degradation, leading to reduction in the reaction time and operating cost (Rosales et al., 2019; Sun et al., 2019). Combining ozonation with a catalyst has been used to enhance the removal efficiencies of DCF and other PhAcs. Ozone combined with hydrogen peroxide (H_2O_2), known as peroxone, has been proved as an efficient method for the degradation of organic compounds, as the ozone is catalyzed to produce OH· (Chen and Wang, 2021). However, H_2O_2 is a strong oxidizer which enhances the combustion of other substances, causing restrictions in its use, storage, and transportation. To solve this limitation, calcium peroxide (CaO_2) has been introduced to use in combination with the ozonation process, because CaO_2 can release H_2O_2 and $Ca(OH)_2$ through a dissolution process (Lu et al., 2017; Xiang et al., 2021). The released H_2O_2 from CaO_2 can react with O_3 to generate OH· and accelerate the degradation of organic compounds (Nuar et al., 2023). Additionally, the released $Ca(OH)_2$ increases the alkalinity of the solution, which promotes O_3 to transform into more OH· (Wang et al., 2016; Javid et al., 2020). Therefore, ozonation using CaO_2 as a catalyst is considered to be a very practical technology for wastewater treatment, due to its high removal efficiency together with the advantages of easy handling, stability, safety, and reasonable cost (Xu et al., 2020). Other studies have revealed that CaO_2 could be effectively used as a catalyst in ozonation process to remove phenol, sulfamethoxazole, and oxytetracycline (Honarmandrad et al., 2021; Xiang et al., 2021). However, there is no published information regarding using CaO_2 as a catalyst in the ozonation process to degrade DCF.

When utilized in combination, the interaction between O_3 and CaO_2 as a source of peroxide results in synergistic effects that influence removal efficiency. These effects vary depending on their interaction mechanisms; either O_3 acts as the activator for the peroxide, or the peroxide acts as the activator for O_3 (Chen et al., 2024). Furthermore, different control parameters, such as pH, CaO_2 dose, and reaction time, influence DCF removal efficiency. Currently, the optimization of these parameters is carried out on a trial-and-error basis. However, traditionally, this involves an experimental technique based on varying a single factor while fixing the remaining parameters at a certain set of conditions (Dwivedi and Sharma, 2015). Additionally, the single-dimensional factor of the experiment is not only time-consuming but also the attained optimum conditions are not accurate due to neglecting interactions between the operating variables (Ferreira et al., 2023). To solve this problem, response surface methodology (RSM) has been suggested to define the effects of individual parameters. RSM is a statistical and mathematical tools that has been proved valuable for the multifactor optimization of various processes (Dehghani et al.,

2016; Norabadi et al., 2020; Jafari et al., 2023). The Box-Behnken experimental design (BBD) is a widely exploited form of RSM, particularly tailored for 3 levels (-1, 0, and +1). BBD is more efficient than other factorial designs including the central composite design (CCD) and requires fewer experiments (Witek-Krowiak et al., 2014). More recently, RSM has been extensively used in the optimization of operating parameters in combined systems (Jasnia et al., 2020).

The novelty of the current research can be attributed to the use of calcium peroxide as a catalyst in the ozonation process for the degradation of DCF in wastewater, along with the statistical analysis using RSM with BBD to examine the effect of selected independent variables (initial DCF concentration, pH, CaO_2 dose, and reaction time) on the DCF removal efficiency. The mathematic model obtained from the study can be applied to determine the optimum conditions and to predict the performance of the catalytic ozonation process using CaO_2 as a catalyst in the removal of DCF. The expected results from this research should inform the use of CaO_2 combined with the ozonation process, with upscaling to treat wastewater contaminants such as DCF, other PhACs, and other emerging pollutants.

2. METHODOLOGY

2.1 Chemicals

Sodium thiosulfate ($Na_2S_2O_3$) and calcium sulfate ($CaSO_4$) were obtained from Ajax (Australia). Potassium hydroxide (KOH) and sodium hydroxide (NaOH) were purchased from KemAus (Australia). Hydrochloric acid (HCl), hydrogen peroxide (H_2O_2), and ethanol (C_2H_6O) were obtained from Qrec (New Zealand). All chemicals used in this experiment were of analytical grade.

2.2 Preparation of CaO_2 catalyst

The CaO_2 catalyst was prepared from calcium sulfate ($CaSO_4$), according to Vijuksungsith et al. (2021). First, 40 g of $CaSO_4$ was dissolved in 400 mL of RO water; then, 160 mL of 1 M potassium hydroxide (KOH) and 208 mL of hydrogen peroxide (H_2O_2) were added to the solution. The mixture was stirred thoroughly for 2 h. After that, the solution was centrifuged at 5,000 rpm for 5 min and the CaO_2 obtained was washed twice using RO water and once again using ethanol. Next, the CaO_2 was dried at 90°C for 24 h before storing in a desiccator until use. The as-prepared CaO_2 was characterized using X-ray diffractometry (XRD) and Fourier-transform infrared spectroscopy (FTIR).

2.3 Preparation of synthetic wastewater

Different concentrations of DCF in the synthetic wastewater were investigated (10, 17.5, or 25 mg/L) to serve as a representative range of DCF contamination levels typically found in wastewater from the pharmaceutical industry. A stock solution of 25 mg/L DCF was prepared from an enteric-coated tablet containing 25 mg DCF. The tablet was ground into powder and dissolved in RO water. After that, the solution was adjusted to 1 L with RO water and then passed through GF/C filter paper to eliminate any residue. The stock solution was diluted to the desired concentrations (10 or 17.5 mg/L) and the DCF concentration was determined using a colorimetric method with a spectrophotometer at a wavelength of 275 nm (Mukkawi et al., 2021).

2.4 Experimental setup

Ozone was generated using a laboratory-scale ozone generator with a production rate of 96.30 mg/h. The ozonation experiment was carried out in batch mode using an acrylic rectangular reactor with dimensions of 12×12×15 cm. Synthetic wastewater containing DCF (1.5 L) was circulated using a pump through a venturi device where a vacuum was created. At this point, ozone gas was fed in and mixed with wastewater before the ozonated wastewater returned to the reactor, as shown in Figure 1. Unreacted ozone gas was trapped by the sodium thiosulfate ($Na_2S_2O_3$) solution contained in two gas absorption bottles in series. In the catalytic ozonation process, the as-prepared CaO_2 catalyst at a specified dosage was filled in the reactor. The catalyst was mixed simultaneously using turbulence from the circulation pump. Aliquot samples of 30 mL were collected at 30, 60, and 90 min. Sodium metabisulfite ($Na_2S_2O_5$) was used to quench any residual ozone in the sample. The samples were passed through 0.45-µm nylon filter to separate any CaO_2 residue prior to analysis. The DCF concentration was determined using a colorimetric method with a spectrophotometer at a wavelength of 275 nm (Mukkawi et al., 2021). All experiments were performed in triplicate. Data presented in figures and tables were averaged from three initial values. The percentage of DCF removal was calculated according to Equation 1.

$$\text{Removal (\%)} = \left(\frac{[DCF]_0 - [DCF]_t}{[DCF]_0}\right) \times 100 \quad (1)$$

Where; $[DCF]_0$ is the initial concentration of DCF and $[DCF]_t$ is the concentration of DCF at time t of the reaction.

2.5 Box-Behnken experimental design and statistical analysis

A Box-Behnken experimental design was used to evaluate the main effect on DCF removal from the operational factors, as well as to determine the operational factor values that achieved maximum DCF removal efficiency. The experimental design involved 4 factors, 3 levels, and 27 experiments. The factors considered as independent variables were initial DCF concentration (x_1), pH (x_2), CaO_2 dosage (x_3) and reaction time (x_4). The percentage DCF removal efficiency (y) was used as the response variable, as shown in Table 1.

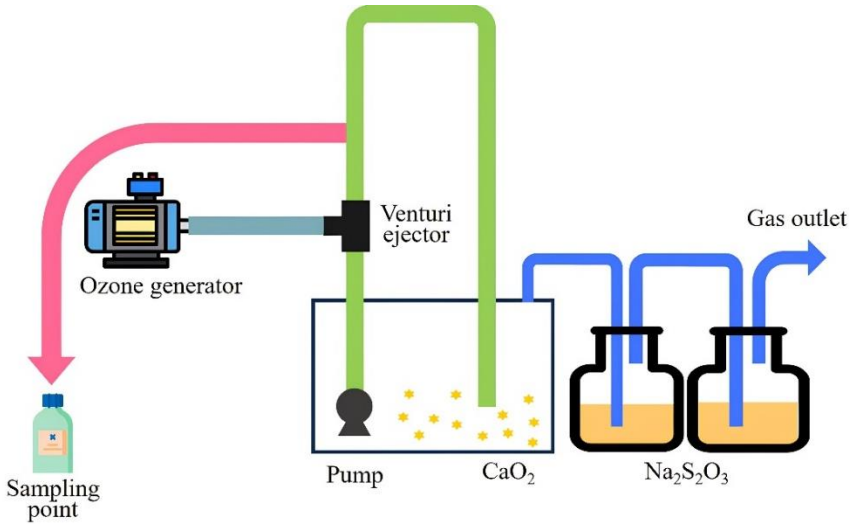

Figure 1. Catalytic ozonation system with venturi type

Table 1. Levels of each factor for Box-Behnken experimental design

Factor	Parameter	Code level		
		1-	0	1
x_1	Initial DCF concentration (mg/L)	10	17.5	25
x_2	pH	5	7	9
x_3	CaO_2 dosage (g/L)	1	2	3
x_4	Reaction time (min)	30	60	90

RSM was used to develop the optimization model and processes. RSM represents independent parameters quantitatively. The relationship between the independent and dependent variables can be illustrated using a quadratic model, as shown in Equation 2.

$$y = \beta_0 + \sum_{j=1}^{k} \beta_j x_j + \sum_{j=1}^{k} \beta_{jj} x_j^2 + \sum_i x \sum_{<j=2}^{k} \beta_{ij} x_i x_j + e_i \quad (2)$$

Where; y is the dependent variable (response parameter); x_i and x_j are the independent variables; β_o is intercept; β_j is the linear coefficient; β_{jj} is the quadratic coefficient; β_{ij} is the interaction coefficient; k is the number of factors studied and optimized in the experiment; and e_i is the random error. The optimum conditions for DCF removal were analyzed based on RSM using different variable combinations, according to the BBD.

Statistical analysis was conducted using analysis of variance (ANOVA) at the 95% confidence level. The quality of fit of the polynomial model was expressed using the coefficient of determination (R^2), as shown in Equation 3. Model accuracy was analyzed using the root mean squared error (RMSE) and the mean absolute percentage error (MAPE), as shown in Equation 4 and Equation 5, respectively.

$$R^2 = 1 - \frac{\sum_{i=1}^{n} (\hat{y}_i - y_i)^2}{\sum_{i=1}^{n} (\bar{y} - y_i)^2} \quad (3)$$

$$RMSE = \sqrt{\sum_{i=1}^{n} \frac{(\hat{y}_i - y_i)^2}{n}} \quad (4)$$

$$MAPE = \frac{\sum_{i=1}^{n} \left| \frac{(\hat{y}_i - y_i)}{\hat{y}_i} \right|}{n} \times 100 \quad (5)$$

Where; $R^2$is the coefficient of determination; $\hat{y}_i$ is the actual value obtained from the experiment; $\bar{y}$ is the average value obtained from the experiment; y_i is the predicted value obtained from the model; and n is the number of experiments.

3. RESULTS AND DISCUSSION

3.1 Characterization of CaO_2

The CaO_2 was synthesized based on the chemical precipitation from mixing $CaSO_4$ and H_2O_2. The representative results of the XRD analysis of the CaO_2 are shown in Figure 2. The XRD spectra show the different diffraction peaks at 2θ values of 31.9°, 35.4°, 47.7°, 54.7°, and 55.2°. These dominant peaks aligned with the XRD patterns of CaO_2 nanoparticles reported by Madan et al. (2017) and Prameswari et al. (2023). However, the XRD spectra also showed diffraction peaks at 2θ values of 14.8°, 25.7°, and 29.7°, corresponding to $CaSO_4$ as reported by Moncea et al. (2016). The contamination by $CaSO_4$ was possibly caused by using excess $CaSO_4$ as the reactant or incomplete reaction of CaO_2 production or both, as shown in Equation 6.

$$CaSO_4 + H_2O_2 \rightarrow CaO_2\,(hydrate) + H_2SO_4 \quad (6)$$

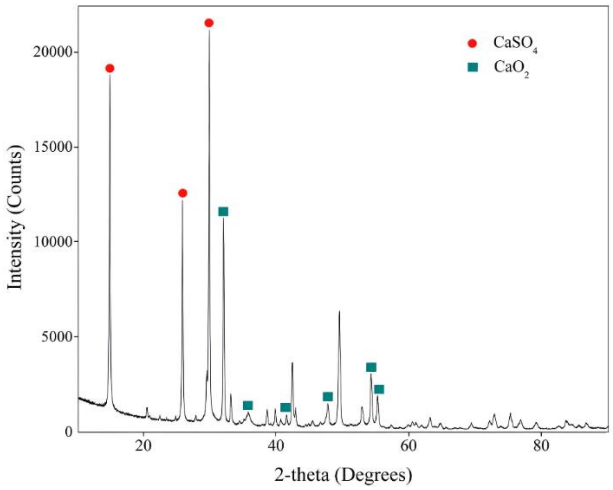

Figure 2. XRD pattern of as-prepared CaO_2 from $CaSO_4$

Figure 3 shows the FT-IR spectra in the wavenumber range 4,000-500 cm^{-1} to identify the functional groups present in the as-prepared CaO_2. According to the spectra, the peak at 599 cm^{-1} and the broad peak at 1,419 cm^{-1} were attributed to O-Ca-O stretching (Madan et al., 2017), whereas the peaks at 867 cm^{-1} corresponded to the O-O vibration of CaO_2 (Li et al., 2022; Dedecan et al., 2022). The FT-IR spectra also exhibited the presence of impurities from the unreacted $CaSO_4$ by the characteristic vibration bands of sulfate at the peaks of 659, 1,007, and 1,173 cm^{-1}. Furthermore, the peak at 1,621 cm^{-1} represented O-H stretching, related to the strongly held water molecules in the hydrated $CaSO_4$ (Melo et al., 2014). The peak at 3,612 cm^{-1} was attributed to O-H stretching vibrations, originating from moisture in the sample (Habte et al., 2019).

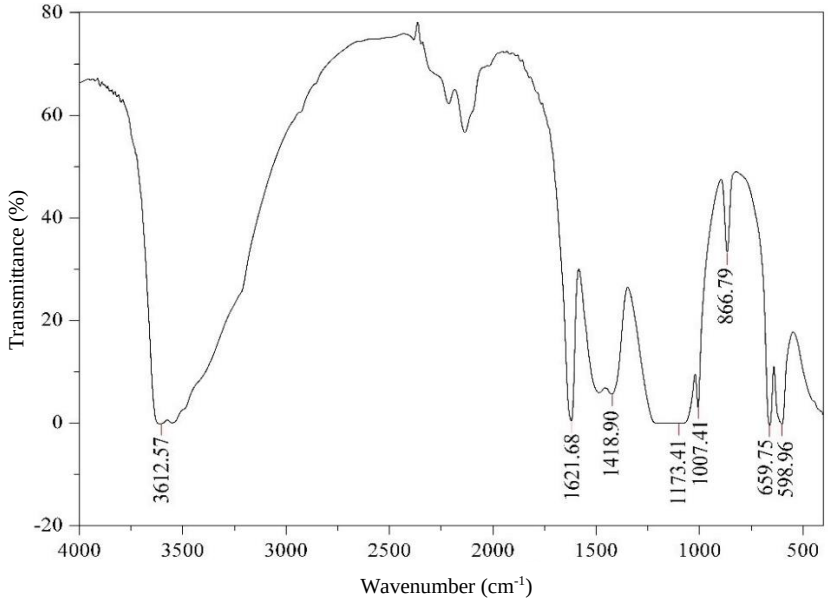

Figure 3. FT-IR spectra of CaO_2 synthesized from $CaSO_4$

3.2 Results from Box-Behnken experimental design and statistical analysis

The experiments involving the DCF removal based on catalytic ozonation using CaO_2 as a catalyst were conducted using a BBD, consisting of 27 experiment sets. The results of the DCF removal as the response variable affected by various factors are presented as a design matrix in Table 2. Statistical analysis revealed that the DCF removal percentage as response variable (y_1) was correlated with four design factors (x_1, x_2, x_3, x_4).

Model suitability analysis was performed to explain the changes in the DCF removal efficiency resulting from the initial DCF concentration, solution pH, CaO_2 dosage, and reaction time. Table 3 presents the statistical analysis of the correlations among these parameters using four models. The coefficient of determination (R^2) is an important parameter for validating model adequacy and this value must be at least 0.80 for the model to be considered a good fit (Aguilar-Ascón et al., 2024). According to Table 3, the full quadratic model had a low standard error of 8.5866 with the highest R^2 and adjusted R^2 values of 84.00% and 65.34%, respectively, demonstrating a good fit to the data and that the quadratic regression model was the most suitable of the tested models to explain DCF removal efficiency.

Table 2. Experimental design matrix and DCF removal based on experimental data results compared to predicted values

Order	DCF concentration (mg/L)	pH	CaO_2 dosage (g/L)	Time (min)	DCF removal efficiency (%)		%Error
	x_1	x_2	x_3	x_4	Actual value	Predicted value	
1	10	5	2	60	96.45	93.96	2.65
2	10	7	1	60	88.00	87.45	0.63
3	10	7	2	30	69.51	66.80	4.06
4	10	7	2	90	95.07	100.00	7.53
5	10	7	3	60	96.00	94.45	1.64
6	10	9	2	60	100.00	98.81	1.21
7	17.5	5	1	60	80.80	76.44	5.70
8	17.5	5	2	30	54.63	57.29	4.66
9	17.5	5	2	90	87.49	85.43	2.40
10	17.5	5	3	60	81.28	78.58	3.44
11	17.5	7	1	30	39.39	46.28	14.90
12	17.5	7	1	90	76.21	77.50	1.66
13	17.5	7	2	60	83.48	83.81	0.39
14	17.5	7	2	60	81.96	83.81	2.21
15	17.5	7	2	60	86.25	83.81	2.91
16	17.5	7	3	30	51.03	57.11	10.65
17	17.5	7	3	90	77.26	77.76	0.64
18	17.5	9	1	60	77.89	70.50	10.48
19	17.5	9	2	30	52.76	56.97	7.40
20	17.5	9	2	90	81.21	80.69	0.64
21	17.5	9	3	60	85.20	79.45	7.24
22	25	5	2	60	80.37	89.08	9.78
23	25	7	1	60	72.93	76.64	4.85
24	25	7	2	30	82.47	64.61	27.63
25	25	7	2	90	87.84	80.47	9.16
26	25	7	3	60	78.01	80.73	3.37
27	25	9	2	60	69.27	79.17	12.50

Table 3. Statistical summary for models predicting DCF removal efficiency

Model	S	R^2 (%)	R^2 (adj) (%)
Linear	11.5778	46.67	36.98
Linear + square	7.7746	71.58	55.73
Linear + interaction	13.1001	50.35	19.32
Full quadratic	8.5866	84.00	65.34

Note: S=standard deviation, R^2=coefficient of determination and R^2(adj)=adjusted R^2

The model for predicting the DCF removal efficiency was obtained from statistical analysis using RSM. This quadratic regression model presented the relationship of DCF removal efficiency with the independent variables of pH, initial DCF concentration, CaO_2 dosage, and reaction time, as shown in Equation 7.

$$\text{DCF removal efficiency (\%)} = -41.1 - 2.23\ \text{DCF} + 6.8\ \text{pH} + 29.8\ CaO_2 + 2.815\ \text{Time} + 0.1335\ \text{DCF} \times \text{DCF} - 0.266\ \text{pH} \times \text{pH} - 6.50\ CaO_2 \times CaO_2 - 0.01405\ \text{Time} \times \text{Time} - 0.246\ \text{DCF} \times \text{pH} - 0.097\ \text{DCF} \times CaO_2 - 0.0224\ \text{DCF} \times \text{Time} + 0.85\ \text{pH} \times CaO_2 - 0.0184\ \text{pH} \times \text{Time} - 0.088\ CaO_2 \times \text{Time} \quad (7)$$

The results of the regression analysis are presented in Table 4, revealing that the initial DCF concentration (x_1) and reaction time (x_4) variables were significant based on the response variable (y) with a p-value of 0.006 (<0.05). These findings suggested that the changes in these parameters significantly affected the DCF removal efficiency at the 95% confidence level. The interactions between variables indicated that DCF^2 (x_1^2) and $Time^2$ (x_1^2) had significant effects on DCF removal efficiency at the 95% confidence level. All the 2-way interactions among the variables had p-values that were greater than the significance level (p>0.05), indicating that those interactions had no significant effects on DCF removal efficiency based on catalytic ozonation using CaO_2 as a catalyst. However, the lack of fit was not significant (p=0.052) in the model, indicating that the model could be used to predict the response of DCF removal efficiency.

Table 4. Response surface model analysis of variance with variables

Source		SS	df	MS	F-value	p-value
Model		4,645.42	14	331.82	4.50	0.006
Linear		2,581.15	4	645.29	8.75	0.002
x_1	DCF	459.65	1	459.65	6.23	0.028
x_2	pH	17.63	1	17.63	0.24	0.634
x_3	CaO_2	93.94	1	93.94	1.27	0.281
x_4	Time	2,009.93	1	2009.93	27.26	0.000
Square		1,861.03	4	465.26	6.31	0.006
x_1^2	DCF×DCF	300.54	1	300.54	4.08	0.066
x_2^2	pH×pH	6.02	1	6.02	0.08	0.780
x_3^2	CaO_2×CaO_2	225.11	1	225.11	3.05	0.106
x_4^2	Time×Time	852.24	1	852.24	11.56	0.005
2-Way Interaction		203.24	6	33.87	0.46	0.825
x_1 x_2	DCF×pH	54.63	1	54.63	0.74	0.406
x_1 x_3	DCF×CaO_2	2.13	1	2.13	0.03	0.868
x_1 x_4	DCF×Time	101.94	1	101.94	1.38	0.262
x_2 x_3	pH×CaO_2	11.64	1	11.64	0.16	0.698
x_2 x_4	pH×Time	4.85	1	4.85	0.07	0.802
x_3 x_4	CaO_2×Time	28.05	1	28.05	0.38	0.549
Error		884.75	12	73.73		
Lack-of-fit		875.30	10	87.53	18.53	0.052
Pure error		9.45	2	4.72		

Note: SS=sum of squares, df=degree of freedom, MS=mean square error

3.3 Influence of parameters on DCF treatment by catalytic ozonation

DCF removal efficiency was optimized using RSM and a BBD, according to different variable factors. Contour plots were constructed to determine the optimum levels of the independent variables and the effects of individual factors were explained.

The regression analysis results indicated that initial DCF concentration and reaction time were significant parameters in the catalytic ozonation process. The effect of reaction time on DCF removal showed that as the reaction time increased, DCF removal efficiency increased. At 30 min, DCF removal efficiency was 69.51%, whereas DCF removal efficiency was 95.07% at 90 min. In the catalytic ozonation process, a long ozonation time was attributed to increased decomposition of the ozone and consequently the generation of the hydroxyl radical (OH·), which is a very powerful radical, that reacted with the DCF (Jabbari et al., 2020). The current findings were consistent with those of Norabadi et al. (2020) and Honarmandrad et al. (2021), which demonstrated that the removal percentage increased with longer reaction times. This observation could be attributed to the extended reaction time facilitating the generation of more hydroxyl radicals, thereby enhancing the degradation of pollutants. As shown in Figure 4, when the DCF concentration increased, the removal efficiency decreased. As a constant ozone concentration was applied to the system, when the DCF concentration increased, ozone and the hydroxyl radical had limited supply to oxidize DCF.

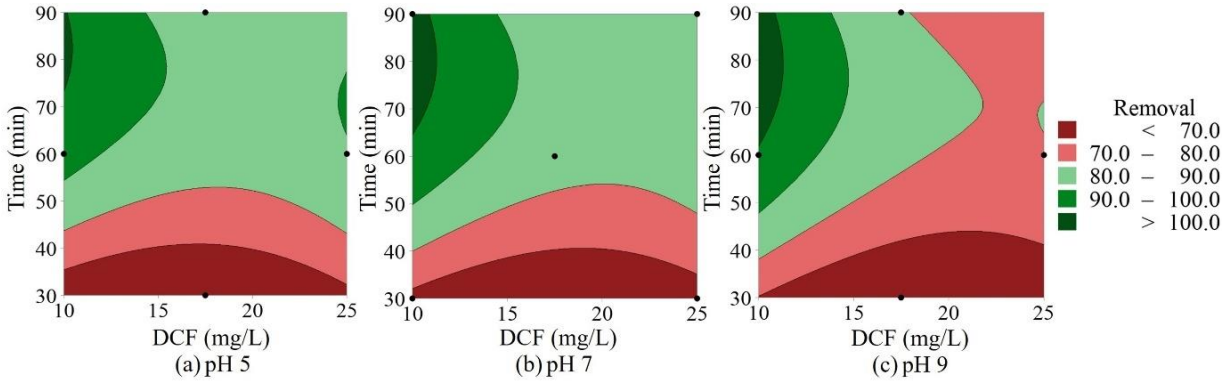

Figure 4. Contour plots of DCF removal efficiency as function of initial DCF concentration and reaction time at different pH levels (a) pH 5 (b) pH 7 and (c) pH 9

Figure 5 illustrates the RSM contour plots of DCF removal efficiency as a function of pH and reaction time at different initial DCF concentrations. It showed that the initial pH did not affect DCF removal efficiency during catalytic ozonation because the CaO_2 generated hydrogen peroxide (H_2O_2) and calcium hydroxide ($Ca(OH)_2$), leading to an increase in the pH, as shown in Equation 8. Under alkaline conditions, the ozone decomposed and produced hydroxyl radicals (OH·), a very powerful radical, as shown in Equations 9-11 (Castro et al., 2019; Wang and Chen, 2020).

$$CaO_2 + 2H_2O \rightarrow H_2O_2 + Ca(OH)_2 \quad (8)$$

$$2H_2O_2 \rightarrow 2H_2O + O_2 \quad (9)$$

$$H_2O_2 + e^- \rightarrow OH\cdot + OH^- \quad (10)$$

$$O_3 + OH^- \rightarrow 2OH\cdot + O_2{}^-\cdot \quad (11)$$

Figure 6(a-c) show the RSM contour plots for DCF removal efficiency as a function of CaO_2 dosage and reaction time at different pH levels. They show that the CaO_2 dosage affected DCF removal efficiency; specifically, as the CaO_2 dosage increased, the removal efficiency increased. This could be explained by during the ozonation process, the CaO_2 produced H_2O_2 and $Ca(OH)_2$ through dissolution. The released H_2O_2 from the CaO_2 reacted with O_3 to generate OH· and accelerated the degradation of the DCF, as mentioned earlier (Xu et al., 2020; Xiang et al., 2021).

3.4 Optimization of DCF treatment based on catalytic ozonation and confirmation test

The regression model obtained from the RSM with BBD provided predicted data from different experimental conditions. The predicted values were calculated using the regression quadratic model with

training and test datasets, and then compared with the experimental data, as listed in Table 2. Figure 7 shows both the experimental and predicted values from the regression model. The observed and predicted values were close to linearity, with RMSE and MAPE values of 5.90 and 6.10%, respectively, suggesting that the regression model could accurately predict DCF removal efficiency.

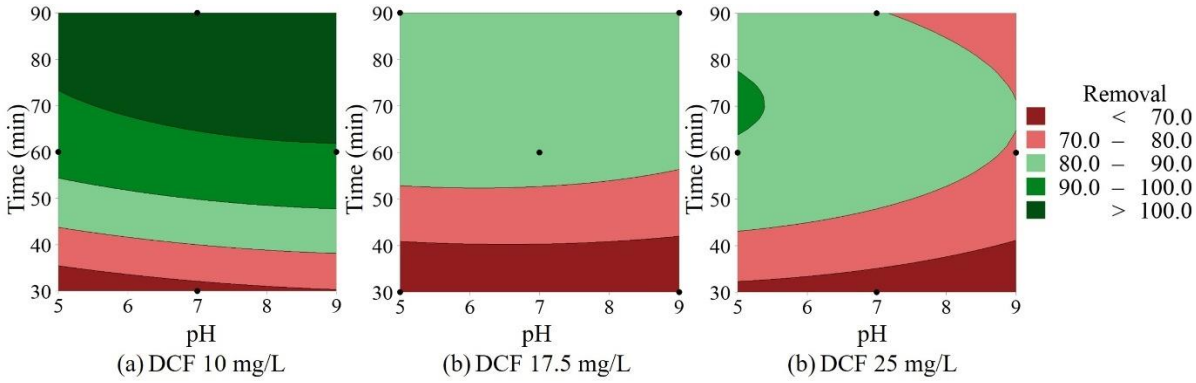

Figure 5. Contour plots of DCF removal efficiency as function of pH and reaction time at different initial DCF concentrations (a) 10 mg/L (b) 17.5 mg/L and (c) 25 mg/L

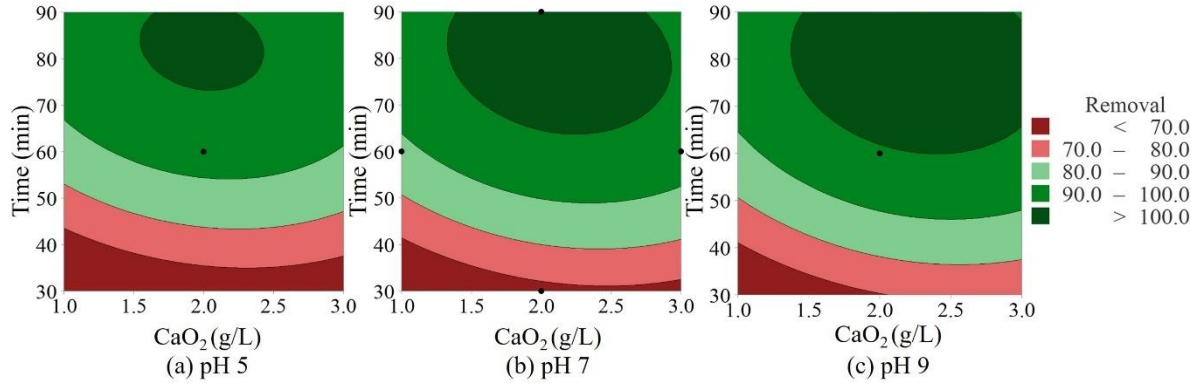

Figure 6. Contour plots of DCF removal efficiency as function of CaO_2 dosage and reaction time at different pH levels (a) pH 5 (b) pH 7 and (c) pH 9

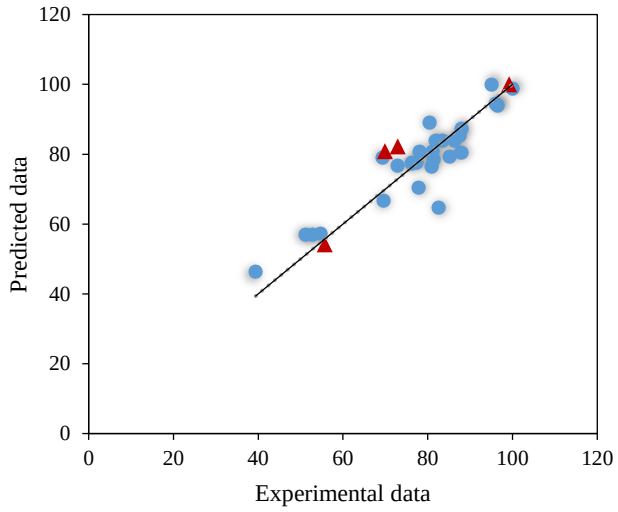

Figure 7. Comparison of predicted and experimental data for DCF removal efficiency (blue dots: training dataset, red triangles: test dataset)

According to Table 2, the DCF removal efficiency of the predicted values was up to 100% for the optimal conditions (initial DCF concentration 10 mg/L, solution pH 7, CaO_2 dosage 2 g/L, and reaction time 90 min). The confirmation test was performed with those optimum factors to validate the predicted optimal conditions. A new experiment was carried out and 97.6% DCF removal efficiency was achieved, as shown in Figure 8. Compared to the experimental data, the RMSE and MAPE values were 4.02 and 6.47%, respectively. These results showed that the regression model obtained from RSM could be effectively used to predict the optimal conditions for DCF treatment based on ozonation catalyzed with CaO_2. Furthermore, the DCF removal efficiency based on catalytic ozonation was compared with that by ozonation alone for the same conditions, which showed that the DCF

removal efficiency based on catalytic ozonation was higher than from using ozonation alone (48.1%), proving that CaO_2 could be effectively used as a catalyst in catalytic ozonation for treatment of DCF contamination in wastewater.

While catalytic ozonation presents an attractive technology for removing emerging contaminants, several studies have indicated that other constituents in wastewater, such as total dissolved solids, total organic carbon, nitrite, and alkalinity, may impair its performance (Kolosov and Yargeau, 2019; Merkus et al., 2023). Additionally, the degradation by-products generated during this process could be more toxic and hazardous than the parent compounds (Malik et al., 2020). Therefore, it is recommended to undertake further investigations into the combined effects of these constituents, the toxicity of by-products, and the cost-effective aspect to ensure the development of more sustainable wastewater treatment solutions.

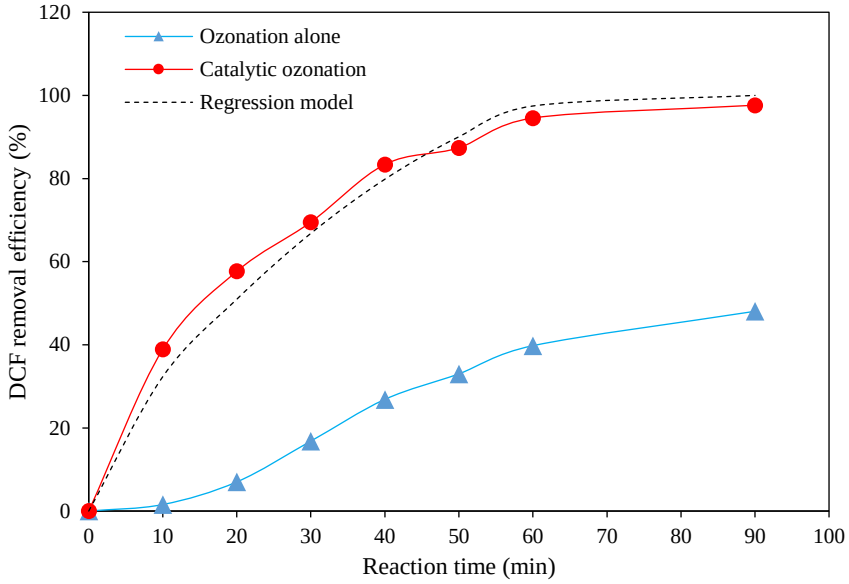

Figure 8. Removal of DCF in synthetic wastewater based on catalytic ozonation using CaO_2 as catalyst (initial DCF concentration 10 mg/L, pH 7, and CaO_2 dosage 2 g/L)

4. CONCLUSION

Catalytic ozonation using CaO_2 as a catalyst was successfully applied to remove DCF in synthetic wastewater. The as-prepared CaO_2 was characterized using XRD and FT-IR to confirm the existence of CaO_2. The results from the RSM with BBD showed that the quadratic regression model was suitable to describe the influence of the studied variables on the DCF removal efficiencies with an R^2 value of 84.00%. According to regression analysis, the initial DCF concentration and reaction time were the key parameters in the catalytic ozonation process. The predicted data obtained from the model were verified with the experimental data, producing RMSE value of 5.90 and a MAPE of 6.10%, indicating that the regression model could be used to optimize and predict DCF removal efficiency. Using the optimal conditions (initial DCF concentration 10 mg/L, solution pH 7, CaO_2 dosage 2 g/L, and reaction time 90 min), the DCF removal efficiency obtained from the experiment was 97.6%, whereas that from the regression model was up to 100%, which was higher than that obtained from ozonation alone (48%). The results from the current research proved that CaO_2 could be effectively used as a catalyst for catalytic ozonation treatment of DCF contamination in wastewater.

ACKNOWLEDGEMENTS

This project was funded by the National Research Council of Thailand (NRCT) (contract no. N41A660178). Support and assistance were provided by the Department of Environmental Technology and Management, Faculty of Environment, Kasetsart University, Bangkok, Thailand.

REFERENCES

Aguilar-Ascón E, Liliana Marrufo-Saldaña L, Neyra-Ascón W. Enhanced chromium removal from tannery wastewater through electrocoagulation with iron electrodes: Leveraging

the Box-Behnken design for optimization, Heliyon 2024;10(3):e24647.

Alessandretti I, Rigueto CVT, Nazari MT, Rosseto M, Dettmer A. Removal of diclofenac from wastewater: A comprehensive review of detection, characteristics and tertiary treatment techniques. Journal of Environmental Chemical Engineering 2021;9(6):Article No. 106743.

Alharbi SK, Ansari AJ, Nghiem LD, Price WE. New transformation products from ozonation and photolysis of diclofenac in the aqueous phase. Process Safety and Environmental Protection 2022;157:106-14.

Alonso E, Sanchez-Huerta C, Ali Z, Wang Y, Fortunato L, Pinnau I. Evaluation of nanofiltration and reverse osmosis membranes for efficient rejection of organic micropollutants. Journal of Membrane Science 2024;693:Article No. 122357.

Beltran FJ, Pocostales P, Alvarez P, Oropesa A. Diclofenac removal from water with ozone and activated carbon. Journal of Hazardous Materials 2009;163(2-3):768-76.

Bilińska M, Bilińska L, Gmurek M. Homogeneous and heterogeneous catalytic ozonation of textile wastewater: Application and mechanism. Catalysts 2022;13(1): Article No. 6.

Castro J, Paz S, Mena N, Urresta J, Machuca-Martinez F. Evaluation of heterogeneous catalytic ozonation process for diclofenac degradation in solutions synthetically prepared. Environmental Science and Pollution Research 2019; 26(5):4488-97.

Chen F, Zhang Y-S, Bai C-W, Huang X-T, Sun Y-J, Chen X-J. Ozone meets peroxides: A symphony of hybrid techniques in wastewater treatment. Chemical Engineering Journal 2024;483:Article No. 149129.

Chen H, Wang J. Degradation and mineralization of ofloxacin by ozonation and peroxone (O_3/H_2O_2) process. Chemosphere 2021;269:Article No. 128775.

Davies NM, Anderson KE. Clinical pharmacokinetics of diclofenac. Clinical Pharmacokinetics 1997;33(3):184-213.

Dedecan T, Baylan N, Inci I. Synthesis, characterization and application of calcium peroxide nanoparticles as a novel adsorbent for removal of malic acid from aqueous solutions. Chemical Physics Letters 2022;797:Article No. 139581.

Dehghani MH, Faraji M, Mohammadi A, Kamani H. Optimization of fluoride adsorption onto natural and modified pumice using response surface methodology: Isotherm, kinetic and thermodynamic studies. Korean Journal of Chemical Engineering 2016;34:454-62.

Dwivedi G, Sharma MP. Application of Box-Behnken design in optimization of biodiesel yield from pongamia oil and its stability analysis. Fuel 2015;145:256-62.

Ferreira N, Viana T, Henriques B, Tavares DS, Jacinto J, Colonia J, et al. Application of response surface methodology and Box-Behnken design for the optimization of mercury removal by *Ulva* sp. Journal of Hazardous Materials 2023;445:Article No. 130405.

Gomes J, Matos A, Gmurek M, Quinta-Ferreira RM, Martins RC. Ozone and photocatalytic processes for pathogens removal from water: A review. Catalysts 2019;9(1):Article No. 46.

Habte L, Shiferaw N, Mulatu D, Thenepalli T, Chilakala R, Ahn JW. Synthesis of nano-calcium oxide from waste eggshell by sol-gel method. Sustainability 2019;11(11):Article No. 3196.

Honarmandrad Z, Javid N, Malakootian M. Removal efficiency of phenol by ozonation process with calcium peroxide from aqueous solutions. Applied Water Science 2021;11(2):Article No. 14.

Jabbari F, Eslami A, Mahmoudian J. Degradation of diclofenac in water using the $O_3/UV/S_2O_8$ advanced oxidation process. Health Scope 2020;9(2):e99436.

Jafari D, Esfandyari M, Mojahed M. Optimization of removal of toluene from industrial wastewater using RSM Box-Behnken experimental design. Sustainable Environment Research 2023;33:Article No. 30.

Jasnia AB, Kamyab H, Chelliapan S, Arumugam N, Krishnan S, Din MFM. Treatment of wastewater using response surface methodology: A brief review. Chemical Engineering Transactions 2020;78:535-40.

Javid N, Honarmandrad Z, Malakootian M. Ciprofloxacin removal from aqueous solutions by ozonation with calcium peroxide. Desalination and Water Treatment 2020;174:178-85.

Kolosov P, Yargeau V. Impact of catalyst load, chemical oxygen demand and nitrite on disinfection and removal of contaminants during catalytic ozonation of wastewater. Science of the Total Environment 2019;651:2139-47.

Li F, Choong TSY, Soltani S, Abdullah LC, Jamil SNA, Nuar NNA. Investigation of glyphosate removal from aqueous solutions using Fenton-like system based on calcium peroxide. Processes 2022;10:Article No. 2045.

Lonappan L, Brar SK, Das RK, Verma M, Surampalli RY. Diclofenac and its transformation products: Environmental occurrence and toxicity: A review. Environment International 2016;96:127-38.

Lu S, Zhang X, Xue Y. Application of calcium peroxide in water and soil treatment: A review. Journal of Hazardous Materials 2017;337:163-77.

Madan SS, Wasewar KL, Kumar CR. Optimization of adsorptive removal of α-toluic acid by CaO_2 nanoparticles using response surface methodology. Resource-Efficient Technologies 2017;3(3):329-36.

Malik SN, Ghosh PC, Vaidya AN, Mudliar SN. Hybrid ozonation process for industrial wastewater treatment: Principles and applications: A review. Journal of Water Process Engineering 2020;35:Article No. 101193.

M'Arimi MM, Mecha CA, Kiprop AK, Ramkat R. Recent trends in applications of advanced oxidation processes (AOPs) in bioenergy production: Review. Renewable and Sustainable Energy Reviews 2020;121:Article No. 109669.

Maryam B, Buscio V, Odabasi SU, Buyukgungor H. A study on behavior, interaction and rejection of paracetamol, diclofenac and ibuprofen (PhACs) from wastewater by nanofiltration membranes. Environmental Technology and Innovation 2020;18:Article No. 100641.

Melo HP, Cruz J, Candeias A, Mirão J, Cardoso M, Oliveira MJ, et al. Problems of analysis by FTIR of calcium sulphate-based preparatory layers: The case of a group of 16th-century Portuguese paintings. Archaeometry 2014;56(3):Article No. 12026.

Merkus VI, Leupold MS, Rockel SP, Lutze HV, Schmidt TC. Effects of organic matter and alkalinity on the ozonation of antiviral purine derivatives as exemplary micropollutant motif. Water Research 2023;242:Article No. 120387.

Moncea AM, Panait AM, Deák G, Poteras G. Binder microstructures developed during the hydration process in the system portland cement - calcium aluminate cement - calcium sulfate. MRS Proceedings 2016;1812:71-6.

Mukkawi R, Shantier S, Gadkariem EA. Spectrophotometric method for the simultaneous analysis of diclofenac sodium and lidocaine hydrochloride in bulk and dosage forms. Pharmaceutical Chemistry Journal 2021;55(8):831-4.

Norabadi E, Panahi AH, Ghanbari R, Meshkinian A, Kamani H, Ashrafi SD. Optimizing the parameters of amoxicillin removal in a photocatalysis/ozonation process using Box-Behnken response surface methodology. Desalination and Water Treatment 2020;192:234-40.

Nuar NNA, Jamil SNA, Choong TSY, Azmi IDM, Romli NAA, Abdullah LC, et al. Synthesis of calcium peroxide nanoparticles with starch as a stabilizer for the degradation of organic dye in an aqueous solution. Polymers 2023; 15(5):Article No. 1327.

Prameswari J, Widayat W, Buchori L, Hadiyanto H. Novel iron sand-derived alpha-Fe_2O_3/CaO_2 bifunctional catalyst for waste cooking oil-based biodiesel production. Environmental Science and Pollution Research 2023;30(44):98832-47.

Rosales E, Diaz S, Pazos M, Sanromán MA. Comprehensive strategy for the degradation of anti-inflammatory drug diclofenac by different advanced oxidation processes. Separation and Purification Technology 2019;208:130-41.

Sathishkumar P, Meena RAA, Palanisami T, Ashokkumar V, Palvannan T, Gu FL. Occurrence, interactive effects and ecological risk of diclofenac in environmental compartments and biota: A review. Science of the Total Environment 2020;698:Article No. 134057.

Sun Q, Lu J, Wu J, Zhu G. Catalytic ozonation of sulfonamide, fluoroquinolone, and tetracycline antibiotics using nano-magnesium hydroxide from natural bischofite. Water, Air, and Soil Pollution 2019;230:Article No. 55.

Thalla AK, Vannarath AS. Occurrence and environmental risks of nonsteroidal anti-inflammatory drugs in urban wastewater in the southwest monsoon region of India. Environmental Monitoring and Assessment 2020;192(3):Article No. 193.

Tra VT, Pham VT, Tran T-D, Tran TH, Tran TK, Nguyen TPT, et al. Enhance diclofenac removal in wastewater by photocatalyst process combination with hydrogen peroxide. Case Studies in Chemical and Environmental Engineering 2023;8:Article No. 100506.

Vijuksungsith P, Satapanajaru T, Chokejaroenrat C, Jarusutthirak C, Sakulthaew C, Kambhu A, et al. Remediating oxytetracycline contaminated aquaculture water using nano calcium peroxide ($nCaO_2$) produced from flue gas desulfurization (FGD) gypsum. Environmental Technology and Innovation 2021;24:Article No. 101861.

Wang H, Zhao Y, Li T, Chen Z, Wang Y, Qin C. Properties of calcium peroxide for release of hydrogen peroxide and oxygen: A kinetics study. Chemical Engineering Journal 2016;303:450-7.

Wang J, Chen H. Catalytic ozonation for water and wastewater treatment: Recent advances and perspective. Science of the Total Environment 2020;704:Article No. 135249.

Wang Y, Zheng K, Guo H, Tian L, He Y, Wang X, et al. Potassium permanganate-based advanced oxidation processes for wastewater decontamination and sludge treatment: A review. Chemical Engineering Journal 2023;452(3):Article No. 139529.

Witek-Krowiak A, Chojnacka K, Podstawczyk D, Dawiec A, Bubala K. Application of response surface methodology and artificial neural network methods in modelling and optimization of biosorption process. Bioresource Technology 2014;160:150-60.

Xiang L, Xie Z, Guo H, Song J, Li D, Wang Y, et al. Efficient removal of emerging contaminant sulfamethoxazole in water by ozone coupled with calcium peroxide: Mechanism and toxicity assessment. Chemosphere 2021;283:Article No. 131156.

Xu Q, Huang QS, Wei W, Sun J, Dai X, Ni BJ. Improving the treatment of waste activated sludge using calcium peroxide. Water Research 2020;187:Article No. 116440.

Zind H, Mondamert L, Remaury QB, Cleon A, Leitner NKV, Labanowski J. Occurrence of carbamazepine, diclofenac, and their related metabolites and transformation products in a French aquatic environment and preliminary risk assessment. Water Research 2021;196:Article No. 117052.

Environment and Natural Resources Journal

Volume 22
Issue 4
2024

Landscape Ecological Structures and Patterns for Green Space Conservation in Forest Monasteries in Northeast Thailand

Prat Kongsombut[1, 2], Sura Pattanakiat[3*], Wee Rawang[1], Pattranit Srijuntrapun[1], Uthaiwan Phewphan[2], Thamarat Phutthai[3], Sirasit Vongvassana[3], and Jirapatch Jumpasingha[3]

[1]Faculty of Social Sciences and Humanities, Mahidol University, Nakhon Pathom 73170, Thailand
[2]Innovation for Social and Environmental Management, Mahidol University, Amnatcharoen Campus, 37000, Thailand
[3]Faculty of Environment and Resource Studies, Mahidol University, Nakhon Pathom 73170, Thailand

ARTICLE INFO

Received: 27 Jan 2024
Received in revised: 3 July 2024
Accepted: 8 July 2024
Published online: 23 Jul 2024
DOI: 10.32526/ennrj/22/20240016

Keywords:
Forest monastery/ Landscape ecology/ Geo-informatics/ Greenspace conservation

*** Corresponding author:**
E-mail: sura.pat@mahidol.ac.th

ABSTRACT

The green spaces in Wat Pah play an important role in forest conservation in Thailand. This study identified and analyzed the structures and patterns of landscape ecology in Wat Pah Nanachart, Ubon Ratchathani Province, to guide a conceptual framework for green space conservation in forest monasteries. Spatial analysis and modeling using geoinformatics technology were employed to recognize and characterize these landscapes. Information on the green space conservation and management of Wat Pah was also obtained using an in-depth interview and site observation. The results revealed that most of the green space in Wat Pah is forest, characterized by an ecological matrix and a dry evergreen forest. The forest structure can be divided into three canopies, dominated by the Dipterocarpaceae family, which has regenerated into upper and lower canopies. It is an edge matrix and ecological corridor connected to the internal and external green spaces of Wat Pah. It plays an important role in supporting cultural, religious, and aesthetic activities for ordained monks and Buddhists . The spatial landscape model can be divided into three main zones: Thoranisangha, Buddhawas, Sanghawas. Thoranisangha is an open space covered with traditional and artificially planted tree species. It is located in front of the temple and designed for public utilities in the context of managing and conserving the remaining trees. Buddhawas is a semi-open space mostly covered with traditional tree species. It represents Buddhism's identity and uniqueness and is used for religious ceremonies and dissemination—listening to sermons, meditating, and praying. Meanwhile, Sanghawas is covered with natural forest and contains residences for monks that are designed to be in harmony with the forest ecosystem.

1. INTRODUCTION

The forest deterioration situation in Thailand is critical. Formerly, the forest area covered more than 70% of the country (Baimai, 2007). Unfortunately, it has significantly declined owing to rapid population growth and economic expansion. Deforestation and forest degradation are mainly caused by utilization activities that exceed the capacity of the forest ecosystem. They include, for instance, forest encroachment for the construction of resorts and golf courses; slash and burn agriculture; and dam and road construction (UN-REDD, 2013). The forest area has gradually reduced from 33.15% in 2000 to 31.57% in 2022 (Royal Forest Department, 2022). The national forest policy proposes that the forest area in Thailand must cover at least 40% of the country, with 25% for conservation forest and 15% for economic and community forest (Royal Forest Department, 2020). In addition, before the 20-Year National Strategy (2018-2037) can be achieved, the green area in Thailand must

Citation: Kongsombut P, Pattanakiat S, Rawang W, Srijuntrapun P, Phewphan U, Phutthai T, Vongvassana S, Jumpasingha J. Landscape ecological structures and patterns for green space conservation in forest monasteries in Northeast Thailand. Environ. Nat. Resour. J. 2024;22(4):366-377. (https://doi.org/10.32526/ennrj/22/20240016)

consist of natural forest, economic forest, and urban/recreation exploitation at 35%, 15%, and 15%, respectively (NESDC, 2023). Therefore, increasing the forest area to meet these targets is very important. Since the forest area is a scattered patch pattern, especially outside protected areas, it needs particular attention regarding conservation. Wat Pah, or forest monasteries, play an important role in this matter.

Buddhism is the predominant religion in Thai society, and temples are Buddhist organizations. Buddhists comprise more than 90% of the population, and the country is home to 43,562 temples (Kanyalak et al., 2015). The northeast is the region with the most temples. In Ubon Ratchathani Province alone, there are as many as 1,848 temples (The National Office of Buddhism, 2021). There are 936 forest monasteries spread over the natural landscape, rural areas, and urban areas, 375 of which are recognized as legitimate (Sornsakda et al., 2013). Numerous forest monasteries preserve a wide range of vegetation and enormous trees, and this conservation was partly influenced by Buddhism (Jirathasanakul, 2001). Monks are tied to the forest, and many role-model noble monks use the forest to practice Dhamma, such as Luang Pu Sao Kantasilo, Luang Pu Man Phurithatto, and Luang Pu Cha Suphattho. Thus, even though there is not much remaining forest, a few places, like Wat Pah Nanachart, Wat Nong Pa Pong, Wat Pah Phrom Thitanusorn, Wat Pah Hua Don, Wat Pah Non Sawan, Wat Pah Nam Bun, and Wat Pah Nong Bua Hi, have status as forest monasteries, which are best suited to preserving the forest conditions, guaranteed by the Species Diversity Index and Importance Value Index. *Aquilaria crassna*, *Dipterocarpus turbinatus*, and *Dalbergia cochinchinensis* are among the critically endangered and endangered plants found in these monasteries (Jumpasingha et al., 2018). This demonstrates that forest monasteries are places where the traditional forest's green spaces have been conserved. Functionally, these monasteries have lush forests that maintain an ecological balance; thus, they can be used as peaceful locations for Dhamma practice and serve as green spaces that support environmental sustainability within a province's landscape system.

Wat Pah monasteries are categorized as elements of the landscape's ecosystem that provide ecosystem services in terms of their ecological value, use for Buddhist religious purposes, beauty, and green spaces (Wonglangka and Han, 2018). These functions are like lungs that purify the air and create a pleasant surrounding environment. Furthermore, there are sporadic communities of forest monasteries in urban, suburban, rural, and natural settings. Even though most forest monasteries today have been disturbed by surrounding land use activities, an abundance of plants is still maintained within certain ones (Wongsanao and Krutasean, 2022), such as Wat Pah Nanachart, owing to their emphasis on environmental preservation and protection. As part of the initiative to improve green space and environmental management in monasteries, Wat Pah Nanachart was certified by the Department of Environmental Quality Promotion in 2019 and given the Excellent Environmental Management Temple Award (Wat Pah Nanachart, 2022a), indicating that this monastery has conserved green spaces to preserve the health of a productive forest. This study aimed to research the principles of landscape ecology, which are crucial for understanding the ecological and cultural significance of these green spaces, recognizing the ecological landscape structure and patterns, as well as the conservation and management strategies at Wat Pah Nanachat, which serves as a representative Buddhist forest conservation site. It successfully maintains forest habitats. Understanding these elements will guide conservation and management efforts, help foster a unique identity, and promote the expansion of green spaces in monasteries. Therefore, this research aims 1) to analyze the ecological structures and patterns of Wat Pah Nanachart to understand the physical, biological, and functional components integrated into the forest monastery landscape system, and 2) to create a landscape ecological model for conserving the green spaces of forest monasteries based on the principles of landscape ecology to establish conservation and management concepts based on the lessons learned and the needs of the monks. This will help us create a framework and present this model as it relates to Ubon Ratchathani Province.

2. METHODOLOGY

2.1 Study area

Situated in Ban Bung Wai, Warin Chamrap District, Ubon Ratchathani Province, Wat Pah Nanachart is one of the temples of the Wat Nong Pa Pong. Originally an abandoned monastery called Wat Nong Pla Keng, it is located in the old Bung Wai cemetery. Owing to the community's faith, monks were invited to practice Dhamma, and this place became a monastery. Vihara was built in the old Sima area (in 1985), consisting of Kuti, buildings, and a chapel for monks to use for chanting and performing

various religious rituals. This forest monastery received the Wisungkhamsima in 1998. The monastery's territory has an area of 365 rai (Wat Pah Nanachart, 2022b) (Figure 1), and is surrounded by community and agricultural areas. The structure of the facilities and transportation routes have been developed, and the community surrounding the monastery has expanded. In both the past and present, forest monasteries conserve and preserve the forest and allow monks to practice their beliefs.

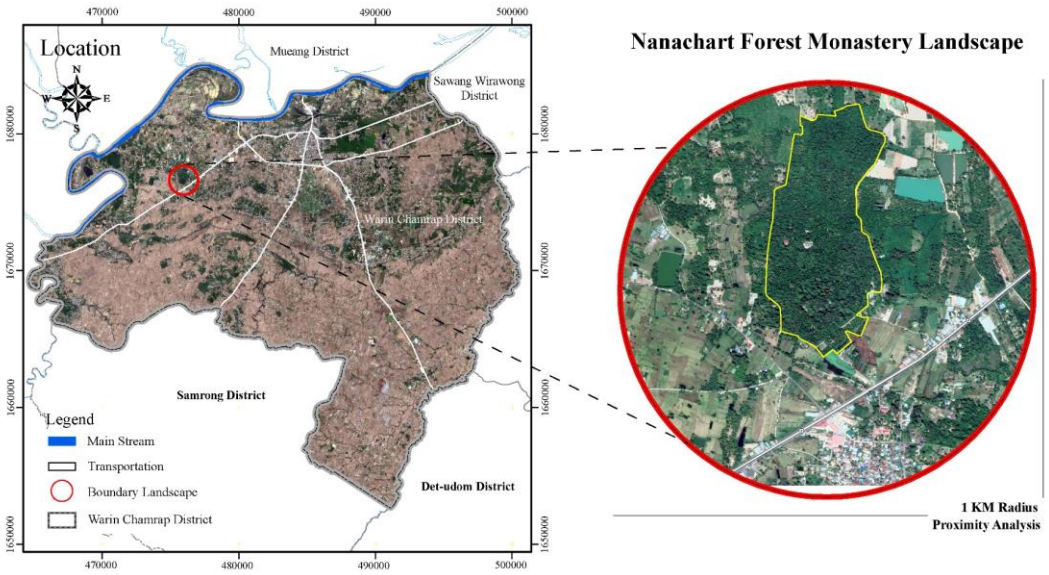

Figure 1. Position and location of Wat Pah, Ban Bung Wai, Warin Chamrap District, Ubon Ratchathani Province

2.2 Methodology

This study was conducted based on landscape design approaches (Ahmadi et al., 2018; Suppakittpaisarn, 2021). These approaches served as a foundation for presenting conservation and management guidelines for the ecological landscape of forest monasteries. This study consisted of the following steps.

2.2.1 Site inventories and user requirements

To create a base plan for surveying, analyzing, and designing, basic data regarding the physical structure and components of the forest monasteries were gathered (Limthongkul, 2019). A survey was conducted with intensive in-field data collection from April to August 2022. The site inventory gathered landscape elements such as locations, morphology, soil, drainage, circulation, plants, and forest habitats. Simple random sampling was used, along with one temporary plot (20×50 meters) in a representative forest habitat selected through purposive sampling, based on a monastery zone identified from aerial photographs taken in 2002 and 2022. Additionally, user needs were explored through in-depth interviews using purposive sampling, which included an abbot and 2 monks. These semi-structured interviews focused on the history, management, use, and concepts of forest conservation. Interviews were also conducted with 2 urban planners to discuss green development concepts and observe activities within the context of the Wat Pah.

2.2.2 Landscape structure analysis

The landscape composition of forest communities was assessed using geo-information techniques, which involved visually interpreting aerial photographs from 2002 and 2022 and worldview satellite imagery from 2022 (Esri, Maxar, USDA, USGS, GeoEye, Getmapping, AeroGRID, IGN, IGP, UPR-EGP, and the GIS user community). This analysis aimed to evaluate forest cover (Pattanakiat, 2018). The forest cover was classified into three categories based on the main green space development concepts (ONEP, 2005), forest, open space, and imperviousness/buildings, followed by the delineation of the dominant land cover type and delineation based on the most extensive and well-connected land cover type, referred to as the matrix (Aminzadeh and Khansefid, 2009; Forman and Godron, 1986; Tangkitngamwong, 2012). Meanwhile, the path and corridor of the dominant landcover were identified by visually interpreting aerial photographs, and a site inventory was used for intensive in-field data collection across the three landscape zones of the forest monastery based on suggestions from the abbot. All tree species

within these zones were identified and recorded. Individual tree characteristics, tree positions, and tree canopies were measured using diameter tape, a hypsometer, and a GPS receiver, respectively.

2.2.3 Recognition and identification of landscape ecology structures and patterns

The "Morphological Spatial Pattern Analysis" (MSPA) model, developed by Soille and Vogt (2009), was employed during this step. This model is a crucial tool in landscape ecology assessment, focused on understanding the spatial configurations of landscape elements. It aids in analyzing the spatial patterns of habitat connectivity and fragmentation, which are essential for identifying and prioritizing areas for conservation and management planning, particularly in the context of Wat Pah monasteries. The MSPA model is a binary segmentation technique that measures the foreground and background. The foreground refers to the forest landscape, while the remaining landscape types are set as the background. Using the Guidos Toolbox software for 8-neighborhood analysis, the edge width was set to 1 pixel (10 meters). The shape, connectivity, and arrangement of the forest areas were used to form 8-connected neighborhoods automatically classified into seven landscape patterns: core, edge, perforation, bridge, loop, branch, and islet. This classification focused on key habitats and corridors that require conservation. Subsequently, post-classification data were analyzed. The results were then presented through a data layout.

2.2.4 Landscape ecology design

Conceptualization was created from site programming based on user needs and analysis of structural space characteristics, patterns, and landscape ecology. The synthesis phase involved three tasks and decision-making steps aimed at site planning for conservation and management. These tasks included: 1) development of the Preliminary Greenspace Concept, 2) establishment of conservation strategies for protecting, preserving, and zoning greenspace, and 3) presentation in Perspective and Isometric Patterns.

3. RESULTS

3.1 Assessment of the landscape's ecological features

Wat Pah Nanachat is on a low terrace along the Mun River, facing southward. The area has an elongated shape extending from south to north, covering approximately 0.55 square kilometers and surrounded by a dry evergreen forest. Aerial photographs in 2002 visually indicate that the Wat Pah area was previously covered by dry evergreen forest (forest cemetery) at the frontal and eastern sections, followed by disturbed forest and agricultural and barren areas. The Wat Pah has a strategic plan for reforestation, restoring the area to one predominantly covered by forest. By 2022, the forested regions were surrounded and predominantly characterized by dry evergreen forest and secondary dry evergreen forest. The land use around the monastery consists of agriculture. The fence and a wall of large trees provide the monastery with privacy; the morphology is slightly undulating, with slopes ranging from 0 to 2% at an elevation of 130 to 149 meters above sea level. The soil conditions are sandy loam with moderate permeability, affecting surface runoff and drainage in both the surface and subsurface soil. These influence the impact on the forest ecosystem and create a local climate that reduces temperatures and is supported by shade from trees, resulting in an optimal environment. The direction of the Sun's path, particularly in the morning, creates an ideal environment for Buddhist activities. Although the temple area receives some sunlight throughout the day in open areas, large trees provide ongoing shade, cover sunlight angles, and create shade from the west and south directions. The planning area is divided using a combination of fences and walls made of trees to separate the zones. This division can be identified by the components and activities in each section with circulation patterns within these areas. The main pathways, accessible to the public, are concrete or paved, providing access to public and interior areas, with some exceptions. Natural dirt pathways, serving as semi-public access, are intended for walking and meditative practices in the central area. The monks' walking pathways, which serve as private access, are designated as living quarters. The forest monastery is divided into three zones: 1) the Public Zone: Known as the Thoranisangha, this area surrounds the monastery and serves as an open space for public benefit activities. 2) the Semi-Public Zone: Referred to as the Buddhawas, this area is located within the interior front part of the monastery and is designated for activities associated with propagating Buddhism. 3) the Private Zone: Known as the Sanghawas, this is the largest area of the monastery used for the monks'activities and living quarters (Figure 2).

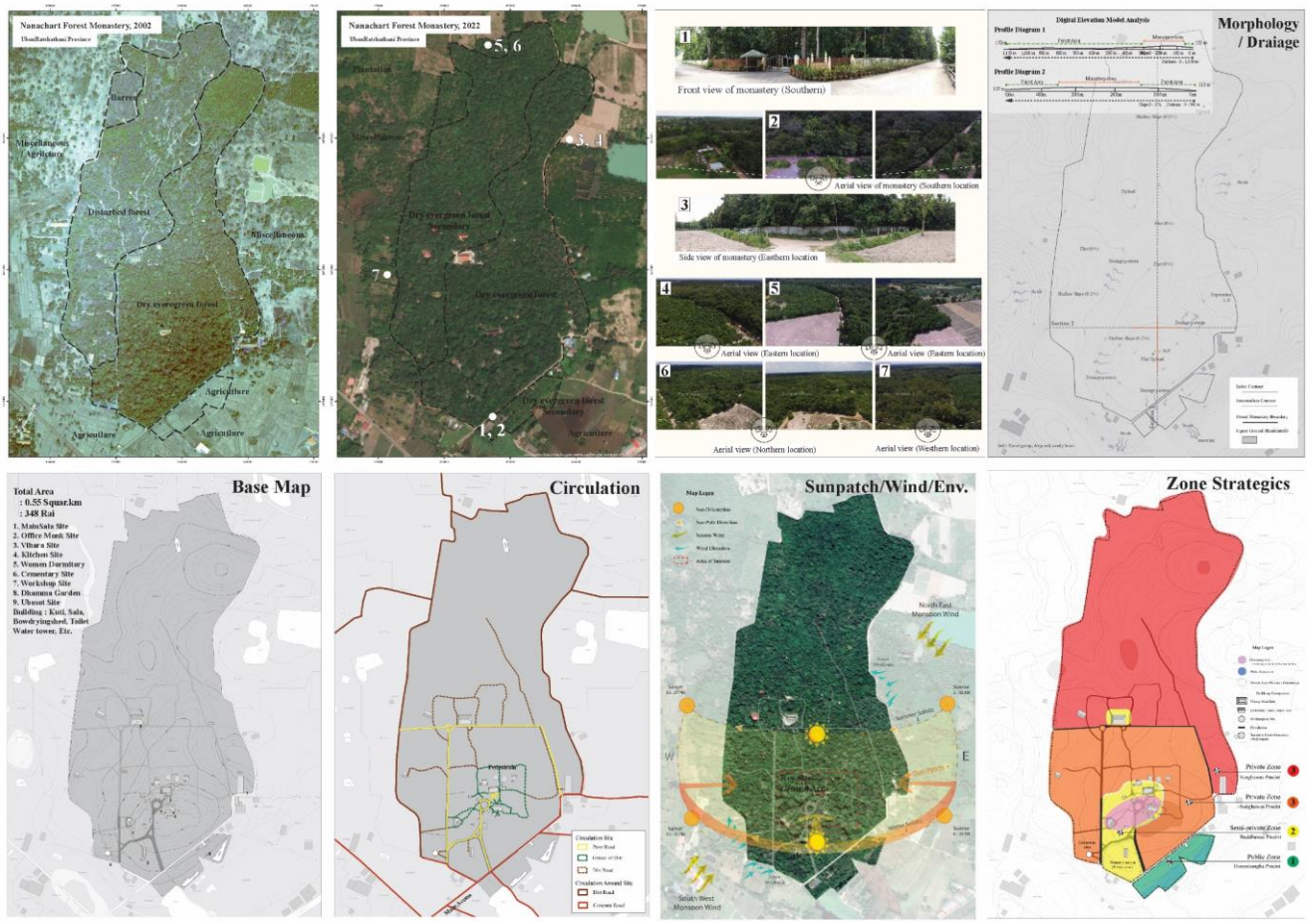

Figure 2. Analysis of spatial data to identify landscape ecological structures and patterns

3.2 Classification and identification of landscape ecological structures

The board structure of the Wat Pah was delineated by interpreting landscape ecology based on aerial photographs and field surveys. Two major dominant cover types were identified: dry evergreen forest, constituting approximately 54.49% of the area, located centrally near the monastery entrance, surrounding the Buddhawas Zone and extending eastward to the Sunghawas zone; reforestation dry evergreen forest, covering about 45.51% of the area, situated in the western part of the monastery, around the outer boundaries and near the Thoranisangha Zone entrance. The forest matrix status was studied using forest community structure analysis in three zones: Sunghawat, Buddhawat, and Thoranisangha. The details are as follows (Figure 3).

1) The Sunghawas area comprises dry evergreen and restored dry evergreen forests characterized by a dense canopy. A survey indicated 84 trees and 24 species, prominent trees are in the Dipterocarpaceae family, resulting in a Shannon-Wiener diversity index of 2.63 and a Richness Index of 3.18. Prominent species include *Aglaia cucullata* (Roxb.) Pellegr. *Dialium cochinchinense* Pierre and *Streblus asper*. The forest structure is stratified into three canopy levels: 1) an upper canopy, reaching heights of 25 meters, with some areas reaching up to 30 meters in height; 2) a middle canopy layer, ranging from 15 to 20 meters; and 3) a lower canopy layer and ground cover consisting of regenerating species. Additionally, introduced patches, including offices, a hospital, a sewing area, a bow-drying shed, Thera, Mahathera, Kuti, and a cemetery, serve specific monastic purposes. These areas are interconnected by semi-natural corridors like dirt and gravel paths, as well as human-made corridors, including paved roads for accessing the ordination hall (Ubosot) and other significant sites within the Sunghawas area.

2) The Buddawas area comprises dry evergreen forest characterized by a dense canopy and a seamlessly interwoven ecotone with the Sanghawas Zone. This area is demarcated by concrete walls and wooden fences and has transitioned from a dense forest structure into a semi-natural state owing to increased Buddhist activities in designated areas, such

as the shrine precinct, the pavilion, the kitchen, and recreational spaces. A survey indicated a total of 76 trees and 21 species, identifying seven species. Prominent trees are in the Dipterocarpaceae, family, contributing to a Shannon-Wiener diversity index of 2.65 and a Richness Index of 3.00. Prominent species include *Hopea odorata* Roxb., *Dipterocarpus alatus* Roxb. ex G. Don., and *Baccaurea ramiflora* Lour. The forest structure is stratified into two canopy levels: 1) an upper canopy reaching heights of 25 meters, with some areas reaching up to 30 meters, and 2) a middle canopy layer ranging from 5 to 15 meters. The ground cover is cleared and managed to enhance recreational activities under the forest canopy, preserve scenic views, and preserve landscape aesthetics. Containers with auspicious trees further enhance the landscape. Additionally, introduced patches such as the pavilion site, the shrine precinct site, the kitchen, and infrastructure buildings serve specific functional purposes and support visits by Buddhist devotees. These patches are interconnected by semi-natural corridors such as gravel paths and human-made corridors, including paved roads leading directly to the Buddhawas Area.

3) The Thoranisangha Area is a restored dry evergreen forest characterized by secondary growth. It interfaces with the Buddhawas and Sanghawas Zones, featuring edge patches along riverbanks and water bodies connected to the agricultural matrix. A survey identified a total of 93 trees and 12 species, including seven species. Prominent trees are in the Fabaceae and Dipterocarpaceae family, contributing to a Shannon-Wiener diversity index of 2.40 and a Richness Index of 2.48. Prominent species include *Sindora siamensis* Teijsm. ex Miq. var. *siamensis*., *Hopea odorata* Roxb., and *Dipterocarpus alatus* Roxb. ex G. Don. The forest structure is stratified into two canopy levels: 1) upper canopy trees, reaching heights of 10-20 meters, and 2) lower canopy trees, reaching 5 meters. The ground cover consists of regenerating species integrated into the primary forest structure. Additionally, introduced patches such as parking areas, public utility spaces, recreational open areas, and the Dhammajukkra Garden support visits by Buddhist devotees. These patches are interconnected internally within the monastery by human-made corridors, including paved roads, and connected to urban areas via concrete roads.

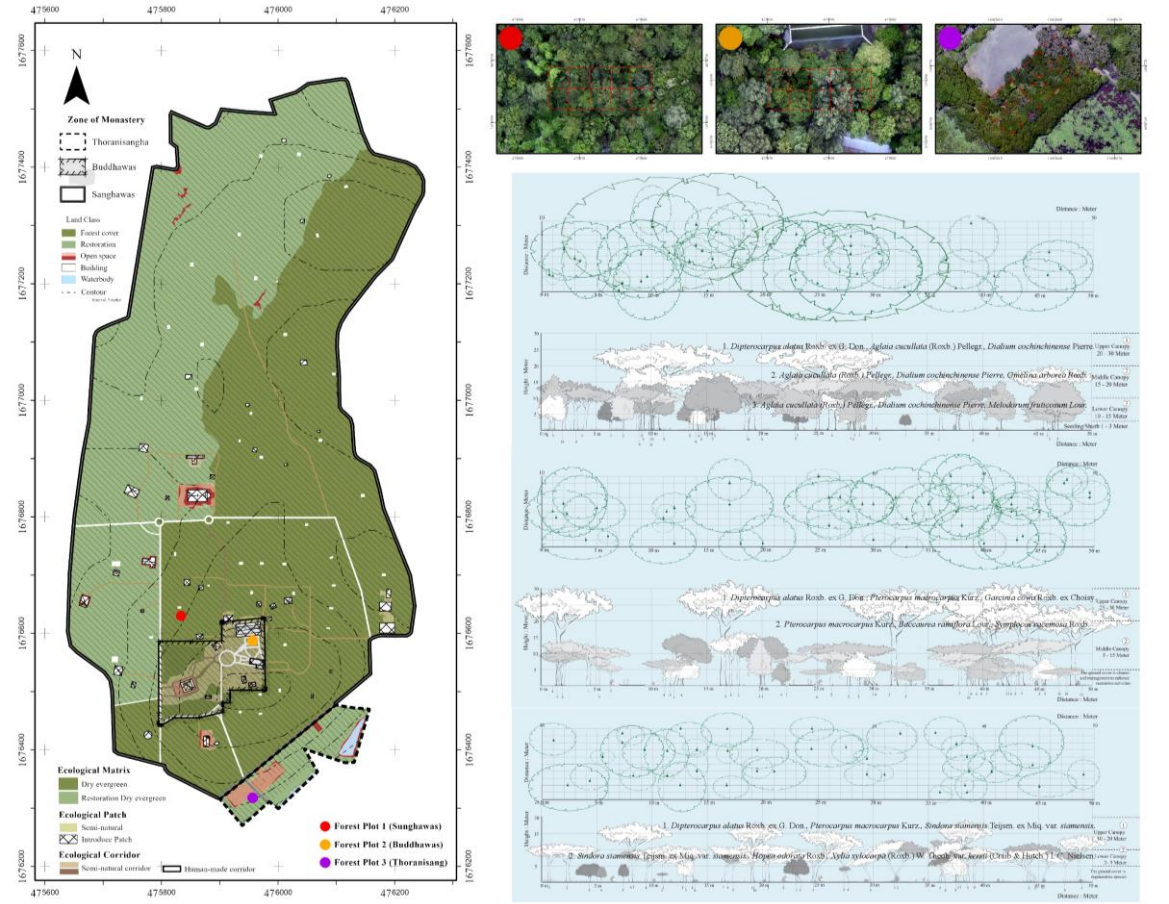

Figure 3. Landscape ecological structure and canopy structure of the Wat Pah

3.3 Recognition and identification of landscape ecology pattern

Figure 4 shows the landscape pattern types generated by the MSPA calculation, overlaid on the Wat Pah zone, divided into three major areas: 1) The Sunghawas area, encompassing 91.97% of the Wat Pah, primarily serves as the main forest matrix landscape. It consists of 96.59% foreground and 3.41% background, with core landscapes comprising the majority at 72.62%. Additionally, edge landscapes cover 19.47%, while the remaining patterns are loop (1.71%), perforation (1.55%), bridge (0.72%), islet (0.47%), and branch (0.06%). 2) The Buddhawas Area accounts for 4.47% of the area and functions as a forest patch adjacent to Buddhist activities within the matrix landscape. It features 75.31% foreground and 24.69% background, predominantly characterized by edge landscapes (26.42%). The area also includes core (20.74%), islet (12.66%), bridge (6.97%), loop (6.48%), and branch (2.03%) patterns. Lastly, 3) the Thoranisangha Area comprises 3.56% of the total area and is a forest remnant patch surrounded by agriculture. It exhibits 71.39% foreground and 28.61% background, with core landscapes covering the largest portion at 25.58%. This area also includes edge (23.29%), loop (19.71%), islet (1.31%), branch (1.27%), and bridge (0.24%) patterns.

The results indicate that the Sunghawas area is a crucial natural forest matrix within the landscape ecosystem, providing continuous habitats for biotic communities and maintaining ecosystem balance. This forest primarily consists of core and edge patterns (72.62% and 19.47%, respectively), emphasizing the need for preservation. In contrast, the Buddhawas Area is a forest patch embedded within the forest matrix, contain significant religious buildings and Buddhist activities. This area exhibits various patterns, including edge, background, core, islet, and loop (26.42%, 24.69%, 20.74%, 12.66%, and 6.48%, respectively). Conservation strategies should focus on minimize impacts on the edge and core areas that connect to the surrounding Sunghawas zone. Meanwhile, the Thoranisangha Area, located on the periphery of the forest monastery, serves as a remnant patch buffering the monastery from adjacent agricultural areas; it also displays diverse landscape patterns, such as background, core, edge, and loop (28.61%, 25.58%, 23.29%, and 19.71%, respectively). Strategies should be developed to increase forest patches and enhance their role as a buffer against the agricultural matrix.

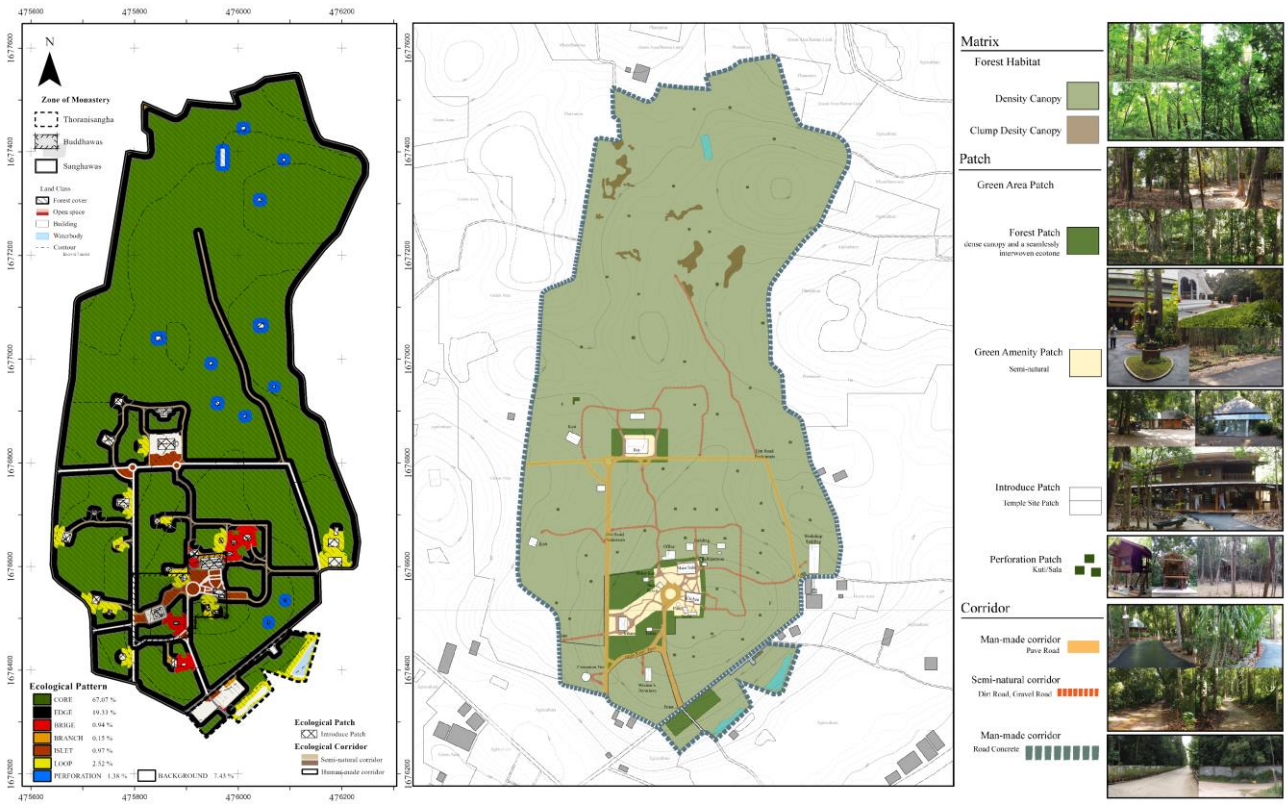

Figure 4. Landscape ecological structures and patterns of the Wat Pah

3.4 Presentation of guidelines for conservation and management

Based on our study of structures, patterns, Buddhist space-planning concepts (Jirathasanakul, 2001; Piromkeat, 2002; Wonglangka and Han, 2018), green space development concepts (Ahmadi et al., 2018; Bentrup, 2008; ONEP, 2005; Tangkitngamwong, 2012), and lessons learned from the concept of conservation and management at forest monasteries (Saardiam, 2020), a framework for site programming can be summarized as follows (Figure 5 and Figure 6).

3.4.1 Forest patch conservation and management in the Thoranisangha Area

Conserving and managing forest patches within the Thoranisangha Area means prioritizing green utility spaces to enhance the environmental quality surrounding the forest monastery and the community. This approach involves expanding forested areas as a buffer before entering the Wat Pah, focusing on native tree species and ornamental plants to preserve biodiversity and enhance the landscape, as illustrated in Diagram A. Located at the entrance of the Wat Pah, adjacent to the main road and the community's land use area, this open space is adorned with native and naturally planted trees. It serves as a distinct boundary for convenience, catering to Buddhists visiting the Wat Pah. Additionally, a garden symbolizing the Buddhist religion enhances the environmental quality and improves the community's quality of life.

3.4.2 Forest patch conservation and management in the Buddhawas Area

In forest patches within the Buddhawas Area, we should prioritize designing buildings that harmonize with the natural environment, emphasizing using native or local plant species as primary shade trees and maintaining local flora. Management should concentrate on undergrowth and utilization areas, integrating auspicious plant species to enhance the landscape and spiritual ambiance on-site. Restoring forest edges along the boundary between the Buddhawas and Sanghawas Areas serves to harmonize these zones and protect core habitats within the Sanghawas Area while also raising awareness of the privacy of the monastic domain. As depicted in Diagram B, the functional green area serves structural purposes and facilitates Buddhist activities at the entrance garden of the temple site. It encompasses buildings, public amenities, meeting areas, and seating spots nestled under original trees, with a line of tree barriers delineating the space. Similarly, Diagram C shows that the landscape amenity green area provides spaces for sitting and listening to Dharma teachings. It integrates pedestrian zones with managed spaces featuring potted plants and preserved trees to create clearings beneath them, guiding viewers toward landmark buildings adorned with plants. This area is demarcated by the forested and temple private zones.

3.4.3 Forest matrix conservation and management in the Sunghawas Area

Forest matrix should serve as a prominent landscape feature, with a strong emphasis on conserving native species and biodiversity. Green conservation areas should be designated to protect various species habitats, surrounded by buffer zones that allow for limited, low-impact activities. As depicted in Diagram D, a temple site within the matrix for performing Buddhist rituals and sangha activities, should be designed to blend seamlessly with the natural environment. An Ubosot area on the monastery land is envisioned as a green space to enhance the landscape; we should incorporate landscape amenities and plant auspicious species to elevate its aesthetic appeal. This area will support activities such as Dharma practices and meditation walks, with natural corridors near forest edges facilitating seamless transitions between spaces. Similarly, Diagram E depicts kuti patches in the green conservation area that will serve as animal habitats and private areas for the monks' Dharma practices. These patches should be integrated into the matrix landscape or constructed without disturbing the natural area, avoiding vegetation clearing and protecting critical habitats. Enclosed with trees to create privacy, the corridors connecting them will be narrow yet functional, effectively mitigating matrix fragmentation.

4. DISCUSSION

Landscape ecology is the study of structures and patterns in landscape systems. It has the potential to help us understand how to use a holistic approach that can create sustainability. In other words, it is a design that considers aspects of the environment, culture, and aesthetics (Makhzoumi, 2000). Integrating landscape design with planning for the Wat Pah Area facilitates the presentation of research findings that can improve our understanding of the spatial links between the monastery's culture and the surrounding environment. This is because this approach integrates landscape

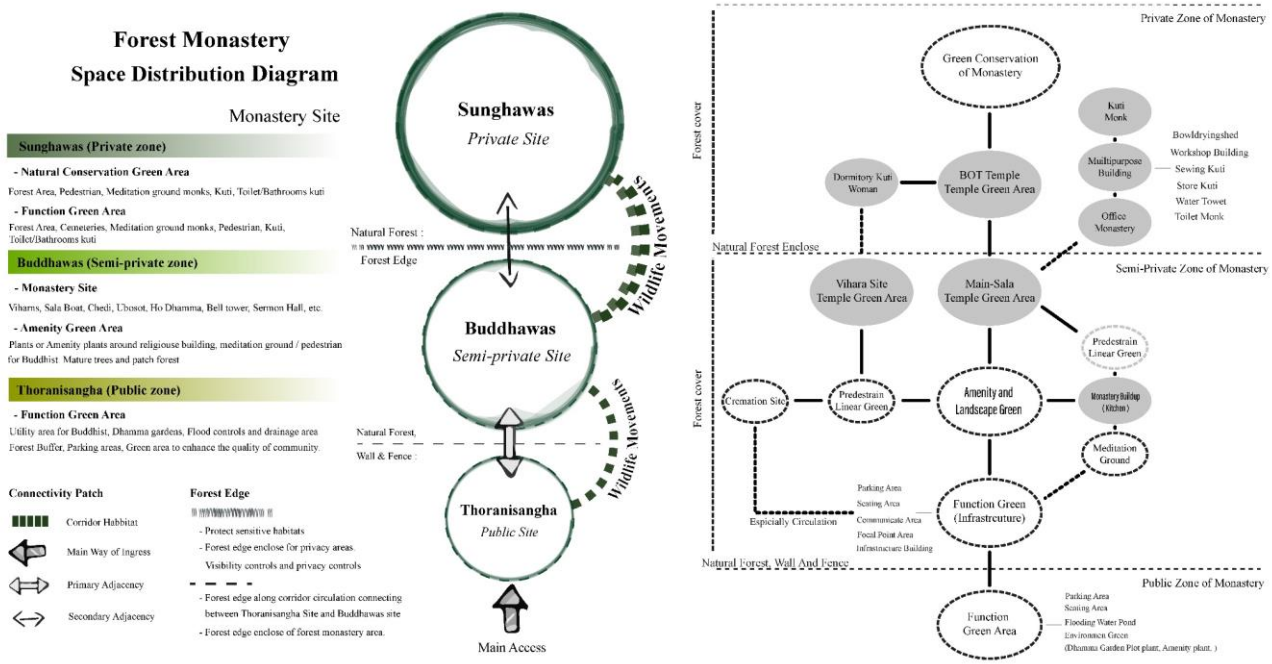

Figure 5. Area planning for ecological landscape conservation management of the Wat Pah

Figure 6. Design and presentation of guidelines for conservation management at the Wat Pah

design with local resources within the framework of the Wat Pah (Chen et al., 2019). For example, native plants are utilized for ecological functions such as barriers, physical control, perspective creation, territorial division, community buffers, and wood replacement in plant community rehabilitation Examples include using native plants as an integral part of the ecological structure (Sittipong and Tongtuam, 2018): as barriers, for physical control, to create perspective, to divide territories, as a buffer between communities, and to serve as replacement wood for plant community rehabilitation. The building's landscaping combines decorative and auspicious trees in strategic locations throughout the monastery with environmentally friendly designs that do not harm the nearby forest. This method places a strong emphasis on preserving natural and cultural capital to raise the value of the environment, establish new ecosystems (Ahmadi et al., 2018), and aid in the understanding the structural components that underpin the categorization and planning of green spaces, such as conservation areas, functional areas, and spaces within Buddhist buildings. This involves using a type of green space that consists of a forest, traditional trees, plants, a hardscape-softscape, and a building area that does not absorb water from different spatial activities; it also involves using the area layouts of the forest monastery. This enables the forest monastery's designer to understand the landscape in every area layout with clarity. To create an aesthetic that strengthens the Buddhist faith, we must establish a conceptual framework to develop the forest monastery's green spaces and enhance its unique traditional value in terms of its surroundings and locations and supporting religious activities (Techaamnuaywit, 2013). This framework also highlights the forest area within a one-kilometer radius of the monastery, which is one of the characteristics of a forest monastery (Chaisuwan and Charoonseang, 2018).

In landscape ecology studies for the conservation and management of green spaces in Buddhist areas, forest monasteries are classified as functional green areas (ONEP, 2005). The ecological landscape in a forest monastery landscape's indicate distinct use in terms of green spaces. For instance, the Sangkawas Area accommodates the monks and their living quarters. The Buddhawas Area promoting both the natural beauty and the distinctive value of Buddhism. The Thoranisangha Area enhance space usage for public benefits, maintain environmental quality, and act as a buffer. Consequently, Wat Pah's green space may be divided into three groups: green utility areas, green amenity areas, and green conservation areas, all under the functional green area category. The guidelines for designing and planning a forest monastery's green space are derived from the lessons that can be ascertained from the conservation and management practices used by the monks there and can be used as information for decision-making when planning the management of urban green spaces in the future. Managing cultural monastic areas is crucial to the growth of green areas improving community's quality of life, and providing additional benefits (Wonglangka and Han, 2018).

Aside from understanding the structures, patterns, and ecological roles of landscapes, it is important to study the selection of plants for a landscape's architecture, as well as to manage forest monastery ecosystems in terms of the structure of each area's layout. Emphasis should be placed on suitable applications for the forest monastery area based on practical uses, such as covering traditional and large trees as integral parts of the landscape (Suteethorn, 2018), the basics of Thai monastery landscape architecture (Kantatian, 2017), and the area's green spaces. This ensures that all dimensions of green spaces are accounted for, including waste, bathrooms, power, the environment, food and water, and sanitation management (Department of Health, 2019). However, Buddhist sites are a delicate matter because of a few limitations. Some of the forest monastery's activities fall outside the monks' purview, and there is a deficiency of detailed information on this subject. Therefore, future studies should clarify their purposes to potential participants to encourage them to engage with the research. This can be achieved by promoting knowledge and understanding regarding forest monastery green spaces in accordance with Thailand's policy and plans to increase its green spaces.

5. CONCLUSION

The plan and guidelines for managing and conserving the green spaces of forest monasteries are based on the structures, patterns, and concepts of conservation and management. Specifically, a space should be designed with Buddhist concepts and teachings at its core, accounting for the organizational management of forest monasteries. In other words, focus should be placed on living in the forest and relying on natural areas, for example, with respect to Vipassana meditation and Buddhist teachings, providing good living strategies for Buddhists who visit the forest monastery. Additionally, there should be guidelines for developing and managing green spaces to promote natural sustainability. As a result, protecting a forest monastery's green spaces involves viewing it as a forest ecology that serves as a habitat for living creatures, provides an environment for Vipassana meditation based on the monk's religious practices, and promotes Buddhism using large trees and/or forest surroundings.

ACKNOWLEDGEMENTS

This publication is based on thesis research and information support for academic works under the following project: Conservation of Green Area in Wat Pah: A Case Study of Ubon Ratchathani Province 2017: Geo-informatics in Resource and Environment Research and Training Center, Mahidol University.

REFERENCES

Ahmadi F, Bemanian M, Ansari M. An introduction to natural landscape restoration method based on landscape ecology approach. The Scientific Journal of NAZAR Research Center For Art, Architecture and Urbanism 2018;14(56):4-14.

Aminzadeh B, Khansefid M. A case study of urban ecological networks and a sustainable city: Tehran's metropolitan area. Urban Ecosystems 2009;13(1):23-36.

Baimai W. Biodiversity Situation in Thailand. Bangkok: The Thailand Research Fund; 2007. p. 79 (in Thai).

Bentrup G. Conservation Buffers: Design Guidelines for Buffers, Corridors, and Greenways (General Technical Report SRS-109). United states: United States Department of Agriculture and Forest Service, Southern Research Station; 2008. p. 3-9.

Chaisuwan P, Charoonseang P. The forest monastery and environment preservation. Inthaninthaksin Journal 2018; 13(2):165-75 (in Thai).

Chen X, Xu D, Fadeleseed S, Li L. Analysis on landscape ecological design in landscape architecture. Research in Ecology 2019;1(1):31-4.

Department of Health. Guide to Environmental Health Management in Monasteries. 1st ed. Bangkok: Samcharoen Panich (Bangkok) co. ltd.; 2019 (in Thai).

Forman RTT, Godron M. Landscape Ecology. New York: John Wiley and Sons; 1986.

Jirathasanakul S. Wat: Buddha of Thai Architecture. 1st ed. Bangkok: Thammasat Printing House; 2001 (in Thai).

Jumpasingha J, Phutthai T, Pattanakiat S. Plants community structure and diversity of flora in forest monastery. Thai Forest Ecological Research Journal 2018;2(1):26-36 (in Thai).

Kantatian W. Landscape architecture of Thai temples, and Buddhist intergrated learning and health promotion.Journal of Graduate Studies Review 2017;13(2):137-49 (in Thai).

Kanyalak Y, Chunchlee M, Suwichai T. The forest monasteries roles on human and social development process. Journal of Education and Social Development 2015;11(2):141-53 (in Thai).

Limthongkul S. Site Analysis: Project Site Analysis. 1st ed. Bangkok: Boonsiri Printing co. ltd; 2019. p. 5 (in Thai).

Makhzoumi JM. Landscape ecology as a foundation for landscape architecture: Application in Malta. Landscape and Urban Planning 2000;50(1-3):167-77.

Office of Natural Resources and Environmental Policy and Planning (ONEP). Water Sensitive Urban Design. 1st ed. Chiangmai: Tone Color Chiangmai Printing; 2005 (in Thai).

Office of the National Economics and Social Development Council (NESDC). National strategy 2018- 2037 [Internet]. 2023 [cited 2023 Jan 17]. Available from: http://nscr.nesdc.go.th/master-plans.

Pattanakiat S. Aerial Photograph: Application in Forestry. 1st ed. Bangkok: S.P. Com Interprint Limited Partnership; 2018. p. 128-85 (in Thai).

Piromkeat S. The Lay-Out of Buddhist Architecture in the Sukhothai Period at the Old Sukhothai City [dissertation]. Nakhon Pathom, Silpakorn University; 2002 (in Thai).

Royal Forest Department. National Forest Policy. Bangkok, Thailand: Planning and Information Office, Royal Forest Department; 2020. p. 34.

Royal Forest Department. National Forest Policy. Bangkok, Thailand: Planning and Information Office, Royal Forest Department; 2022: p. 8.

Saardiam T. Wat Nong Pah Pong: The model of organization administration according to the buddhist way. Journal of MCU Modern Education Studies 2020;1(1):17-21 (in Thai).

Sittipong Y, Tongtuam Y. Lanna cultural landscape ecology and the landscape Architecture Integration to Reducing Hydrological Surface Runoff Impact of Land Cover Change: A case study of Chiangmai-Lamphun Basin. Built Environment Inquiry Journal 2018;18(1):19-35.

Sornsakda S, PhrakruDhammathornSiriwat S, PhraSawai C. Patterns and processes of buddhist community forest conservation in Ubonratchathani. Journal of MCU Peace Studies 2013;1(2):11-28 (in Thai).

Suppakittpaisarn P. Research and Design in Landscape Architecture. 1st ed. Bangkok: O. S. Printing House co. ltd; 2021. p. 131 (in Thai).

Suteethorn K. Urban Forests in Temple Landscapes, The Cultural Services of an Urban Forest within a Temple Garden: The Bangkok Experience [dissertation]. Berkeley, University of California; 2018.

Tangkitngamwong O. Landscape ecology: The application to landscape planning for natural area conservation and management in Thailand. NAJUA: Architecture, Design and Built Environment 2012;25:263-87 (in Thai).

Techaamnuaywit P. The study of architectural design which support the acquixition of Sappaya in order to design Wat Pa Vimuttayalaya. Academic Journal Faculty of Architecture Khonkean University 2013;12(1):15-26 (in Thai).

The National Office of Buddhism. Report the number of temples in Thailand [Internet]. 2021 [cited 2021 Aug 8]. Available from: https://www.onab.go.th/th/content/category/index/id/805.

The United Nations Collaborative Programme on Reducing Emissions from Deforestation and Forest Degradation (UN-REDD). Readiness Preparation Proposal (R-PP) for Country: Thailand. Bangkok: Forest Carbon Partnership Facility; 2013. p. 62.

Wat Pah Nanachart. Wat Pah Nanachart. 1st ed. Ubonratchathani: Siritham Offset Printing House; 2022a (in Thai).

Wat Pah Nanachart. Wat Pah Nanachat Ubosatha Hall. 1st ed. Ubonratchathani: Siritham Offset Printing House; 2022b (in Thai).

Wonglangka W, Han F. Lanna buddhist temple: The cultural landscape as urban green space. Journal of Environmental Design 2018;5(1):106-29 (in Thai).

Wongsanao K, Krutasaen W. The study of spatial identity of forests temples and temple development standards of buddhist monastery department, National office of buddhism. Journal of MCU Peace Studies 2022;11(3):1219-33 (in Thai).

Environment and Natural Resources Journal

Volume 22
Issue 4
2024

Biomass and Carbon Stock Estimation through Remote Sensing and Field Methods of Subtropical Himalayan Forest under Threat Due to Developmental Activities

Vivek Dhiman[1,2] and Amit Kumar[1*]

[1]*RS-GIS Laboratory, Environmental Technology Division, CSIR-Institute of Himalayan Bioresource Technology, Palampur, Himachal Pradesh-176 061, India*
[2]*Academy of Scientific and Innovative Research (AcSIR), Ghaziabad- 201002, India*

ARTICLE INFO

Received: 29 Jan 2024
Received in revised: 8 Jul 2024
Accepted: 11 Jul 2024
Published online: 25 Jul 2024
DOI: 10.32526/ennrj/22/20240018

Keywords:
REDD+/ Regional climate/ Forest restoration/ Policymaking

*** Corresponding author:**
E-mail: amitkr@ihbt.res.in

ABSTRACT

Mixed subtropical forests possess a high amount of carbon pool owing to their rich species diversity and carbon sequestration potential. The Dhaulasidh forest is located in Himachal Pradesh within the subtropical Himalayan region. This research aimed to identify: (1) Optimal satellite-derived Sentinel-2A indices for predicting biomass, (2) the best-fitting model for biomass estimation, and (3) changes in above-ground carbon stock due to biomass loss, using satellite remote sensing and quadrat-based approaches. Results indicated that Band 3 (Green), Band 5 (Red edge), the vegetation (VEG) index, and the Carotenoid reflectance index (CRI) were suitable for estimating above-ground biomass (AGB). Shannon and Simpson's diversity indices were calculated as 0.89 and 0.73, respectively. Significant contributors to AGB included *Mallotus philippensis*, *Emblica officinalis*, *Cassia fistula*, *Acacia catechu*, *Ehretia laevis*, *Kydia calycina*, and *Lannea coromandelica*. The AGB prediction model based on vegetation indices demonstrated a strong correlation between observed and predicted biomass (R^2=0.65, $p<0.001$), with a mean absolute percentage error of 20% and root mean square error of 7.33 tonnes per pixel. The study predicted a total loss of 22,917.15 tonnes of CO_2 in mixed subtropical forests, representing a 12.04% reduction in carbon stock within the study area. These findings offer critical baseline data for environmental management and carbon balance in the forest ecosystem, recommending that forest management practices after deforestation should be reviewed for remedial measures for any developmental activities.

1. INTRODUCTION

The estimation of carbon loss is a crucial element for national carbon accounting. The United Nations Framework Convention on Climate Change (UNFCCC) recommends that developing countries should adhere to the Intergovernmental Panel on Climate Change (IPCC) protocol for CO_2 emission estimation (UNFCCC, 2009). Preparation of a parametric model for measuring these changes requires the collection of plot-level activity data, such as forests under degradation, carbon loss into the atmosphere due to forest degradation, and forests required to be monitored after degradation. This information may be retrieved from forest inventory data and remote sensing techniques. Forest degradation can be attributed to the loss of carbon stock within forest land (UNFCCC, 2008), mostly due to deforestation (Peres et al., 2006). To a larger extent, forest degradation contributes to 12-20% of greenhouse gas (GHG) emissions globally (CFU, 2020). Pearson et al. (2017), estimate that due to annual forest degradation, 2.1 billion tonnes of CO_2 were emitted across developing countries. From various anthropogenic activities, about 10.34% of the global forest cover was lost between 1990 and 2020 (Lousada et al., 2022). In Euthopia, Moisa et al. (2023), reported that from 1992 to 2022, forest degradation resulted in a

Citation: Dhiman V, Kumar A. Biomass and carbon stock estimation through remote sensing and field methods of subtropical Himalayan Forest under threat due to developmental activities. Environ. Nat. Resour. J. 2024;22(4):378-393. (https://doi.org/10.32526/ennrj/22/20240018)

decline in the carbon stock of 58,883.4 tonnes/km^2, and the past three decades exhibited 2,418,083.91 tonnes of carbon emission annually.

The functioning of the ecosystem is influenced by the change in regional biomass due to forest degradation as per the Reducing Emissions from Deforestation and Forest Degradation (REDD+) programme. The biomass changes are a combination of five carbon pools: above-ground biomass (AGB), below-ground biomass, soil organic matter (SOM), deadwood, and litter (IPCC, 2003). Among these, AGB accounts for CO_2 emitted due to deforestation, ultimately responsible for climatic changes (Lu et al., 2005). Carbon losses exert a substantial impact on ecosystems, posing significant threats to ecological stability and function, underscoring the critical need for evaluation (Lingbing and Jing, 2022). Research on land-use carbon emissions primarily focuses on carbon emission accounting (Luo et al., 2024; Zhang and Zhang, 2023) and low-carbon optimisation (Yan et al., 2023). In these scenarios, accurate estimation of AGB loss is central for precise quantification of CO_2 emission.

Initially, species-specific allometric equations were used for AGB estimation (Navar, 2009; Pearson et al., 2005). Allometric equations estimate biomass using parameters measured from trees (e.g., height, diameter at breast height (DBH), and wood density). These equations establish a scaling relationship between tree form and function to predict total biomass (West et al., 1999). Later, remote sensing technology gained attention for forest biomass estimation after the launch of resource-monitoring satellites (Lu et al., 2016). Consequently, allometric equations derived from the field, along with modelled remote sensing equations, were used for AGB and carbon stock estimation in forest ecosystems (Brown, 1993; Vashum and Jayakumar, 2012).

Remote sensing-based methods are widely utilised for AGB estimation due to their advantages, such as the repeatability of data collection and high correlations between spectral bands and vegetation parameters. However, selecting the spatial resolution of data is crucial as it influences the performance of image texture and discrimination of land covers, especially in complex forest stand structures (Lingbing and Jing, 2022).

According to Houghton et al. (2009), satellite missions provided the opportunity for measurement and mapping of biomass and carbon emission changes on local to global scales. Data retrieved from satellite sensors were used in measurements of different vegetation traits estimations such as the leaf area index, tree density, tree volume, tree crown size, and tree height. These traits are used in biomass estimation (Isbaex and Coelho, 2021). Information derived from the amalgamation of quadrats laid in the forest with remote sensing images is widely used in forest studies (Chen et al., 2019), embedding predictive models for monitoring AGB and carbon estimation (Castillo et al., 2017). Satellite images provide varied spatial, temporal, and spectral resolutions (Timothy et al., 2016). Low spatial resolution images with broad bandwidth were found inappropriate for AGB estimation of subtropical forests consisting of high species diversity (Mutanga and Skidmore, 2004; Pandit et al., 2018) and require high spatial resolution, narrow-bandwidth spectral images that provide comparatively more accurate AGB estimation.

The multispectral sensor of Sentinel 2 is the types of high spatial resolution (<10 m) images that are resampled to match sample plot field data. Thus, vegetation indices (VI), spectral bands, and biophysical variables (Isbaex and Coelho, 2021; Zhang et al., 2017) derived from Sentinel images can improve the accuracy of AGB predictor models. Sentinel 2 images are freely accessible at the European Space Agency (ESA) hub (Zhang et al., 2017). Chrysafis et al. (2017), found a significant relationship between growing stock volume and VI (R^2=0.63; RMSE of 63.11 m^3/ha) of Sentinel 2 MSI imagery for the heterogeneous forest in northeastern Greece. Accurate biomass estimation is crucial for analysing the impact of deforestation on regional environmental degradation in the global climate change scenario. Biomass loss estimation is also important to meet compensation actions of the REDD+ programme and the net-zero carbon emission plan of UNFCCC. These targets can be achieved using Sentinel 2 imagery, which provides an opportunity for improved and accurate AGB estimation with modelling of image-driven VI and field-measured vegetation traits (Castillo et al., 2017).

In the above background, we aimed to find Sentinel-derived best predictive indices for biomass estimation, the best-fitting model for biomass estimation, and changes in carbon stock in terms of AGB loss in the study area.

2. METHODOLOGY

2.1 Study area

Dhaulasidh is part of the subtropical Himalayan forest located at 31.80477 N latitude and 76.43964 E longitude in the Hamirpur District of Himachal Pradesh, India (Figure 1). Annual mean temperature and rainfall of the region vary from 17.96 to 27.9°C and 42.86 mm, respectively. A total of 142.6 ha area is under forest cover, having an elevation of 469-869 m AMSL. A 66W hydel power project is proposed to build on Beas River flowing in the study area. This hydel project will generate hydroelectricity and will add 304 million units of energy to the national budget. It will provide irrigation facilities to over 200 village surroundings. Worldwide hydroelectric projects contribute to approximately 16% of global electricity (IHA, 2024). For developing countries, these renewable sources are crucial to meet energy demands, but at the same time, environmental loss due to the hydel projects need to be taken care. For dam construction, a connecting road, and related infrastructure of this hydel project, tree felling was permitted by the local Himachal Pradesh government. It is assumed that approximately 10,000 trees were cut in this exercise (SIAU, 2019).

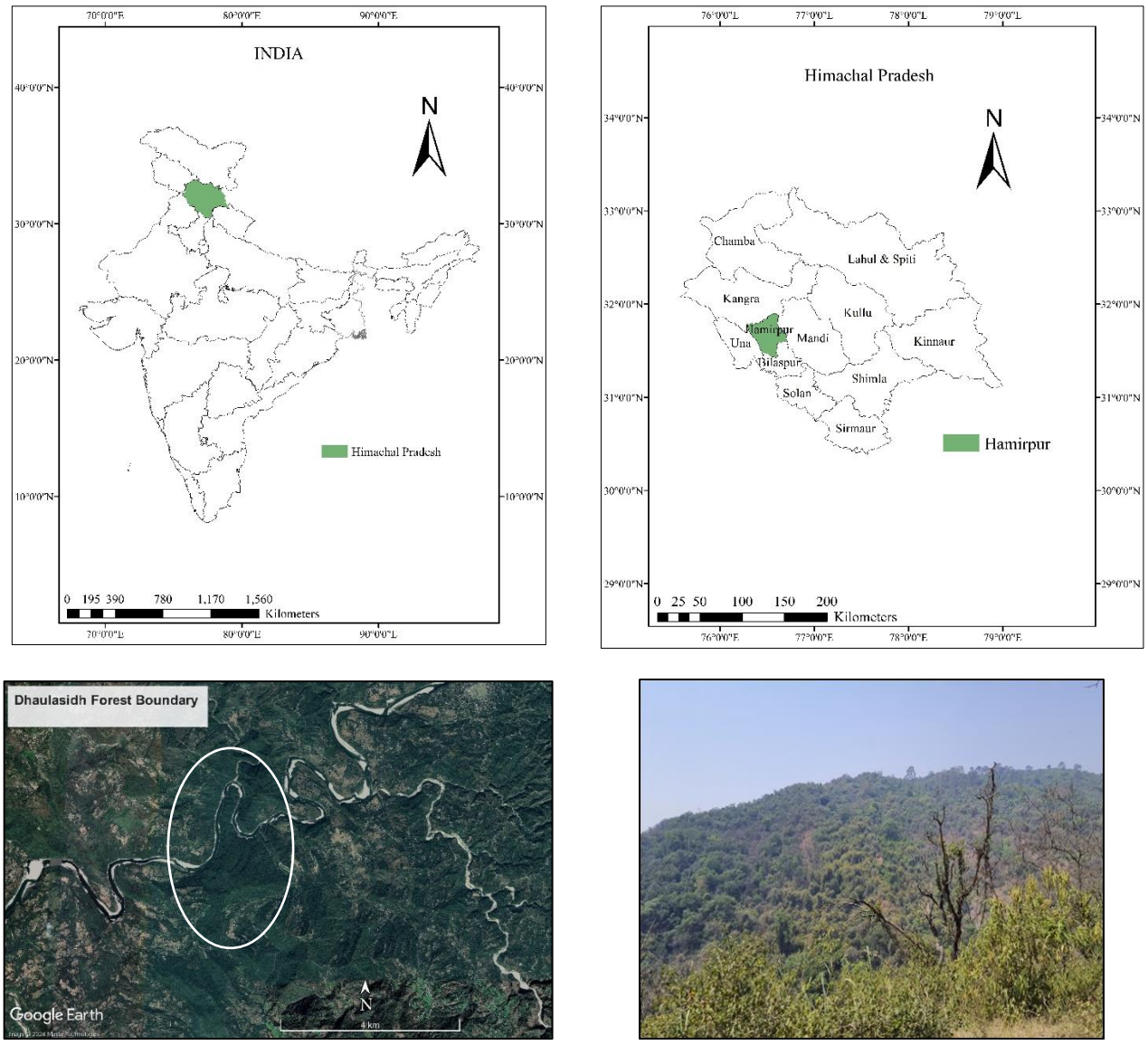

Figure 1. (a) Study area located on country map, (b) state map, (c) Google Earth imagery, and (d) in the field

2.2 Materials and methods

The overall methodology for estimating AGB of the Dhaulasidh forest is shown in Figure 2. An extensive field survey was conducted before the start of tree felling on 15-16 March 2021. A total of 15 quadrats (10×10 m) were established at 300-m

intervals to adequately represent the tree felling area (Figure 3). The geographical coordinates of each plot were recorded using a handheld Global Positioning System device. The DBH of each tree was measured using a tape measure, and tree height was measured using a clinometer. Soil samples from the study area were collected and analysed for nutrient availability, including nitrogen, phosphorus, potassium, and SOM.

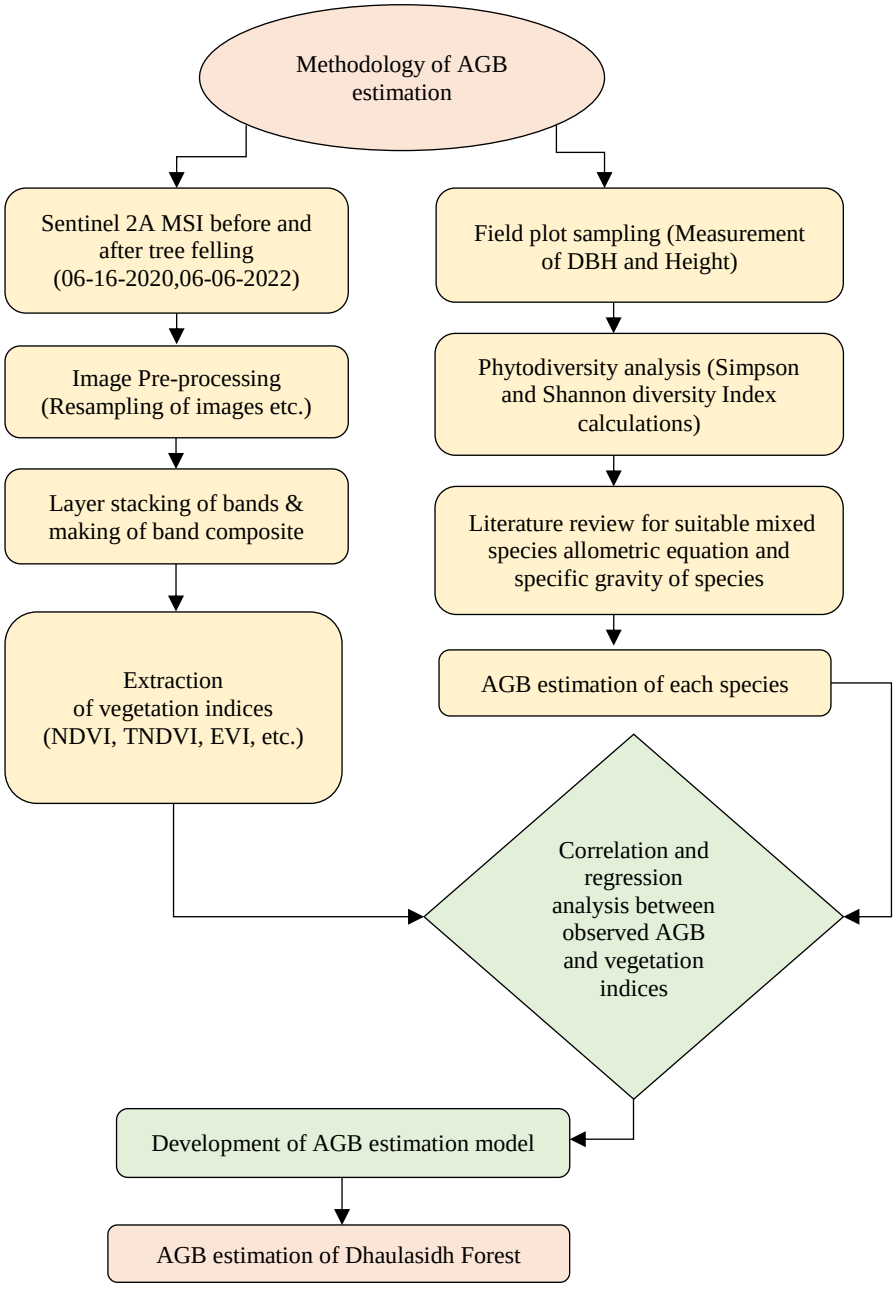

Figure 2. Flow diagram of the methodology for the biomass estimation

Before tree felling, Sentinel-2A MSI image Level-1C (16 June 2020) of the study area was acquired from the ESA for AGB estimation. Raw images were downloaded and pre-processed in the Sentinel Application Platform (SNAP) software, containing 13 spectral bands with spatial resolutions of 20 m and 60 m. In the radiometric correction process, the raw Digital number (DN) values of the Level1-C product were converted into Top of Atmosphere (TOA) radiance using sensor-specific calibration coefficients provided in the metadata. Subsequently, TOA radiance was converted to TOA reflectance. Additionally, the data required resampling and subsetting to match the field variables. Therefore, in the geometric correction method of SNAP, the radiometric corrected images were resampled to 10-m resolution to match the size of the field quadrats. Sentinel images (6 July 2022) were used for AGB loss

estimation after tree felling. Using the supervised classification method, these satellite images were classified (Figure 4) in Erdas Imagine software version 16, and the land cover map was prepared. The training dataset for classification was identified through visual image interpretation. The maximum likelihood parametric decision rule was applied to image pixels and the land cover map prepared, resulting in forest classes mixed with open/barren lands. Forest canopy cover >70% was categorised as very dense forest, 50-70% as dense forest, 40-50% as moderately dense forest, 10-40% as open forest, and <10% canopy cover as scrub forest (Farooq and Rashid, 2010).

Figure 3. 10×10-meter quadrat-based vegetation sampling in the study area

The accuracy of the classified image was assessed using sensitivity, specificity, and true skill statistical (TSS) analysis in the R software package. A 2×2 confusion matrix was applied to the classified images to determine true positives (a), false positives (b), false negatives (c), and true negatives (d) using Equations (1-3) (Allouche et al., 2006).

$$\text{Sensitivity} = \frac{a}{a+c} \quad (1)$$

$$\text{Specificity} = \frac{d}{b+d} \quad (2)$$

$$\text{TSS} = \text{Sensitivity} + \text{Specificity} - 1 \quad (3)$$

The phytodiversity of the study area was calculated using Simpson (Simpson, 1949) and Shannon-Weiner Indices (Shannon and Weaver, 1949) using Equations 4 and 5. The Simpson diversity index measures the presence and abundance of species in their habitat, while the Shannon-Weiner index measures uncertainty of the species and community diversity. Lower uncertainty indicates lower community diversity and vice versa.

$$\text{Simpson diversity index (D)} = 1/\sum_{i=1}^{s} p_i^2 \quad (4)$$

Where; p = proportion (n/N) of individuals of one particular species (n) divided by total number of individuals (N), Σ is the sum of the calculations, and s=number of species.

$$\text{Shannon-Weiner Index (H)} = -\sum_{i=1}^{s} p_i \ln p_i \quad (5)$$

Where; p=proportion (n/N) of individuals of one particular species (n) divided by the total number of individuals (N), ln is natural log, Σ is the sum of the calculations, and s=number of species.

Global, regional, and local biomass estimations are influenced by the choice of biomass estimation equation. Therefore, the selection of an equation is

crucial as it affects accuracy when applied with remote sensing data for regional biomass prediction (Mitchard et al., 2013). Several allometric equations are available for AGB estimation (Chaturvedi and Raghubanshi, 2013; Rawat and Singh, 1988); among them, the equation proposed by Nath et al. (2019), (Equation 6) was considered the most accurate for AGB estimation of mixed woody species and was used in this study.

$$AGB\ (kg/m^3) = 0.32*p*D\text{^}2* H\text{^}0.75 *1.34 \quad (6)$$

Where; p=wood density, D=diameter at breast height, H=height.

Wood density or wood specific gravity (WSG) is an important factor in forest biomass calculations (Fearnside, 1997). It represents the density of oven-dried wood relative to water density and varies between species due to water content differences (Kuyah et al., 2012; Mukuralinda et al., 2021). In this study, WSG values for plant species (Table 1) were obtained from a subtropical species-based wood density database (Reyes, 1992) and literature on Himalayan woody species. These WSG values were used for quadrat-wise AGB estimation (Equation 6).

The carbon stock of the study area was calculated using Equation 7 by multiplying biomass with a carbon fraction value of 0.47 (IPCC, 2006).

$$C = AGB \times CF \quad (7)$$

Where; C=carbon stock, CF=carbon fraction value.

A review of literature was conducted to identify spectral VI used in biomass estimation (Table 2). These indices were calculated for Sentinel images before tree felling. The shapefile of the quadrat overlaid on the spectral vegetation index image allowed the retrieval of indices for each quadrat. An AGB prediction model was developed by correlating spectral VI with biomass for each quadrat. This model was applied to the Sentinel image of the study area for regional biomass estimation.

Table 1. Various wood specific gravity values used in the present study

Serial No.	Species with wood specific gravity values	Source
1	*Bauhinia veriegata*=0.59, *Lannea coromandelica*=0.46, *Bombax malabaricum*=0.33, *Casearia elliptica*=0.64, *Toona ciliata*=0.55, *Ehretia laevis*=0.56, *Melia azedarach*=0.69, *Acacia catechu*=0.77, *Ficus auriculata*=0.44, *Dalbergia sissoo*=0.68, *Cassia fistula*=0.81, *Ougeniao ojeinensis*=0.60, *Grewia optiva*=0.71, *Syzygium cumini*=0.66, *Mallotus philippinensis*=0.64, *Emblica officinalis*=0.61	Sheikh et al. (2011)
2	*Terminalia chebula*=0.96, *Kydia calycina*=0.72, *Crataeva religiosa*=0.53, *Albizia lebbeck*=0.55, *Zanthoxylum rhetsa*=0.33	Reyes (1992)
3	*Ehretia laevis*=0.56, *Eugenia jambolana* Lam.=0.89	ICRAF (2007)
4	*Ficus religiosa* L.=0.51, *Ziziphus mauritiana*=0.49	Bisleshna et al. (2019)

Table 2. Spectral vegetation indices for biomass estimation used in the present study

Vegetation Indices	Formula	Reference
Woebbecke index (WI)	G–B/R–G	Woebbecke et al. (1995)
Normalized Difference Vegetation Index (NDVI)	(NIR–R)/(NIR+R)	Rouse et al. (1974)
Wide Dynamic Range Vegetation Index (WDRVI)	(0.1*NIR–R)/(0.1*NIR+R)	Gitelson (2004)
Colour Index of Vegetation (CIVE)	0.441*R0.881*G+0.385*B+18.78745	Kataoka et al. (2003)
Vegetative (VEG)	$G/(R^aB^{(1-a)})$; a= 0.66	Marchant and Onyango (2000)
Excess Green Index (ExG)	2*G–R –B	Woebbecke et al. (1995)
Visible Atmospherically Resistant Index (VARI)	G–R/G+R–B	Gitelson et al. (2003)
Excess Green minus Excess Red (ExGR)	ExG –1.4*R – G	Meyer and Neto (2008)
Ratio Vegetation Index (RVI)	NIR/R	Pearson and Miller (1972)
Green Leaf Index (GLI)	2*G–R–B)/(2*G+R+B)	Hunt et al. (2011)
Normalized Green Red Difference Index (NGRDI)	G–R/G+R	Gitelson et al. (2002a)
Carotenoid Reflectance Index (CRI)	$1/R_G+1/R_{NIR}$	Gitelson et al. (2002b)

Table 2. Spectral vegetation indices for biomass estimation used in the present study (cont.)

Vegetation Indices	Formula	Reference
Transformational Vegetation Index(TVI)	$\sqrt{NDVI + 0.5}$	Broge et al. (2001)
SAVI (Soil-Adjusted Vegetation Index)	$(R_{NIR}–R_R)/(R_{NIR}+R_R+0.5)\times1.5$	Huete (1988)
Optimized Soil-Adjusted Vegetation Index (OSAVI)	$(R_{NIR}–R_R)/(R_{NIR}+R_R+1.6)\times1.16$	Rondeaux et al. (1996)
Green-NDVI (GNDVI)	$(R_{NIR}–R_G)/(R_{NIR}+R_G)$	Gitelson (1996)
Ratio Vegetation Index (RVI)	R_{NIR}/R_R	Baret et al. (1991)
Enhanced Vegetation Index (EVI)	$2.5\times(R_{NIR}–R_R)/(1+R_{NIR}+6\times R_R–7.5\times R_B)$	Liu and Huete (1995)
Modified Simple Ratio Index (MSR)	$((R_{NIR}/R_R)–1)/\sqrt{R_{NIR}/R_R + 1}$	Chen (1996)
Nonlinear Vegetation Index (NLI)	$(R_{NIR}\times R_{NIR}–R_R)/(R_{NIR}\times R_{NIR}+R_R)$	Goel and Qin (1994)
Re-normalized Difference Vegetation Index (RDVI)	$(R_{NIR}–R_R)/\sqrt{R_{NIR}+R_R}$	Ke et al. (1998)
Modified Triangular Vegetation Index 2 (MTVI2)	$1.5\times[1.2\times(R_{NIR}–R_G)–2.5\times(R_R–R_G)/\sqrt{2\times(R_{NIR}+1)^2 – 6\times R_{NIR} + 5\times\sqrt{R_R – 0.5}}$	Haboudane et al. (2004)

3. RESULTS

Analysis of the land cover map of the Dhaulasidh forest before and after deforestation (Figure 4, Figure 5, and Table 3) revealed significant decreases in forest types post-tree felling: a 2.55% decrease in very dense forests (from 196.18 ha in 2020 to 186.06 ha in 2022), 1.25% reduction in dense forests (from 160.26 ha to 155.05 ha), 1.71% decrease in moderately dense forests (from 43.51 ha to 36.43 ha), 0.26% decline in open forests (from 9.56 ha to 8.45 ha), and 0.29% reduction in barren land (from 6.23 ha to 5.02 ha).

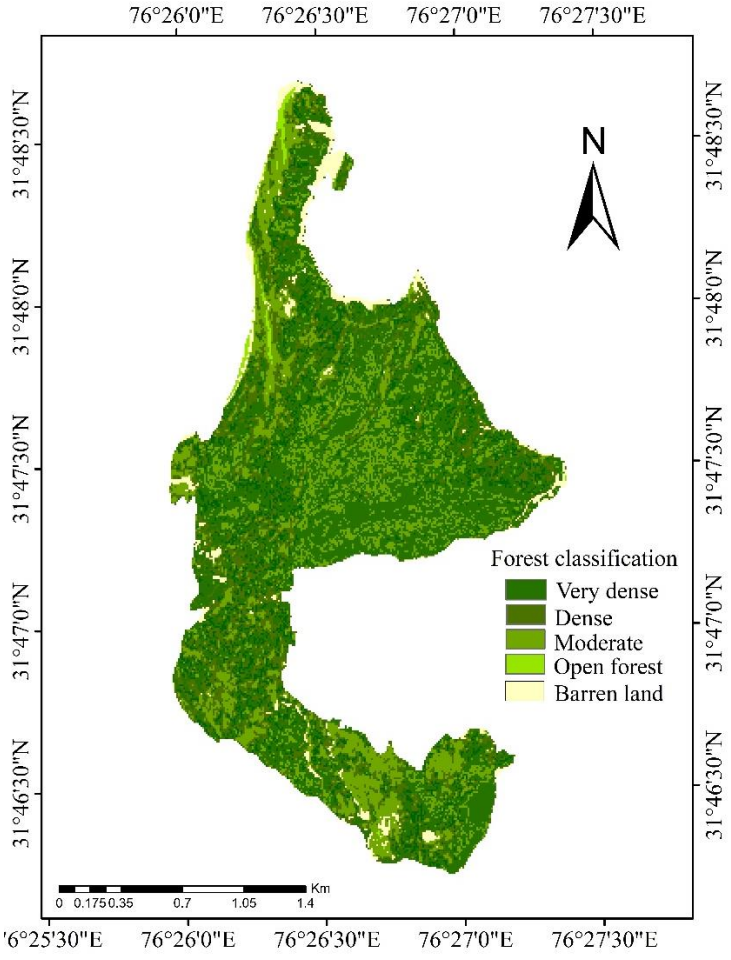

Figure 4. Classified land cover map of 2020 of the study area before tree felling

Table 3. Forest type and representation area of land cover map of 2020 before tree felling

Land cover type	2020 before tree felling area (ha)	2022 after tree felling area (ha)	Change (%)
Very dense forest	196.18	186.06	-2.55%
Dense forest	160.26	155.05	-1.25%
Moderately dense forest	43.51	36.43	-1.71%
Open forest	9.56	8.45	-0.26%
Barren land	6.23	5.02	-0.29%

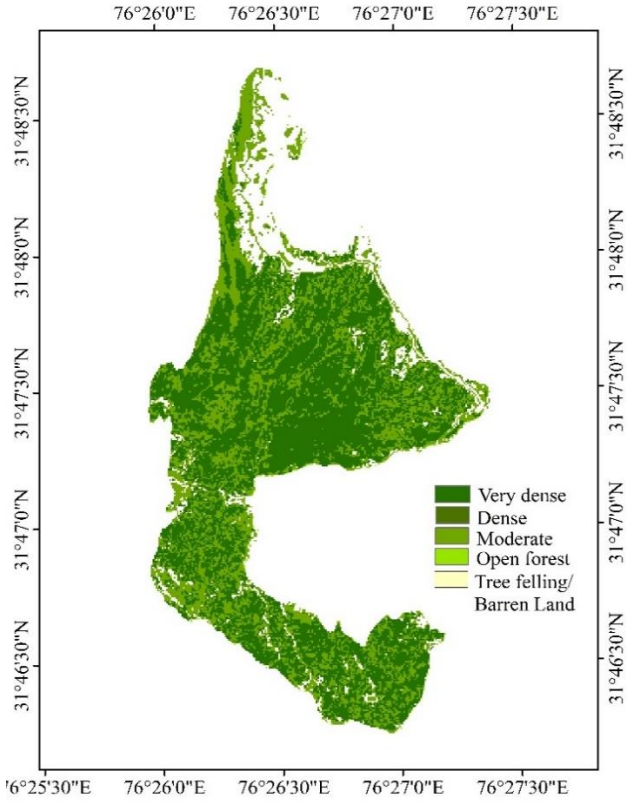

Figure 5. Classified land cover map of 2022 of the study area after tree felling

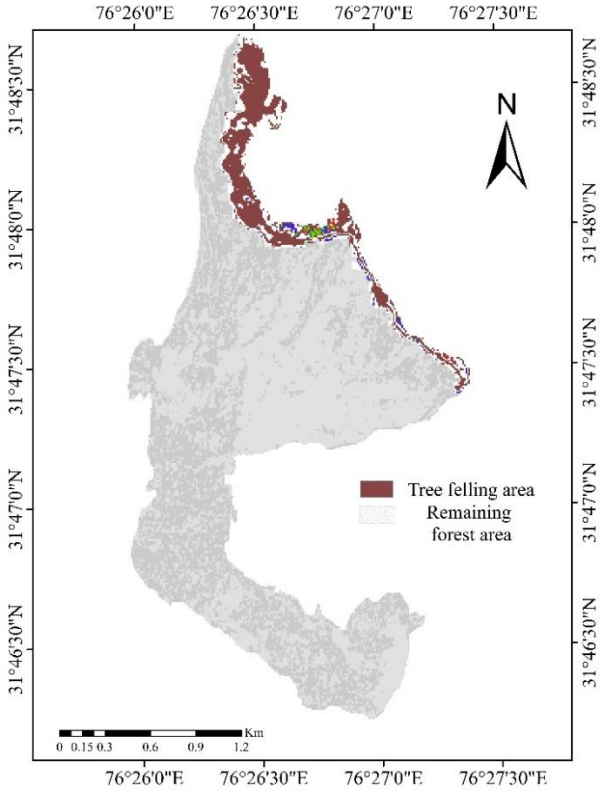

Figure 6. Forest area underwent tree felling for hydel project

The accuracy assessment of the classified image provided sensitivity, specificity, and TSS values of 0.8633, 0.9420, and 0.8059, respectively. It was unaffected by the occurrence and size of the validation set (Allouche et al., 2006), calculated commission and omission errors, and assessed results ranging from –1 to +1, where +1 indicates ideal agreement and values towards 0 and below indicate poorer results.

3.1 Quadrat-wise AGB

The quadrat-wise AGB of the Dhaulasidh forest was estimated (Table 4) using Equation 6 with WSG values (Table 1) of individual species. The 13th quadrat had the lowest AGB (2.56 tonnes/ha), whereas the 5th quadrat had the highest AGB (25.5 tonnes/ha). Phytodiversity analysis found Simpson diversity index (D) ranging from 0 to 0.89 and Shannon-Weiner Index (H) from 0 to 0.73. The 2nd quadrat showed zero diversity due to dominance by *Mallotus philippinensis*. The 9th quadrat possessed the highest species diversity, hosting six species: *Cassia fistula*, *Bombax malabaricum*, *Emblica officinalis*, *Acacia catechu*, *Mallotus philippinensis*, and *Crataeva religiosa.*

A total of 25 woody species were recorded across 15 quadrats during field surveys. These species were *Ziziphus mauritiana*, *Zanthoxylum rhetsa*, *Mallotus philippinensis*, *Albizia lebbeck*, *Ficus religiosa*, *Syzygium cumini*, *Grewia optiva*, *Ougenia oojeinensis*, *Eugenia jambolana*, *Cassia fistula*, *Emblica officinalis*, *Dalbergia sissoo*, *Mangifera indica*, *Acacia catechu*, *Ehretia laevis*, *Melia azedarach*, *Ficus auriculata*, *Casearia tomentosa*, *Toona ciliata*, *Bombax malabaricum*, *Crataeva*

religiosa, *Kydia calycina*, *Lannea coromandelica*, *Terminalia Chebula*, and *Bauhinia variegata*.

Table 4. Quadrat-wise biomass of the study area

Quadrat No.	Area (m^2)	AGB (ton/ha)
1	100	17.94
2	100	23.04
3	100	7.79
4	100	7.29
5	100	25.5
6	100	6.91
7	100	3.47
8	100	4.93
9	100	2.72
10	100	3.86
11	100	5.83
12	100	15.72
13	100	2.56
14	100	4.33
15	100	12.98

3.2 Derivation of AGB from Sentinel image

Polynomial R^2 values of Sentinel image-based spectral bands and vegetation indices (Table 2) with field-observed AGB ranged from 0.13 to 0.68. Second-order polynomial regression was chosen because AGB values for forest species were nonlinear, and a linear regression model would not provide the best-fit line, limiting prediction accuracy.

Predictive variables Green (Band 3), VNIR (Band 5), VEG, and CRI yielded significant coefficient values (Ostertagova, 2012): R^2=0.59, 0.51, 0.59, and 0.68, respectively (Figure 7). Other indices (EVI, NDVI, NDVI45, NLI, ExG, and GLI) showed lower coefficients of determination R^2=0.18, 0.36, 0.26, 0.41, 0.34, and 0.30. Therefore, insignificant predictive variables were excluded from the regression analysis due to multicollinearity, resulting in high variance in prediction (Chen et al., 2018).

Using significant predictor variables, a polynomial regression model (Equation 8) was developed for AGB prediction. Equation 8 was used to calculate AGB values for individual image pixels, providing AGB estimates for the entire forest area. Over- and underestimated pixels were normalised by assigning the mean value of nearby pixels. The derived AGB map of the Dhaulasidh forest (Figure 9(a)) provided biomass estimates ranging from 8 to 38 tonnes/pixel.

$$AGB = \{(327{,}792\times B3^2-57{,}779\times B3+2{,}551.3) + (12{,}840\times B5^2-24{,}919\times B5+1{,}213.9) + (327{,}792\times VEG^2-57{,}779\times VEG+2{,}551.3) + (3.803\times CRI^2-111.1\times CRI+814.64)\} \quad (8)$$

3.3 Model validation for AGB prediction

For validation of the prediction model, predicted and observed AGB values were plotted on the goodness-of-fit line, showing a strong relation with R^2=0.65 (Figure 8) and multiple R=0.61 (p-value<0.5, i.e., 0.01). Mean absolute percentage error (MAPE) was 20% (RMSE=7.33 tonnes/pixel). A MAPE of 10-20% suggests good prediction (Makridakis et al., 1998) and acceptable accuracy (Lewis, 1982). Using the AGB prediction model (Equation 8), a total of 404,686.51 tonnes of AGB was estimated in the 415.74 ha area of the Dhaulasidh forest before tree felling. Similarly, 355,926.63 tonnes of AGB was estimated after tree felling.

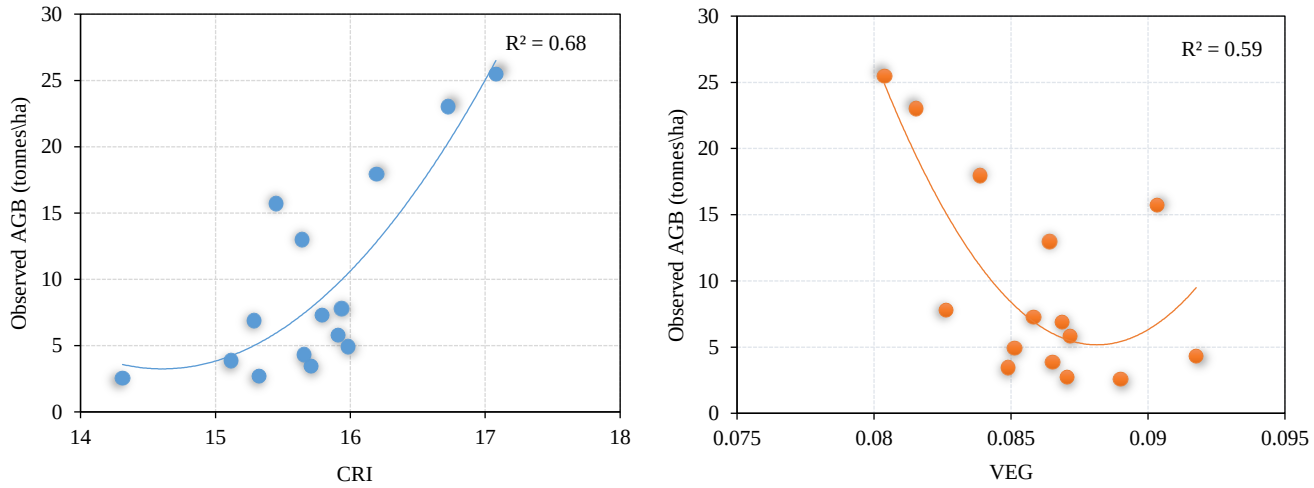

Figure 7. Polynomial regression between spectral values and vegetation indices of image with observed AGB in the field

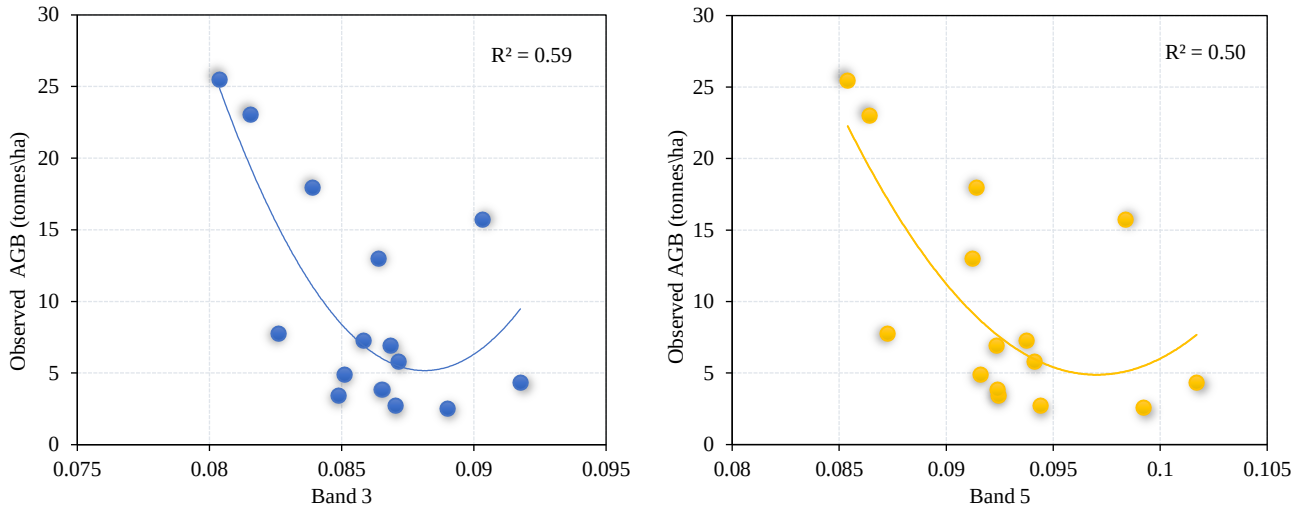

Figure 7. Polynomial regression between spectral values and vegetation indices of image with observed AGB in the field (cont.)

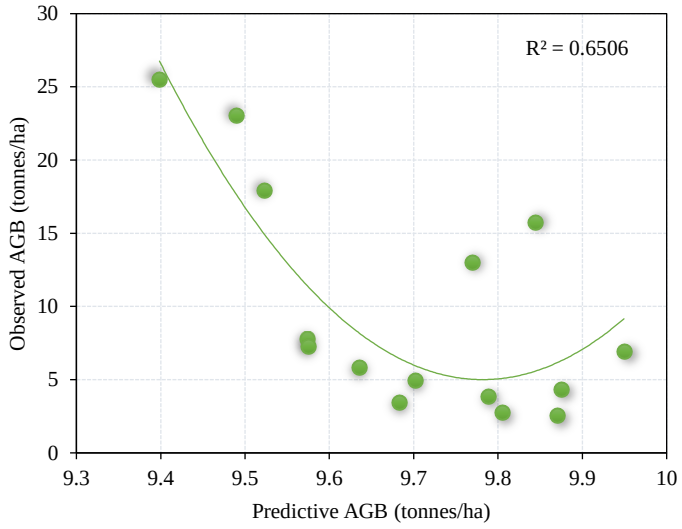

Figure 8. Regression coefficient (R^2) of estimated and observed AGB

3.4 Carbon stock estimation

Using Equation 7 the total above-ground carbon stock was estimated as 190,202.66 C/tonnes/pixel (Figure 9(a)). After tree felling, 167,285.51 C/tonnes/pixel of carbon was estimated. The change in carbon stock of the Dhaulasidh forest was calculated using Equation 9. Thus, a total of 22,917.15 tonnes of carbon loss was estimated due to the tree felling drive for the hydel project in the study area. The obtained results indicate 48,759.88 tonnes of AGB (Figure 9(b)) loss in the Dhaulasidh forest, leading to a reduction in the natural carbon sink. In addition, a total 12.04% loss was observed in AGB and carbon stock of the forest.

Change in carbon stock (ton) = Total Carbon before tree felling – Total carbon after tree felling (9)

4. DISCUSSION

The Green (Band 3) and Red edge (Band 5) bands of Sentinel 2 are efficient in predicting forest-related parameters, including biomass (Astola et al., 2019), which was also found to be significant in our study. The AGB is influenced by the Red edge band due to its presence between high chlorophyll reflectance (red region) and absorption (NIR) regions. The Red edge band, ranging from 680 to 740 nm, reflects the canopy of the forest and is crucial for assessing vegetation and their pigments (Clevers and Gitelson, 2013). Any changes in leaf properties of vegetation can be observed in this region (Slonecker et al., 2009). VEG and CRI indices show a strong

relationship with quadrat AGB, as the reflectance of the Green band strongly influences vegetation indices. Other indices, such as NDVI and EVI, did not show a significant relationship with observed AGB due to pixel saturation caused by high biomass and other factors such as soil, clouds, and atmospheric effects (Nandy et al., 2017).

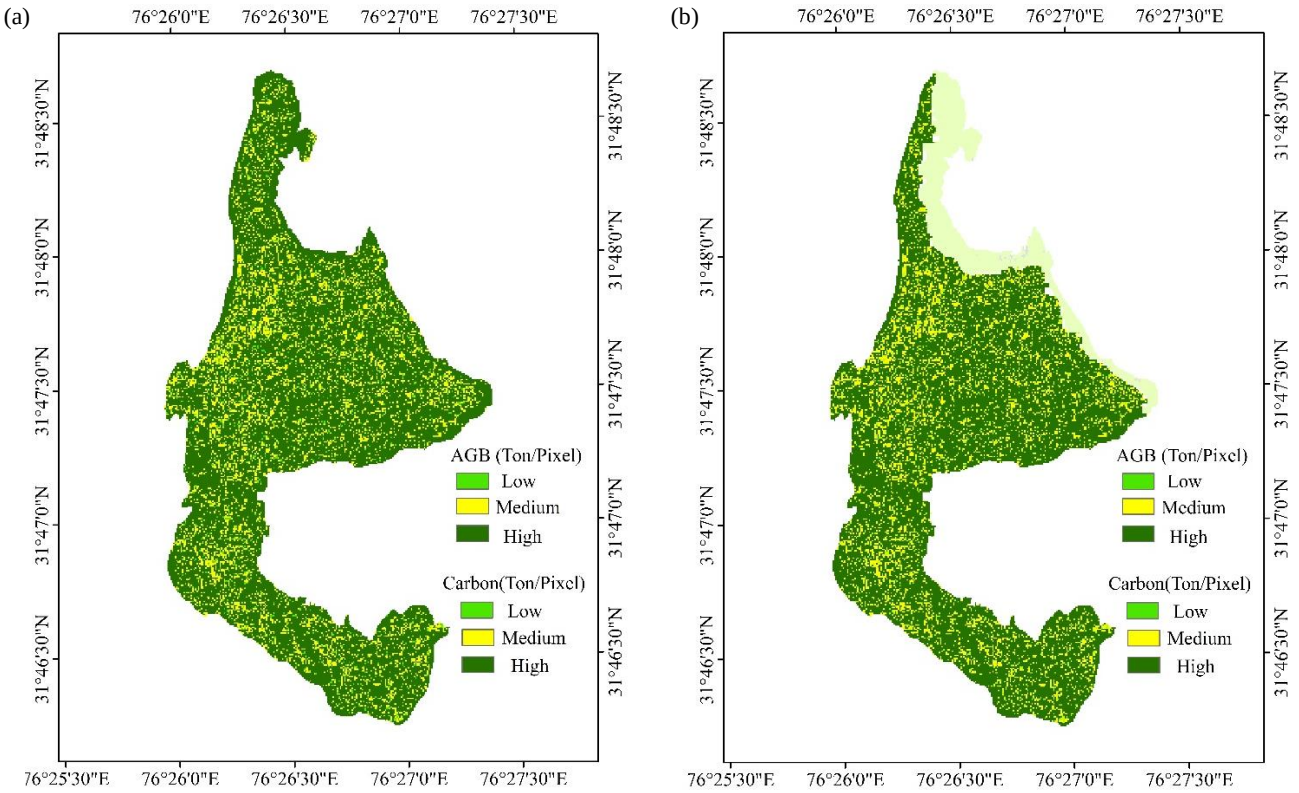

Figure 9. Before and after deforestation AGB and Carbon stock map (a, b) of the study area

The present results of the polynomial model were consistent with those of Ali et al. (2023), where the strongest polynomial regressions of 0.70, 0.70, and 0.72 were observed between AGB and Sentinel 2A-derived indices NDVI, RVI, and ARVI in natural Chir-pine forests. However, a 5% regression value was lower in present study due to the high species diversity in the forest than in mono-plantations. Similar findings for biomass prediction were associated with Lu et al. (2012), indicating that 1st- and 2nd-order polynomial regression models provide accurate prediction results.

While regression models are widely used to analyse factors influencing carbon emissions (Zwane et al., 2023), their integration with diverse space-borne datasets is crucial. This approach not only aids in estimating forest AGB and associated uncertainties but also provides insights into the value of different space-borne datasets, considering coverage area, spatial, and spectral resolution. Such integration allows for biomass estimation in a manner that is both time- and cost-efficient. Khan et al. (2024), examined various remote sensing techniques for estimating forest AGB and found that different forms of regression models are the second most commonly used after random forest models, with varying parameters of space-borne data. Although in the diverse nature of forest environments, it is challenging to identify specific remote sensing datasets, and regression models perform best among others.

The AGB of the study area was calculated as 975 tonnes/hectare, consistent with the AGB range of mixed Himalayan forests at 808.05 tonnes/hectare (Nandy et al., 2017). Species such as *Mallotuss philippensis*, *Emblica officinalis*, *Cassia fistula*, *Acacia catechu*, *Ehretia laevis*, *Kydia calycina*, and *Lannea coromandelica* were found to possess high AGB derived from the quadrat method, similar to findings from the central Himalayan region (Joshi et al., 2021). The mean carbon stock of *Mallotus philippensis* was found to be 0.3473 megagram, and the mean carbon stock of other species was calculated as 0.2350 megagram. The mean basal area was retrieved as 323.1749 square feet/acre for *M.*

philippensis, while for other species, it was 130.39 square feet/acre. The results of Shannon and Simpson diversity analysis, with values of 0.89 and 0.73 respectively, indicate medium to high diversity, underscoring the contribution of mixed species to high AGB in the study area.

Before tree felling, the average AGB of the Dhaulasidh forest was estimated as 9.74 tonnes/pixel, with a minimum of 8.70 tonnes/pixel and a maximum of 38 tonnes/pixel, indicating high AGB levels. After tree felling, the average AGB was observed to be 9.65 tonnes/pixel, with a minimum of 8.70 tonnes/pixel and a maximum of 20.68 tonnes/pixel. AGB ranges were classified as low (8-12 tonnes/pixel), medium (12-16 tonnes/pixel), and high (>16 tonnes/pixel) (Figure 9(a, b)). Soil analysis showed that the soil was highly rich in nutrient contents, with nitrogen ranging from 175.68 to 407.8 kg/ha, phosphorus from 3.96 to 56.13 kg/ha, potassium from 108.03 to 685.66 kg/ha, and SOM from 5.27% to 10.09%. The presence of water bodies within the forest also provides optimal conditions for the growth of the Dhaulasidh forest. These conditions may favour the accumulation of high AGB content.

The study area witnessed mass tree felling (Figure 6), resulting in conditions favourable for an increase in surface albedo, which is the ratio of total radiation reflected from a surface to the total incoming radiation illuminating the surface (Yan et al., 2021). Deforestation influences biogenic volatile organic compounds emitted by forests and affects short-lived climate forcers such as aerosols, ozone, and methane (Scott et al., 2018). Due to deforestation, the incident radiation absorbed by land surfaces may warm the local climate, which needs to be investigated in future studies. While this process is gradual, warming will occur more rapidly in deliberate deforestation scenarios as observed in the present case. Mixed forests promote high biological diversity, carbon storage, and productivity (Nadrowski et al., 2010). Changes in forest cover respond to rainfall patterns and moisture content, affecting evaporative cooling limits due to rainfall (Pitman et al., 2011). The loss of 22,917.15 tonnes of carbon dioxide in the study area due to AGB loss may increase water use efficiency, reducing evapotranspiration (ET). ET is the sum of evaporation from plant surfaces, canopy litter interception, and evaporation from the soil (Baldocchi et al., 2001; Levia et al., 2011). Changes in ET could potentially alter atmospheric moisture content and reduce the local cooling effect (Lawrence et al., 2022), leading to soil erosion and changes in the watershed regime of the forest area. According to Aber and Federer (1992), plant transpiration is closely related to ecosystem productivity and carbon sequestration. Changes in regional climate may influence leaf energy balance, succession stage, morphology stage, and leaf nutrients. A long-term case study of subtropical forests by Zhou et al. (2013), demonstrated that due to temperature rise DBH, height, and biomass of individuals decrease. Also, vegetation shifts are noted as climax communities are replaced by smaller individuals (herbs, shrubs, small trees) due to an imbalance between mortality and recruitment rates. In the Dhaulasidh forest, the invasion of pioneer species over climax species may result from the boundary region of the felling area spreading towards the core zone of the forest. Therefore, species such as *Albizia lebbeck*, *Ficus religiosa*, *Acacia catechu*, *Emblica officinalis*, *Bombax malabaricum*, etc., with high DBH ranges may be considered under threat from pioneer species such as *Lantana camara* and *Murraya koenigii*.

The remaining forests after deforestation need to be prioritised for conservation efforts, which may help in recovering AGB and enhancing the carbon pool in the existing forest (Gann et al., 2019). Already degraded sites should be selected instead of focusing on non-forest land to tackle desertification (Liu et al., 2020), utilising technologies such as drones and LiDAR (Deere et al., 2020). Multiple stakeholders and local communities should participate in reforestation projects.

Assisted natural regeneration could be applied by selectively planting missing species and clearing weeds to boost natural regeneration (FAO, 2019). The framework species approach may be followed by planting mixed species that shade out herbaceous weeds, which attract seed dispersal by animals. Selection of mixed species for plantation is important over monoculture (Brancalion and Chazdon, 2017). When natural regeneration is insufficient, tree plantation is necessary for forest restoration following the Nucleation approach of planting trees in small groups (Zahawi et al., 2013). Prioritisation should be given to native species while avoiding invasive species to achieve a high level of biodiversity with biomass. The key outcome of such plantations is to maximise functional diversity alongside natural diversity. The above conservation and management strategies are of utmost importance for biomass accumulation and biodiversity recovery after deforestation in the study area.

5. CONCLUSION

This research focused on carbon stock estimation due to deforestation in the subtropical Himalayas and revealed that CRI and VEG are the most effective indices, and the Green and Red edge bands of Sentinel 2A products are appropriate for biomass estimation in mixed forests. The best-fitting polynomial model was established between these indices and observed biomass. Therefore, a 12.04% loss in carbon stock might indicates significant ecological shifts in species due to potential consequences of deforestation, such as an increase in surface albedo contributing to local climate warming and altered rainfall patterns in the study area. Concurrently, shifts in vegetation composition may occur, with climax communities potentially being replaced by pioneer species. As such, urgent attention and prioritisation are required for conservation efforts in the study area. Moreover, this study has provided important baseline information for policymakers and established a framework for estimating carbon loss resulting from deforestation. We recommend proactive environmental management strategies that consider carbon sequestration dynamics in any developmental activities.

ACKNOWLEDGEMENTS

Authors thank Director, CSIR-IHBT, Palampur, India for providing his encouragement and facilities in carrying out this research. We are thankful to CCF, Hamirpur forest circle, Himachal Pradesh State Forest Department and staff members of Environmental Technology, CSIR-IHBT for lending their support during in the field work. Mr. Sunil Kumar, research scholar, AcSIR-CSIR-IHBT is acknowledged for his suggestions in the preparation of this manuscript. Author Vivek Dhiman acknowledges the University Grant Commission (UGC) (commencement No. 190510008590) for providing SRF fellowship.

Funding: This work is funded by University Grant Commission (UGC) (commencement No. 19051 0008590) of providing SRF Fellowship to author Vivek Dhiman. Also, this work was carried out under CSIR in-house funded project entitled “Assessing, monitoring, conserving Himalayan bio resources vis-a-vis understanding plant strategies and functions for its sustainable utilization (MLP-0206)”. This article represents CSIR-IHBT communication number 5333.

Declaration of Interest Statement: The authors declare no conflict of interests.

Data availability: The authors declare that all the raw, processed and analysed data related to the present study is with us and may be made available from the corresponding author upon reasonable requests, which is subject to further official formalities and approval from the competent authority.

REFERENCES

Aber JD, Federer CA. A generalized, lumped-parameter model of photosynthesis, evapotranspiration and net primary production in temperate and boreal forest ecosystems. Oecologia 1992;92:463-74.

Allouche O, Tsoar A, Kadmon R. Assessing the accuracy of species distribution models: Prevalence, kappa and the true skill statistic (TSS). Journal of Applied Ecology 2006; 43(6):1223-32.

Ali N, Saad M, Ali A, Ahmad N, Khan IA, Ullah H, et al. Assessment of aboveground biomass and carbon stock of subtropical pine forest of Pakistan. Journal of Forest Science 2023;69:287-304.

Astola H, Hame T, Sirro L, Molinier M, Kilpi J. Comparison of Sentinel-2 and Landsat 8 imagery for forest variable prediction in boreal region. Remote Sensing of Environment 2019; 15(223):257-73.

Baldocchi D, Falge E, Gu L, Olson R, Hollinger D, Running S, et al. FLUXNET: A new tool to study the temporal and spatial variability of ecosystem-scale carbon dioxide, water vapor, and energy flux densities. Bulletin of the American Meteorological Society 2001;82(11):2415-34.

Baret F, Guyot G. Potentials and limits of vegetation indices for LAI and APAR assessment. Remote Sensing of Environment 1991;35(2-3):161-73.

Bisleshna T, Sarkar BC, Pala NA, Gopal S, Sofi PA. Wood specific gravity of some tree species in sub-tropical humid climate of India. Indian Forester 2019;145(7):637-42.

Brancalion PH, Chazdon RL. Beyond hectares: Four principles to guide reforestation in the context of tropical forest and landscape restoration. Restoration Ecology 2017;25(4):491-6.

Broge NH, Leblanc E. Comparing prediction power and stability of broadband and hyperspectral vegetation indices for estimation of green leaf area index and canopy chlorophyll density. Remote Sensing of Environment 2001;76(2):156-72.

Brown S. Tropical forests and the global carbon cycle: The need for sustainable land-use patterns. Agriculture, Ecosystems and Environment 1993;46(1-4):31-44.

Castillo JA, Apan AA, Maraseni TN, Salmo III SG. Estimation and mapping of above-ground biomass of mangrove forests and their replacement land uses in the Philippines using Sentinel imagery. ISPRS Journal of Photogrammetry and Remote Sensing 2017;134:70-85.

Chaturvedi RK, Raghubanshi AS. Aboveground biomass estimation of small diameter woody species of tropical dry forest. New Forests 2013;44:509-19.

Chen L, Wang Y, Ren C, Zhang B, Wang Z. Assessment of multi-wavelength SAR and multispectral instrument data for forest aboveground biomass mapping using random forest kriging. Forest Ecology and Management 2019;447:12-25.

Chen JM. Evaluation of vegetation indices and a modified simple ratio for boreal applications. Canadian Journal of Remote Sensing 1996;22(3):229-42.

Chen L, Ren C, Zhang B, Wang Z, Xi Y. Estimation of forest above-ground biomass by geographically weighted regression and machine learning with sentinel imagery. Forests 2018;9(10):Article No. 582.

Chrysafis I, Mallinis G, Siachalou S, Patias P. Assessing the relationships between growing stock volume and Sentinel-2 imagery in a Mediterranean forest ecosystem. Remote Sensing Letters 2017;8(6):508-17.

Clevers JG, Gitelson AA. Remote estimation of crop and grass chlorophyll and nitrogen content using red-edge bands on Sentinel-2 and -3. International Journal of Applied Earth Observation and Geoinformation 2013;23:344-51.

Climate Funds Update (CFU). Climate Finance Thematic Briefing: REDD+ Finance. Washington, USA: Heinrich Boll Stiftung; 2020.

Deere NJ, Guillera-Arroita G, Swinfield T, Milodowski DT, Coomes DA, Bernard H, et al. Maximizing the value of forest restoration for tropical mammals by detecting three-dimensional habitat associations. Proceedings of the National Academy of Sciences 2020;117(42):26254-62.

Food and Agricultural Organization (FAO). Restoring Forest Landscapes through Assisted Natural Regeneration (ANR): A Practical Manual. Bangkok: Food and Agriculture Organization of the United Nations; 2019.

Farooq M, Rashid H. Spatio temporal change analysis of forest density in Doodhganga Forest range, Jammu and Kashmir. International Journal of Geomatics and Geosciences 2010; 1(2):132-40.

Fearnside PM. Wood density for estimating forest biomass in Brazilian Amazonia. Forest Ecology and Management 1997;90(1):59-87.

Gann GD, McDonald T, Walder B, Aronson J, Nelson CR, Jonson J, et al. International principles and standards for the practice of ecological restoration. Restoration Ecology 2019;27(S1):1-46.

Gitelson AA, Vina A, Arkebauer TJ, Rundquist DC, Keydan G, Leavitt B. Remote estimation of leaf area index and green leaf biomass in maize canopies. Geophysical Research Letters 2003;30(5):Article No. 1199.

Gitelson AA. Wide dynamic range vegetation index for remote quantification of biophysical characteristics of vegetation. Journal of Plant Physiology 2004;161(2):165-73.

Gitelson AA. Use of a green channel in remote sensing of global vegetation from EOSMODIS. Remote Sensing of Environment 1996;58:289-98.

Gitelson AA, Kaufman YJ, Stark R, Rundquist D. Novel algorithms for remote estimation of vegetation fraction. Remote Sensing of Environment 2002a;80(1):76-87.

Gitelson AA, Zur Y, Chivkunova OB, Merzlyak MN. Assessing carotenoid content in plant leaves with reflectance spectroscopy. Photochemistry and Photobiology 2002b; 75(3):272-81.

Goel NS, Qin W. Influences of canopy architecture on relationships between various vegetation indices and LAI and FPAR: A computer simulation. Remote Sensing Reviews 1994;10(4):309-47.

Haboudane D, Miller JR, Pattey E, Zarco-Tejada PJ, Strachan IB. Hyperspectral vegetation indices and novel algorithms for predicting green LAI of crop canopies: Modeling and validation in the context of precision agriculture. Remote Sensing of Environment 2004;90(3):337-52.

Houghton RA, Hall F, Goetz SJ. Importance of biomass in the global carbon cycle. Journal of Geophysical Research: Biogeosciences 2009;114:148-227.

Huete AR. A soil-adjusted vegetation index (SAVI). Remote Sensing of Environment 1988;25(3):295-309.

Hunt Jr ER, Daughtry CS, Eitel JU, Long DS. Remote sensing leaf chlorophyll content using a visible band index. Agronomy Journal 2011;103(4):1090-9.

The European Union and the World Agroforestry Centre (ICRAF). Wood Density Database [Internet]. 2007 [cited 2024 Jun 21]. Available from: https://apps.worldagroforestry.org/treedb/index.php?keyword=Timber.

Isbaex C, Coelho AM. The potential of Sentinel-2 Satellite Images for land-cover/land-use and forest biomass estimation: A review. In: Cristina GA, Sousa A, Malico I, editors. Forest Biomass - From Trees to Energy. IntechOpen; 2021. p. 2-25.

Intergovernmental Panel on Climate Change (IPCC). IPCC National Greenhouse Gas Inventories Programme: Good Practice Guidance for Land Use, Land-Use Change and Forestry. Japan: Institute for Global Environmental Strategies; 2003.

Intergovernmental Panel on Climate Change (IPCC). IPCC Guidelines for National Greenhouse Gas Inventories: Volume 1-5. Hayama, Japan: Institute for Global Environmental Strategies; 2006.

International Hydropower Association (IHA). Hydropower: the facts [Internet]. 2024 [cited 2024 Jun 21]. Available from: https://www.hydropower.org/net-zero.

Vashum KT, Jayakumar S. Methods to estimate above-ground biomass and carbon stock in natural forests: A review. Journal of Ecosystem and Ecography 2012;2(4):1-7.

Joshi VC, Negi VS, Bisht D, Sundriyal RC, Arya D. Tree biomass and carbon stock assessment of subtropical and temperate forests in the Central Himalaya, India. Trees, Forests and People 2021;6:Article No. 100147.

Kataoka T, Kaneko T, Okamoto H, Hata S. Crop growth estimation system using machine vision. Proceeding of the IEEE/ASME International Conference on Advanced Intelligent Mechatronics; 2003 July 20-24; Kobe, Japan; 2003.

Ke W, Zhangquan S, RenChao W. Effects of nitrogen nutrition on the spectral reflectance characteristics of rice leaf and canopy. Journal of Zhejiang Agricultural University 1998;24(1);93-7.

Khan MN, Tan Y, Gul AA, Abbas S, Wang J. Forest aboveground biomass estimation and inventory: Evaluating remote sensing-based approaches. Forests 2024;15(6):Article No. 1055.

Kuyah S, Dietz J, Muthuri C, Jamnadass R, Mwangi P, Coe R, et al. Allometric equations for estimating biomass in agricultural landscapes: II. Belowground biomass. Agriculture, Ecosystems and Environment 2012;158:225-34.

Lawrence D, Coe M, Walker W, Verchot L, Vandecar K. The unseen effects of deforestation: Biophysical effects on climate. Frontiers in Forests and Global Change 2022;5:Article No. 756115.

Levia DF, Carlyle-Moses D, Tanaka T. Forest Hydrology and Biogeochemistry: Synthesis of Past Research and Future Directions. Springer; 2011.

Lewis CD. Industrial and Business Forecasting Methods: A Practical Guide to Exponential Smoothing and Curve Fitting. Boston, London: Butterworth Scientific; 1982.

Liu HQ, Huete A. A feedback-based modification of the NDVI to minimize canopy background and atmospheric noise. IEEE

Transactions on Geoscience and Remote Sensing 1995; 33:457-65.

Liu Q, Zhang Q, Yan Y, Zhang X, Niu J, Svenning JC. Ecological restoration is the dominant driver of the recent reversal of desertification in the Mu Us Desert (China). Journal of Cleaner Production 2020;268:Article No. 122241.

Lingbing L, Jing SH. The potential carbon losses estimation with remote sensing-based data: Case study in Nova Vida Ranch, Rondonia, Brazil. Proceedings of the International Archives of the Photogrammetry, Remote Sensing and Spatial Information Sciences; 2022 June 6-11; Nice, France; 2022.

Lousada S, Cabezas J, Castanho RA, Gomez JM. Land-use changes in insular urban territories: A retrospective analysis from 1990 to 2018. The case of Madeira Island-Ribeira Brava. Sustainability 2022;14(24):Article No. 16839.

Lu D, Chen Q, Wang G, Liu L, Li G, Moran E. A survey of remote sensing-based aboveground biomass estimation methods in forest ecosystems. International Journal of Digital Earth 2016;9(1):63-105.

Lu D, Batistella M, Moran E. Satellite estimation of aboveground biomass and impacts of forest stand structure. Photogrammetric Engineering and Remote Sensing 2005; 71(8):967-74.

Lu D, Chen Q, Wang G, Moran E, Batistella M, Zhang M, et al. Aboveground forest biomass estimation with Landsat and LiDAR data and uncertainty analysis of the estimates. International Journal of Forestry Research 2012;2012:Article No. 436537.

Luo H, Gao X, Liu Z, Liu W, Li Y, Meng X, et al. Real-time characterization model of carbon emissions based on land-use status: A case study of Xi'an City, China. Journal of Cleaner Production 2024;434:Article No. 140069.

Makridakis S, Wheelwright SC, Hyndman RJ. Forecasting Methods and Applications. New York: John Wiley and Sons; 2008.

Marchant JA, Onyango CM. Shadow-invariant classification for scenes illuminated by daylight. Journal of the Optical Society of America 2000;17(11):1952-61.

Meyer GE, Neto JC. Verification of color vegetation indices for automated crop imaging applications. Computers and Electronics in Agriculture 2008;63(2):282-93.

Mitchard ET, Saatchi SS, Baccini A, Asner GP, Goetz SJ, Harris NL, et al. Uncertainty in the spatial distribution of tropical forest biomass: A comparison of pan-tropical maps. Carbon Balance and Management 2013;8:1-3.

Moisa MB, Dejene IN, Deribew KT, Gurmessa MM, Gemeda DO. Impacts of forest cover change on carbon stock, carbon emission and land surface temperature in Sor watershed, Baro Akobo Basin, Western Ethiopia. Journal of Water and Climate Change 2023;14(8):2842-60.

Mukuralinda A, Kuyah S, Ruzibiza M, Ndoli A, Nabahungu NL, Muthuri C. Allometric equations, wood density and partitioning of aboveground biomass in the arboretum of Ruhande, Rwanda. Trees, Forests and People 2021;3:Article No. 100050.

Mutanga O, Skidmore AK. Narrow band vegetation indices overcome the saturation problem in biomass estimation. International Journal of Remote Sensing 2004;25(19):3999-4014.

Nadrowski K, Wirth C, Scherer-Lorenzen M. Is forest diversity driving ecosystem function and service. Current Opinion in Environmental Sustainability 2010;2(1-2):75-9.

Nandy S, Singh R, Ghosh S, Watham T, Kushwaha SP, Kumar AS, et al. Neural network-based modelling for forest biomass assessment. Carbon Management 2017;8(4):305-17.

Nath AJ, Tiwari BK, Sileshi GW, Sahoo UK, Brahma B, Deb S, et al. Allometric models for estimation of forest biomass in North East India. Forests 2019;10(2):Article No. 103.

Navar J. Allometric equations for tree species and carbon stocks for forests of northwestern Mexico. Forest Ecology and Management 2009;257(2):427-34.

Ostertagova E. Modelling using polynomial regression. Procedia Engineering 2012;48:500-6.

Pandit S, Tsuyuki S, Dube T. Estimating above-ground biomass in sub-tropical buffer zone community forests, Nepal, using Sentinel 2 data. Remote Sensing 2018;10(4):Article No. 601.

Pearson T, Wolker S, Brown S. Source Book for Land Use, Land Use Change and Forestry Projects. USA: Winrock International and the Bio Carbon Fund, World Bank; 2005.

Pearson RL, Miller LD. Remote mapping of standing crop biomass for estimation of the productivity of the shortgrass prairie, Pawnee National Grasslands, Colorado. Proceedings of the 8th International Symposium on Remote Sensing of Environment; 1972 Oct 2-6; Ann Arbor, Michigan: 1972.

Pearson TR, Brown S, Murray L, Sidman G. Greenhouse gas emissions from tropical forest degradation: An underestimated source. Carbon Balance and Management 2017;12:1-11.

Peres CA, Barlow J, Laurance WF. Detecting anthropogenic disturbance in tropical forests. Trends in Ecology and Evolution 2006;21(5):227-9.

Pitman AJ, Avila FB, Abramowitz G, Wang YP, Phipps SJ, de Noblet-Ducoudre N. Importance of background climate in determining impact of land-cover change on regional climate. Nature Climate Change 2011;1(9):472-5.

Rawat YS, Singh JS. Structure and function of oak forests in central Himalaya. I. Dry matter dynamics. Annals of Botany 1988;62(4):397-411.

Reyes G. Wood Densities of Tropical Tree Species. US Department of Agriculture, Forest Service: Southern Forest Experiment Station; 1992.

Rondeaux G, Steven M, Baret F. Optimization of soil-adjusted vegetation indices. Remote Sensing of Environment 1996; 55(2):95-107.

Rouse JW, Haas RH, Schell JA, Deering DW. Monitoring vegetation systems in the Great Plains with ERTS. NASA Special Publication 1974;351(1):Article No. 309.

Scott CE, Monks SA, Spracklen DV, Arnold SR, Forster PM, Rap A, et al. Impact on short-lived climate forcers increases projected warming due to deforestation. Nature Communications 2018;9(1):Article No. 157.

Shannon CE, Weaver W. The Mathematical Theory of Communication. Urbana, IL: University of Illinois Press; 1949.

Sheikh MA, Kumar M, Bhat JA. Wood specific gravity of some tree species in the Garhwal Himalayas, India. Forestry Studies in China 2011;13:225-30.

Simpson E. Measurement of diversity. Nature 1949;163:Article No. 688.

Social Impact Assessment Unit (SIAU) Social Impact Assessment Study for the Purpose of Proposed Land Acquisition in District Hamirpur and Kangra for Dhaulasidh Hydroelectric Project (66 MW) [Internet]. 2019 [cited 2024 Jun 21]. Available from: https://sjvnindia.com/UploadFiles/GroupLinks/127_1_SIA_Dhaulasidh_Eng.pdf.

Slonecker T, Haack B, Price S. Spectroscopic analysis of arsenic uptake in Pteris ferns. Remote Sensing 2009;1(4):644-75.

Timothy D, Onisimo M, Riyad I. Quantifying aboveground biomass in African environments: A review of the trade-offs between sensor estimation accuracy and costs. Tropical Ecology 2016;57(3):393-405.

United Nations Framework Convention on Climate Change (UNFCCC). Informal Meeting of Experts on Methodological Issues relating to Reducing Emissions from Forest Degradation in Developing Countries. Bonn, Germany: UNFCCC; 2008.

United Nations Framework Convention on Climate Change (UNFCCC). Report of the Conference of the Parties on its 15th session. Copenhagen, Denmark: UNFCCC; 2009.

West GB, Brown JH, Enquist BJ. A general model for the structure and allometry of plant vascular systems. Nature 1999;400:664-7.

Woebbecke DM, Meyer GE, Von Bargen K, Mortensen DA. Color indices for weed identification under various soil, residue, and lighting conditions. Transactions of the American Society of Agricultural and Biological Engineers 1995;38(1):259-69.

Yan H, Wang S, Dai J, Wang J, Chen J, Shugart HH. Forest greening increases land surface albedo during the main growing period between 2002 and 2019 in China. Journal of Geophysical Research: Atmospheres 2021;126(6): e2020JD033582.

Yan D, Liu C, Li P. Effect of carbon emissions and the driving mechanism of economic growth target setting: An empirical study of provincial data in China. Journal of Cleaner Production 2023;415:Article No. 137721.

Zahawi RA, Holl KD, Cole RJ, Reid JL. Testing applied nucleation as a strategy to facilitate tropical forest recovery. Journal of Applied Ecology 2013;50(1):88-96.

Zhang T, Su J, Liu C, Chen WH, Liu H, Liu G. Band selection in sentinel-2 satellite for agriculture applications. Proceedings of the 23rd International Conference on Automation and Computing (ICAC); 2017 Sep 7; IEEE; 2017. p. 1-6.

Zhang X, Zhang D. Urban carbon emission scenario prediction and multi-objective land use optimization strategy under carbon emission constraints. Journal of Cleaner Production 2023; 430:Article No. 139684.

Zhou G, Peng C, Li Y, Liu S, Zhang Q, Tang X, et al. A climate change-induced threat to the ecological resilience of a subtropical monsoon evergreen broad-leaved forest in Southern China. Global Change Biology 2013;19(4):1197-210.

Zwane TT, Udimal TB, Pakmoni L. Examining the drivers of agricultural carbon emissions in Africa: An application of FMOLS and DOLS approaches. Environmental Science and Pollution Research 2023;(19):56542-57.

INSTRUCTION FOR AUTHORS

Publication and Peer-reviewing processes of Environment and Natural Resources Journal

Environment and Natural Resources Journal is a peer reviewed and open access journal that is published in six issues per year. Manuscripts should be submitted online at https://ph02.tci-thaijo.org/index.php/ennrj/about/submissions by registering and logging into this website. Submitted manuscripts should not have been published previously, nor be under consideration for publication elsewhere (except conference proceedings papers). A guide for authors and relevant information for the submission of manuscripts are provided in this section and also online at: https://ph02.tci-thaijo.org/index.php/ennrj/author. All manuscripts are refereed through a **single-blind peer-review** process.

Submitted manuscripts are reviewed by outside experts or editorial board members of **Environment and Natural Resources Journal**. This journal uses double-blind review, which means that both the reviewer and author identities are concealed from the reviewers, and vice versa, throughout the review process. Steps in the process are as follows:

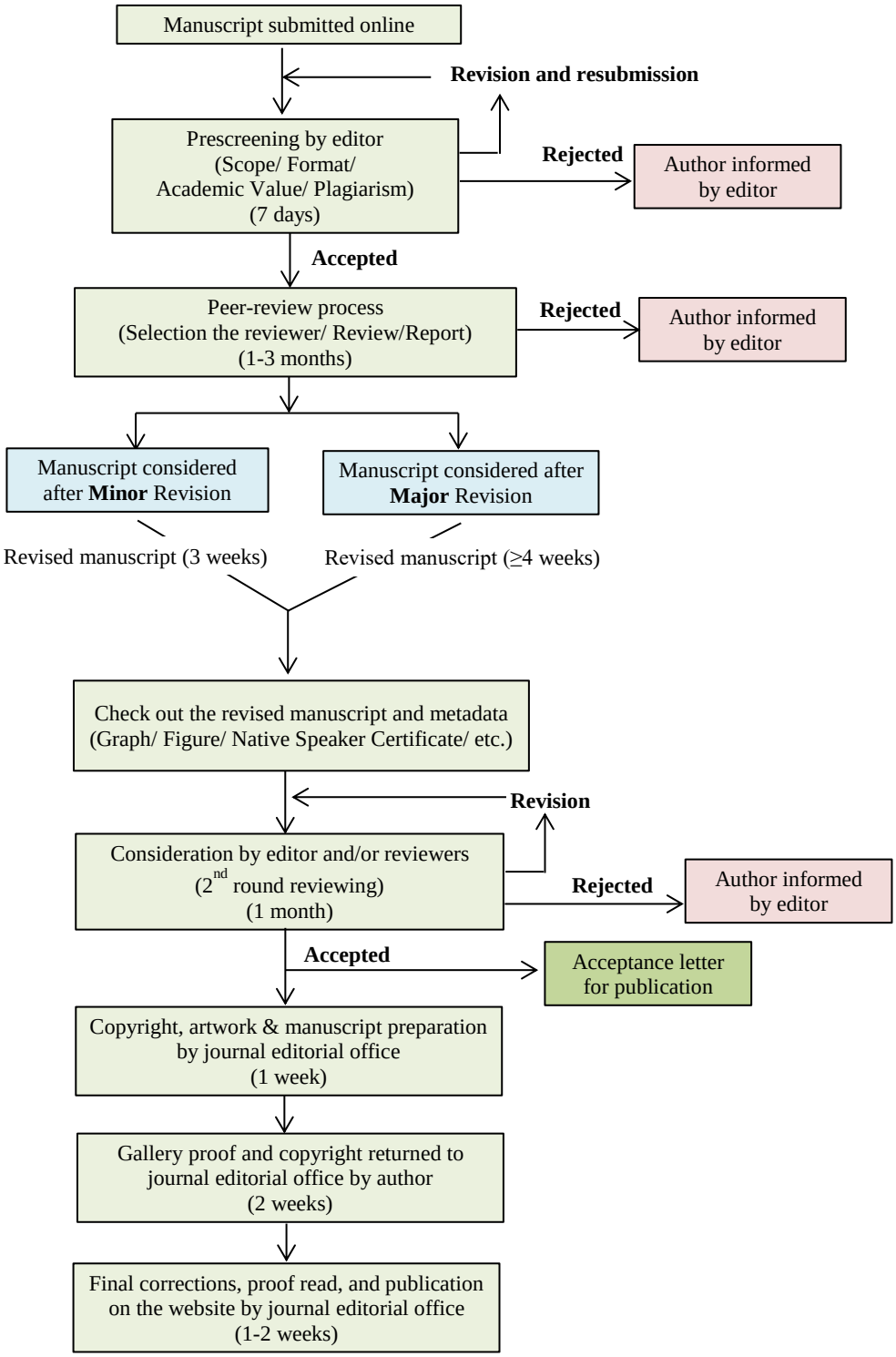

The Environment and Natural Resources Journal (EnNRJ) accepts 2 types of articles for consideration of publication as follows:

- *Original Research Article:* Manuscripts should not exceed 3,500 words (excluding references).
- *Review Article (by invitation):* This type of article focuses on the in-depth critical review of a special aspect in the environment and also provides a synthesis and critical evaluation of the state of the knowledge of the subject. Manuscripts should not exceed 6,000 words (excluding references).

Submission of Manuscript

Cover letter: Key points to include:

- Statement that your paper has not been previously published and is not currently under consideration by another journal
- Brief description of the research you are reporting in your paper, why it is important, and why you think the readers of the journal would be interested in it
- Contact information for you and any co-authors
- Confirmation that you have no competing interests to disclose

Manuscript-full: Manuscript (A4) must be submitted in Microsoft Word Files (.doc or .docx). Please make any identifying information of name(s) of the author(s), affiliation(s) of the author(s). Each affiliation should be indicated with superscripted Arabic numerals immediately after an author's name and before the appropriate address. Specify the Department/School/Faculty, University, Province/State, and Country of each affiliation.

Manuscript-anonymized: Manuscript (A4) must be submitted in Microsoft Word Files (.doc or .docx). Please remove any identifying information, such as authors' names or affiliations, from your manuscript before submission and give all information about authors at title page section.

Reviewers suggestion *(mandatory)*: Please provide the names of 3 potential reviewers with the information about their affiliations and email addresses. *The recommended reviewers should not have any conflict of interest with the authors. Each of the reviewers must come from a different affiliation and must not have the same nationality as the authors.* Please note that the editorial board retains the sole right to decide whether or not the recommended potential reviewers will be selected.

Preparation of Manuscript

Manuscript should be prepared strictly as per guidelines given below. The manuscript (A4 size page) must be submitted in Microsoft Word (.doc or .docx) with Times New Roman 12 point font and a line spacing of 1.5. *The manuscript that is not in the correct format will be returned and the corresponding author may have to resubmit*. The submitted manuscript must have the following parts:

Title should be concise and no longer than necessary. Capitalize first letters of all important words, in Times New Roman 12 point bold.

Author(s) name and affiliation must be given, especially the first and last names of all authors, in Times New Roman 11 point bold.

Affiliation of all author(s) must be given in Times New Roman 11 point italic.

Abstract should indicate the significant findings with data. A good abstract should have only one paragraph and be limited to 250 words. Do not include a table, figure or reference.

Keywords should adequately index the subject matter and up to six keywords are allowed.

Text body normally includes the following sections: 1. Introduction 2. Methodology 3. Results and Discussion 4. Conclusions 5. Acknowledgements 6. References

Reference style must be given in Vancouver style. Please follow the format of the sample references and citations as shown in this Guide below.

Unit: The use of abbreviation must be in accordance with the SI Unit.

Format and Style

Paper Margins must be 2.54 cm on the left and the right. The bottom and the top margin of each page must be 1.9 cm.

Introduction is critically important. It should include precisely the aims of the study. It should be as concise as possible with no sub headings. The significance of problem and the essential background should be given.

Methodology should be sufficiently detailed to enable the experiments to be reproduced. The techniques and methodology adopted should be supported with standard references.

Headings in Methodology section and Results and Discussion section, no more than three levels of headings should be used. Main headings should be typed (in bold letters) and secondary headings (in bold and italic letters). Third level headings should be typed in normal and no bold, for example;

2. Methodology
2.1 Sub-heading
2.1.1 Sub-sub-heading

Results and Discussion can be either combined or separated. This section is simply to present the key points of your findings in figures and tables, and explain additional findings in the text; no interpretation of findings is required. The results section is purely descriptive.
Tables Tables look best if all the cells are not bordered; place horizontal borders only under the legend, the column headings and the bottom.
Figures should be submitted in color; make sure that they are clear and understandable. Please adjust the font size to 9-10, no bold letters needed, and the border width of the graphs must be 0.75 pt. *(Do not directly cut and paste them from MS Excel.)* Regardless of the application used, when your electronic artwork is finalized, please 'save as' or convert the images to TIFF (or JPG) and separately send them to EnNRJ. The images require a resolution of at least 300 dpi (dots per inch). If a label needed in a figure, its font must be "Times New Roman" and its size needs to be adjusted to fit the figure without borderlines.

All Figure(s) and Table(s) should be embedded in the text file.

Conclusions should include the summary of the key findings, and key take-home message. This should not be too long or repetitive, but is worth having so that your argument is not left unfinished. Importantly, don't start any new thoughts in your conclusion.

Acknowledgements should include the names of those who contributed substantially to the work described in the manuscript but do not fulfill the requirements for authorship. It should also include any sponsor or funding agency that supported the work.

References should be cited in the text by the surname of the author(s), and the year. This journal uses the author-date method of citation: the last name of the author and date of publication are inserted in the text in the appropriate place. If there are more than two authors, "et al." after the first author' name must be added. Examples: (Frits, 1976; Pandey and Shukla, 2003; Kungsuwas et al., 1996). If the author's name is part of the sentence, only the date is placed in parentheses: "Frits (1976) argued that . . ."

Please be ensured that every reference cited in the text is also present in the reference list (and vice versa).

In the list of references at the end of the manuscript, full and complete references must be given in the following style and punctuation, arranged alphabetically by first author's surname. Examples of references as listed in the References section are given below.

Book
Tyree MT, Zimmermann MH. Xylem Structure and the Ascent of Sap. Heidelberg, Germany: Springer; 2002.

Chapter in a book
Kungsuwan A, Ittipong B, Chandrkrachang S. Preservative effect of chitosan on fish products. In: Steven WF, Rao MS, Chandrkachang S, editors. Chitin and Chitosan: Environmental and Friendly and Versatile Biomaterials. Bangkok: Asian Institute of Technology; 1996. p. 193-9.

Journal article
Muenmee S, Chiemchaisri W, Chiemchaisri C. Microbial consortium involving biological methane oxidation in relation to the biodegradation of waste plastics in a solid waste disposal open dump site. International Biodeterioration and Biodegradation 2015;102:172-81.

Published in conference proceedings
Wiwattanakantang P, To-im J. Tourist satisfaction on sustainable tourism development, amphawa floating marketSamut songkhram, Thailand. Proceedings of the 1st Environment and Natural Resources International Conference; 2014 Nov 6-7; The Sukosol hotel, Bangkok: Thailand; 2014.

Ph.D./Master thesis

Shrestha MK. Relative Ungulate Abundance in a Fragmented Landscape: Implications for Tiger Conservation [dissertation]. Saint Paul, University of Minnesota; 2004.

Website

Orzel C. Wind and temperature: why doesn't windy equal hot? [Internet]. 2010 [cited 2016 Jun 20]. Available from: http://scienceblogs.com/principles/2010/08/17/wind-and-temperature-why-doesn/.

Report organization:

Intergovernmental Panel on Climate Change (IPCC). IPCC Guidelines for National Greenhouse Gas Inventories: Volume 1-5. Hayama, Japan: Institute for Global Environmental Strategies; 2006.

Remark

** Please be note that manuscripts should usually contain at least 15 references and some of them must be up-to-date research articles.*

** Please strictly check all references cited in text, they should be added in the list of references. Our Journal does not publish papers with incomplete citations.*

Changes to Authorship

This policy of journal concerns the addition, removal, or rearrangement of author names in the authorship of accepted manuscripts:

Before the accepted manuscript

For all submissions, that request of authorship change during review process should be made to the form below and sent to the Editorial Office of EnNRJ. Approval of the change during revision is at the discretion of the Editor-in-Chief. The form that the corresponding author must fill out includes: (a) the reason for the change in author list and (b) written confirmation from all authors who have been added, removed, or reordered need to confirm that they agree to the change by signing the form. Requests form submitted must be consented by corresponding author only.

After the accepted manuscript

The journal does not accept the change request in all of the addition, removal, or rearrangement of author names in the authorship. Only in exceptional circumstances will the Editor consider the addition, deletion or rearrangement of authors after the manuscript has been accepted.

Copyright transfer

The copyright to the published article is transferred to Environment and Natural Resources Journal (EnNRJ) which is organized by Faculty of Environment and Resource Studies, Mahidol University. The accepted article cannot be published until the Journal Editorial Officer has received the appropriate signed copyright transfer.

Online First Articles

The article will be published online after receipt of the corrected proofs. This is the official first publication citable with the Digital Object Identifier (DOI). After release of the printed version, the paper can also be cited by issue and page numbers. DOI may be used to cite and link to electronic documents. The DOI consists of a unique alpha-numeric character string which is assigned to a document by the publisher upon the initial electronic publication. The assigned DOI never changes.

Mahidol University

Wisdom of the Land

Faculty of Environment and Resource Studies, Mahidol University, Thailand
999 Phutthamonthon Sai 4 Rd, Salaya, Phutthamonthon District, Nakhon Pathom 73170
E-mail: ennrjournal@gmail.com